Investigating Proteomic Profiles of Skin Mucus and Blood Plasma of Rainbow Trout (*Oncorhynchus mykiss*) exposed to Low Concentrations of Waterborne Nickel

by

Urvi Pajankar

A thesis submitted to the
School of Graduate and Postdoctoral Studies in partial
fulfillment of the requirements for the degree of

Master of Applied Bioscience

Faculty of Science

University of Ontario Institute of Technology (Ontario Tech University)

Oshawa, Ontario, Canada

August 2022

THESIS EXAMINATION INFORMATION

Submitted by: **Urvi Pajankar**

Masters of Science in **Applied Bioscience**

Thesis title: Investigating Proteomic Profiles of Skin Mucus and Blood Plasma of Rainbow Trout (*Oncorhynchus mykiss*) exposed to Low Concentrations of Waterborne Nickel

An oral defense of this thesis took place on August 4, 2022 in front of the following examining committee:

Examining Committee:

Chair of Examining Committee	Dr. Dario Bonetta
Research Supervisor	Dr. Denina Simmons
Examining Committee Member	Dr. Theresa Stotesbury
Thesis Examiner	Dr. Jon Midwood, Department of Fisheries and Oceans, Canada

The above committee determined that the thesis is acceptable in form and content and that a satisfactory knowledge of the field covered by the thesis was demonstrated by the candidate during an oral examination. A signed copy of the Certificate of Approval is available from the School of Graduate and Postdoctoral Studies.

ABSTRACT

The Ontario Ring of Fire located in the James Bay Lowlands is a nickel rich ore with ongoing mining proposals. This raises the possibility of nickel contamination in one of Ontario's most precious freshwater regions and peatlands. However, impacts of nickel exposure on freshwater fish species remain elusive. To study the impacts in fish when they are exposed to low, environmentally relevant concentrations of nickel (1 – 46 ppb), we examined changes in protein profiles of skin mucus and blood plasma of rainbow trout using untargeted proteomics. The use of non-lethal blood sampling and non-invasive mucus sampling is becoming increasingly desirable to study toxicological effects. Findings suggest that the proteome of rainbow trout is sensitive to low doses of nickel. Primarily, proteins involved in neurological development were impacted in both plasma and mucus proteins. We also find an increase in nickel burden in blood plasma of trout at these concentrations.

Keywords: Nickel; non-lethal and non-invasive sampling; proteomics; fish

AUTHOR'S DECLARATION

I hereby declare that this thesis consists of original work of which I have authored. This is a true copy of the thesis, including any required final revisions, as accepted by my examiners.

I authorize the University of Ontario Institute of Technology (Ontario Tech University) to lend this thesis to other institutions or individuals for the purpose of scholarly research. I further authorize University of Ontario Institute of Technology (Ontario Tech University) to reproduce this thesis by photocopying or by other means, in total or in part, at the request of other institutions or individuals for the purpose of scholarly research. I understand that my thesis will be made electronically available to the public.

The research work in this thesis that was performed in compliance with the regulations of Animal Care Committee under **16421**.

_____ URVI PAJANKAR

STATEMENT OF CONTRIBUTIONS

I hereby certify that I am the sole author of this thesis and that no part of this thesis has been published or submitted for publication. I have used standard referencing practices to acknowledge ideas, research techniques, or other materials that belong to others. Furthermore, I hereby certify that I am the sole source of the creative works and/or inventive knowledge described in this thesis.

ACKNOWLEDGEMENTS

First, I would like to acknowledge my supervisor, Dr. Denina Simmons. The past two years have been challenging to say the least, and through it all she has been understanding, patient, compassionate, uplifting and accommodating of my struggles. Her fiery passion for her work is undeniable and infectious, and I strive to share the same energy with others in the field as I move on forward. I can say without a doubt that she is a role model for aspiring women scientists, and I, along with many others, look up to her for inspiration. Thank you, Nina, for being there for me as a mentor and a professor.

Next, I would like to thank my peers for their constant support during my experiment. To Amy, Almira, Faiz, Chase, Simon, Linda, David, Nancy and Shreya; thank you all for helping me set up for the exposures and sampling days. I know those days started early, with all of us on our feet for hours on end. Sampling days were tedious and stressful, however, each moment spent with them made me feel like I was having the best time. Not only was I able to make great connections, but also some great friends during this time. I am proud to say I have worked with brilliant minds. I could not have done any of this without them, and I am so very grateful.

To my best friend Alice; you have been there for me during my personal and academic struggles. Your incredible contribution and guidance for my data analysis was integral to my thesis. I strongly believe and hope that your mastery over data analysis and inquisitive nature will be a gift to whomever you work with in the future. Thank you for tolerating my long voice-messages and inquiries even when you were busy. I am beyond grateful that I was able to consult my best friend, and have fun while doing so!

Lastly, and certainly not the least, I want to thank my dear parents and my sister. They have been my strongest pillars of support, and the best family anyone could ask for. Although being away from them during this time has been incredibly hard, their encouragement and love through video calls gave me strength when I needed it the most. This would not have been possible without their blessings and sacrifices, and I hope that I have made them proud.

♥

TABLE OF CONTENTS

LIST OF TABLES

CHAPTER 2. Methodology

CHAPTER 3. Results

Appendix F. Over-represented pathways and GO terms in CPDB networks

LIST OF FIGURES

CHAPTER 2. Methodology

CHAPTER 3. Results

Appendix C. Voom Diagnostic Plots

Appendix D. HSI and Condition factor of Rainbow trout

Appendix E. PCA plots

Appendix G. Volcano plots

LIST OF ABBREVIATIONS AND SYMBOLS

AB	Ammonium Bicarbonate
ANOVA	Analysis of Variance
AUP	Animal Utilization Protocol
BLAST	Basic Local Alignment Search Tool
BSA	Bovine Serum Albumin
CPDB	ConsensusPathDB
DDA	Data Dependent Acquisition
DO	Dissolved Oxygen
DOC	Dissolved Organic Content
FDR	False Discovery Rate
GO	Gene Ontology
HDPE	High Density Polyethylene
HSI	Hepatosomatic Index
HPLC	High-Performance Liquid Chromatography
IAA	Iodoacetamide
ICP-MS	Inductively Coupled Plasma Mass Spectrometer
K	Condition factor
LC-HR-MS/MS	Liquid Chromatography High Resolution Tandem Mass-Spectrometry
LOAEL	Lowest Observed Adverse Effects Level
LOQ	Limit of Quantification
OROF	Ontario Ring of Fire
PCA	Principal Component Analysis
PFTE	Polytetrafluoroethylene
QTOF	Quadrupole Time of Flight
RBCs	Red Blood Cells
SGS	Standard Global Services
TCEP	Tris(2-carboxyethyl) Phosphine Hydrochloride
VBA	Visual Basic for Applications
WHO	World Health Organization

Chapter 1. Introduction

1.1 Significance

Currently, aquatic wildlife such as fish are threatened by an array of anthropogenic compounds including heavy metals. Expansion of industrial activities such as mining, smelting, and refining of metals have been one of the major contributors of heavy-metal contamination in waters. The proposed development of the nickel-rich mineral site in the Ontario Ring of Fire (OROF) located in the James Bay Lowlands could be a potential source of nickel contamination. This peatland watershed is interspersed with lakes, rivers, and streams, which ultimately drain into the Hudson Bay. Thus, a locally initiated nickel mining contamination event could also impact marine life in the arctic ocean. Complicating this scenario further is that the effects of nickel on teleost fish are understudied and not well understood.

In humans and other animals, nickel compounds are known to be carcinogenic and cause skin allergies, cardiovascular, and renal disorders (Denkhuas and Salnikow, 2002). Limited research of nickel exposure on fish has revealed adverse impacts on behaviour, respiration, and reproduction at the organismal level (Pane et al., 2003; Zheng et al., 2014.; Kienle et al., 2009). Nickel is known to accumulate in the gills, plasma, liver, and most predominantly in the kidney of fish. Nickel bioaccumulation can induce structural damage within these organs leading to the previously described adverse effects (Athikesavan et al., 2006.; Pane et al., 2004a,b). However, the molecular mechanisms behind these impairments remain elusive.

It is well known that fish exposed to contaminants elicit molecular responses such as modifications in protein levels to maintain optimal fish health. These changes can be detected in the blood plasma, the fluid component of blood, which is the main transport and communication system between various tissues in the body. They can also be detected in the skin mucus of fish, since it is in constant contact with the external environment and thus functions as the first line of defense against pathogens and contaminants. More importantly, these biofluids can be sampled non-lethally, without the need to sacrifice the fish for the purposes of research. Monitoring changes in protein profiles of plasma and mucus upon exposure using a proteomics approach can establish nickel specific biomarkers and indicators of contamination. The main goal of this thesis is to understand the proteomic responses of fish exposed to environmentally relevant nickel concentrations and identify biomarkers of nickel exposure using non-lethal sampling of blood plasma and skin mucus.

1.2 James Bay Lowlands and the Ontario Ring of Fire

The James Bay Lowland region is a part of the Hudson Bay Lowlands, which is the second largest peatland ecosystem of the world. This type of wetland system is highly rich in organic carbon, trapping carbon dioxide from decaying vegetation and animal matter, and preventing its release into the atmosphere. Thus, peatlands help to prevent global warming through carbon sequestration. The wetlands in the James Bay Lowland mostly consist of bogs, fens, swamps, and marshes which are classified based on water chemistry, soil nutrient and moisture regime (National Wetlands Working Group, 1997). Several sources of freshwater such as lakes, rivers, and ponds are scattered in this area and are formed due to the flooding of water in the permeable peatland soils. However, the development of the OROF for mineral extraction may threaten the integrity of this land. One of the many metal

deposits in the OROF is a large nickel deposit named ‘Eagle’s Nest’. The spread of aqueous nickel can threaten the wildlife inhabiting this ecosystem, leading to deleterious effects on aquatic populations. Moreover, the impacts of metal contamination on different types of wetlands are not well explored in general, and in particular the effects of nickel on aquatic wildlife in wetland ecosystems are understudied.

1.3 Overview of nickel

Nickel (Ni) is a group II transition metal, having an atomic and mass number of 28 and 58.69, respectively. It can exist in several oxidation states including -1, 0, +1, +2, +3, +4 with +2 being the most environmentally common (Pyle and Couture, 2012). Commercially, it is in high demand due to its stable, non-corrosive, malleable, conductive, and ductile properties. Ni is predominantly used as an alloy in the manufacture of stainless-steel due to its shiny and silvery finish and due to its ability to tolerate high temperatures. In recent years, Ni has been used as a popular component in the construction of rechargeable batteries for computers, hybrid and electrical vehicles (Nickel Institute, 2020). Additionally, nickel demand is projected to increase with the rise in manufacture of electric automotive batteries (Roskill, 2021).

Biologically, Ni is an essential trace metal in plants and terrestrial animals. In aquatic plants, it operates as a cofactor for enzymes responsible for nitrogen fixation and hydrogen metabolism (Muyssen et al., 2004). However, its essentiality in humans and aquatic animals remains disputed and unestablished. Attempts at investigating the vitality of Ni in fish favor Ni being classified as an essential metal. A few of the studied mechanisms of Ni homeostasis are comparable to other essential metals (Sreedevi et al., 1992; Chowdhury et al., 2008). However, additional research is required to provide a conclusive result.

Conversely, some papers refer to Ni as a non-essential metal in fish since a biological molecule containing Ni has yet to be discovered in teleosts (Denkhuas and Salnikow, 2002). Identifying the essentiality of metals is important for refining policies and water quality guidelines since the regulation of metals is dependent on their biological requirement.

The regulation and effects of Ni in aquatic organisms remains understudied because it is relatively less toxic than other harmful and heavily researched metals such as Cd, Pb, Cu, Ag, and Zn (Pyle and Couture, 2012). However, several studies have documented the toxic effects of Ni in animals which include skin allergies, carcinogenesis, cardiovascular, and renal disorders (Denkhuas and Salnikow, 2002). In Canada, Ni is listed as a contaminant of concern in the Priority Substances List and Toxic Substances List under the Canadian Environmental Protection Act, 1999 (CEPA 1999). Moreover, with the increasing use of Ni for economic and commercial purposes, the mining and extraction of Ni is projected to increase, thereby altering the levels of Ni entering and possibly contaminating the environment. Hence, further studies to understand the effects and responses of aquatic wildlife to nickel contamination are warranted.

1.4 Occurrence of nickel in aquatic environments

Nickel occurs naturally within the earth's crust and core as Ni laterite or sulfidic ores. It can infiltrate waters due to the natural process of weathering of rocks or due to industrial activities such as mining, smelting, and refining of nickel ores. In the 20th century, Sudbury, one of the leading producers of Ni in Canada, witnessed extensive contamination of soil and water due to local mining and smelting activities. Concentration of Ni detected in unaffected surface waters ranged between 1 to 10µg/L (Chau and Kulikovsky-Cordeiro,

1995). However, contaminated areas had higher concentrations of around 2000 µg/L with an average of 131µg/L among lakes sampled in the vicinity (Dixit et al., 1992). Polluted water and soils created toxic conditions for aquatic and terrestrial wildlife, leading to loss of local fish and fish habitat along with the notable destruction of vegetation. Beginning in 1978 and throughout several decades of effort, soils contaminated by years of unsustainable mining practices were remediated and restored by a successful environmental reclamation project, and 40 years afterwards the Sudbury area appears to be in recovery.

Compounds of Ni that are most soluble in water include nickel chloride ($NiCl_2$) and nickel sulphate ($Ni(SO_4)$) and their hydrates ($NiCl_2.6H_20$, $Ni(SO_4).6H_20$, $Ni(SO_4).7H_20$). Therefore, most studies analyzing the impacts of Ni in aquatic environments use these compounds for waterborne exposures. Metal toxicity in fish is dependent on water chemistry such as pH, temperature, dissolved oxygen (DO) content, presence of other metal ions, salinity, and hardness of water. Altering these factors can affect the oxidation state, and therefore the speciation of the metal, which affects bioavailability. Free divalent nickel (Ni^{2+}) is the most bioavailable form in water and can therefore be absorbed at the gill and skin or be ingested by fish and enter the bloodstream. After uptake, Ni^{2+} can bind and interfere with biomolecules, making it the most toxic form of Ni in aquatic animals (Niyogi and Wood, 2004). The toxicity of Ni^{2+} can be reduced by increasing DOC and water hardness (Hoang et al., 2004). Additionally, lower pH confers a slightly protective effect against Ni toxicity compared to neutral pH aquatic environments (Pyle et al., 2002) and toxicity of Ni increases with pH compared to neutral pH conditions (Hoang et al., 2004; Deleebeck et al., 2007).

1.5 Regulation of nickel in fish

1.5.1 Uptake

During waterborne exposure, the primary route of Ni exposure is via the gills, an organ that is in constant contact with the external environment. Likewise, Ni is absorbed through gut epithelial cells during diet-borne exposure. However, the mechanism of uptake of Ni through the epithelial cells present in the gills and the gut of fish have not been explicitly researched (Chowdhury et al., 2008). It is suggested that these mechanisms might be comparable to the ones that have been identified in mammals, i.e., the iron and magnesium transport systems (Tallkvist et al., 2003; Goytain and Quamme., 2005). Specifically, divalent metal transporter 1 (DMT1) has been identified and implicated in the transport of Ni in mammals (Gunshin et al., 1997).

1.5.2 Storage and accumulation

Fish chronically exposed to waterborne Ni have shown trends of accumulation in the gills, kidney, gonads, and gut (Pane et al., 2004b; Chowdhury et al., 2008; Driessnack et al., 2017). The kidney is the predominant site of Ni accumulation, along with blood and gills in trout (Tjalve et al., 1988; Chowdhury et al., 2008). Ni was also detected in the cerebrospinal fluid and spinal cord of *Salmo trutta* (brown trout) exposed acutely and chronically to Ni (Tjalve et al., 1988). Ni accumulates in the red blood cells (RBCs) of fish upon prolonged exposure (Chowdhury et al., 2008). Plasma acts as a sink for Ni upon chronic waterborne exposure as exhibited by adult rainbow trout which had much higher Ni in plasma than unexposed trout (Pane et al., 2004a, Chowdhury et al. 2008). In addition, Ni levels in plasma plateaued towards the end of the chronic exposure. This implies that

this metal might be actively regulated in fish (Brix et al., 2004). The amount of Ni in plasma could be a function of the amount of Ni uptake through the gills from water and the Ni clearance from blood plasma by the kidneys (Pane et al., 2004a; Pane et al., 2005).

Ni accumulation in other tissues can be influenced by the extent of vascularization. Using the estimates of salmonid ^{125}I in plasma space values for each tissue from Olson (1992), Ni loads in the liver and heart tissues of rainbow trout exposed to 384 and 2034 µg/L of Ni were found to be mostly due to the accumulation of Ni present in the blood plasma (Pane et al., 2004a). However, Ni found in the gill and kidney were not explained by perfusion of blood and was most likely due to the exposure of gills and kidney to water and urine (Pane et al., 2004a,b). High loads of Ni in plasma could be explained by an affinity for plasma proteins such as serum albumin (Pane et al., 2004a).

Upon chronic dietary exposure, Ni accumulates in a concentration-dependent manner in the gut, intestine, bile, kidney, scales and gall bladder of trout (Ptashynski et al 2001; Ptashynski and Klaverkamp, 2002; Chowdhury et al., 2008). It also accumulated in the brains of zebrafish (Alsop et al., 2014). Ni remains within the intestine due to absorption whereas it remains in the kidney due to its role in accumulation, detoxification and excretory functions (Eisler, 1998). Ni accumulation in the liver, gallbladder, and bile might also implicate the liver in the detoxification and elimination of dietary Ni in fish (Ptashynski et al., 2001). Adult lake trout and lake whitefish had upregulated renal and hepatic metallothioneins (MTs) when exposed to diet-borne Ni, suggesting a protective role of MTs against Ni (Ptashynski et al., 2001).

1.5.3 Excretion

Kidney is the main site of reabsorption and excretion of Ni in rainbow trout (Pane et al., 2005). Additionally, transport of Ni in the kidney is dependent on the temperature of water and presence of Mg^{2+} ions (Pane et al., 2006 a, b). Another site of storage and elimination of Ni are the scales of fish exposed through diet-borne Ni and might therefore be involved in the detoxification of Ni (Ptashynski and Klaverkamp, 2002; Chowdhury et al., 2008). Ingested Ni is mostly excreted via feces or absorbed through the intestine and eliminated through urine (Chowdhury et al., 2008).

1.6 Effects of nickel on fish

1.6.1 Acute studies

Acute exposure to waterborne Ni (>10 mg/L) can affect ionoregulation, circulation, renal function, respiration, and protein metabolism. Ni^{2+} competes with Mg^{2+} through antagonism in the kidney and thus increases loss of Mg^{2+} through urine, consequently decreasing the level of Mg^{2+} in the plasma of adult rainbow trout (Pane et al., 2005). Zebrafish acutely exposed to Ni experienced loss in whole body Na^{+} ions (Alsop and Wood, 2011). Nile tilapia exhibited a dose-dependent increase of iron (Fe) content in kidneys, and kidney lesions were observed in rainbow trout acutely exposed to Ni (Ghazly et al., 1992; Pane et al., 2005). Carp demonstrated proteolytic activity in the kidneys along with decreased protein content, increased protease activity and free amino acid content in the kidney (Sreedevi et al., 1992). Respiratory effects include the decrease in the partial pressure of oxygen (PO_2) and increase in levels of plasma lactate because of a decrease in gas exchange and aerobic metabolism (Pane et al., 2003). Structural damages due to increased Ni burden

in the gills of trout might be linked to the observed respiratory effects (Pane et al., 2003, Pane et al., 2004).

Cellular level effects include reduction in lymphocyte and leukocyte count, suggesting that acute nickel stress causes negative impacts on immune response (Ghazaly et al., 1992; Kubrak et al., 2012). In contrast, an increase in erythrocyte numbers was observed in Nile tilapia, which may be compensation due to respiratory impairment (Ghazaly et al., 1992). In addition, goldfish and zebrafish exhibited decreased locomotor activity after acute exposure to 10-100 mg/L of nickel (Zheng et al., 2014; Kienle et al 2009). Oxidative stress indicated by altered antioxidant activity such as lipid peroxidase (LPO), superoxide dismutase (SOD), and glutathione peroxidase (GPx) among many others were observed in tissues such as the livers, kidneys, brain and hearts of goldfish due to acute nickel toxicity (Kubrak et al., 2012; Zheng et al., 2014; Kubrak et al., 2014).

1.6.2 Chronic studies

The gill is a major organ for Ni accumulation upon chronic waterborne exposure which leads to histopathological changes in the tissue, decreasing the diffusive capacity of the gill, and ultimately disrupting respiratory function (Pane et al., 2004 a,b). Histopathologies observed in the gills include proliferation of mucus cells present on the epithelium, fusion of structures known as the secondary lamellae that are responsible for increasing the surface area for substance exchange, and hypertrophy of epithelial cells (Athikesavan et al., 2006). Exposure to sublethal waterborne Ni did not affect the resting physiology but impaired maximum oxygen consumption of rainbow trout (Pane et al., 2004). Therefore, Ni is a respiratory toxicant leading to respiratory disorders (Pane et al., 2003 a, 2004a, b; Brix et al., 2004). Additionally, Ni significantly decreased Na^+ and Cl^- ions, elevated Mg^{2+}

ion concentration, and increased protein and ammonia levels significantly in the plasma (Pane et al., 2004b).

Fathead minnows that were chronically exposed to sublethal waterborne Ni experienced a significant decrease in egg production, implying deleterious effects on the fecundity of fish (Pickering, 1974; Driessnack et al., 2017). Zebrafish embryo-larval toxicity tests demonstrated delays and inhibition of the hatching of embryos (Dave and Xiu, 1991). Delays in embryo hatching were also documented in fathead minnows, carp, and Atlantic salmon (Pickering 1974; Baylock and Frank 1979; Grande and Anderson, 1983). However, the mechanism behind delayed hatching has still not been established. Chronic exposure to Ni also significantly upregulated the vitellogenin and metallothionein genes in liver, and significantly decreased plasma estradiol levels in female fathead minnows (Driessnack et al., 2017).

Waterborne Ni is also an implicated neurotoxin and alters fish behaviour due to impairment of the nervous system, but it does not accumulate in the brain tissue of rainbow trout and goldfish (Pane et al., 2003; Kubrak et al., 2014). Additionally, there was a strong induction of c-FOS activity in the brain and brain tissues which indicated signs of demyelination and necrotic changes (Topal et al., 2015). Ni also induces oxidative stress in fish. Rainbow trout that were exposed to waterborne 1 and 2 mg/L of Ni for 21 days demonstrated significant increase in activity of antioxidant enzymes including SOD, LPO, and GSH, but significantly decreased AChE and CAT enzyme activities in the brain, gills and kidney (Topal et al., 2015, 2017). It is thought that oxidative stress can result in genotoxicity. Micronuclei are structures that form within the cell when chromosomes or their fragments are not incorporated into the daughter cell nuclei during cell division. The formation of

these structures indicates cellular damage due to genotoxicity. This was studied in a spotted snakehead, where fish exposed to chronic waterborne nickel (50 µg/L) had significantly greater occurrence of micronuclei in red blood cells compared to the control treatments (Singh et al., 2019).

A transcriptomic analysis of liver and kidney tissues of yellow perch exposed to 542 µg/L of Ni for 45 days revealed disruption of iron metabolism and iron homeostasis, which could lead to iron deficiency (Bougas et al., 2013). There was also reduced expression of genes involved in regulation, translation, and ribosome biogenesis (Bougas et al., 2013). Thus, Ni causes adverse effects at the organismal, tissue and cellular, and organelle level of fish, however the molecular events that lead to these effects have not been fully studied. A deeper understanding of molecular level impacts is required to understand higher level impacts to important biological functions such as neurological effects.

1.7 Proteomics

Proteomics is the study of sets of proteins, known as the proteome, in a defined biological system. The term ‘proteome’ was first coined by Marc Wilkins, and first used in a paper by Wasinger et al. (1995). Proteomics attempts to identify and quantify the proteins in a biological sample in a high-throughput manner. Studying the proteome is useful because it can be used to understand physiological responses of organisms at the molecular level due to changes in gene expression. Proteins control different levels of phenotype, for instance, structural proteins mediate physical form of biological entities and enzymes catalyze biochemical reactions to form products (Liang et al., 2019). Thus, the proteins can be considered direct mediators of phenotypic response in an organism (Liang et al., 2019).

The proteome can be studied using two different approaches: targeted and non-targeted. With the targeted approach, a specific protein is examined and quantified, whereas a non-targeted approach examines the whole set of proteins present in a sample. Also known as 'discovery proteomics', non-targeted proteomics involves the identification of several proteins without priori knowledge. This technique can be applied to discover biomarkers at early stages, and can be combined with targeted proteomics to isolate and validate the biomarkers of interest (Sobsey et al., 2020).

A general non-targeted proteomics workflow involves the retrieval of the biological sample, followed by the reduction, alkylation and fragmentation of the proteins into peptides (also known as shotgun proteomics). The peptides are then separated using a liquid chromatogram and detected using a mass spectrometer. Spectral peaks obtained are used to identify the peptide sequences, which are then matched to reference proteomes using special softwares to identify the proteins present in the sample.

An important application of proteomics is to identify potential biomarkers of effect when an organism is exposed to contaminants. This can be done by inspecting the alterations in the abundance of multiple proteins when exposed to a particular contaminant and associating them with toxicological or physiological pathways. Consequently, this helps identify pathways and proteins that weren't previously characterized as a response to the contaminant, providing the mechanistic basis of effects observed due to exposure. Finally, key proteins that seem to be linked to an adverse outcome or are supported by previous studies can be narrowed down as potential biomarkers of effect. For instance, proteomics was employed to examine pathways affected due to exposure of trout to hypoxia revealing impacts on angiogenesis (Leger et al., 2021) and of fathead minnows to 17α-

ethinylestradiol (oestrogen in birth pills) revealing proteins involved in cellular and endocrine pathways (Martyniuk et al., 2010). Thus, proteomics can be used as an important tool to identify pathways and assess biomarkers, and eventually be used to predict exposure when incorporated into environmental biomonitoring programs for risk assessment.

1.8. Non-lethal and non-invasive sampling

An important aspect of my research is to contribute to the development of non-lethal and non-invasive sampling techniques to study the impacts of contamination in freshwater organisms. Traditional methods usually involve the sacrifice of fish to sample and study their organs, which is unfavourable and contradicts the 3R principles of ethical animal research (Replacement, Reduction and Refinement). Non-lethal and non-invasive tools are particularly beneficial because they can be used to study species at risk. They also offer the ability to sample the same fish repeatedly with a temporal design, improving the strength of the study, and providing a robust analysis of effects observed. Because of this, the use of non-lethal and non-invasive techniques, such as blood and epidermal mucus sampling, have become more desirable in recent years (Thortensen et al., 2022).

Since the blood plasma is a dynamic biological matrix and transports proteins from the whole organism, this biological matrix is highly informative and suitable for proteomic analyses. Previous research in our lab using rainbow trout has shown that the blood plasma proteome shares tissues-specific proteins, which can be used to analyze the status of organs, and thus the overall health of the organism (Tannouri, 2021, *unpublished*). This a novel premise, given that most medical testing for humans and mammals begins with a blood sample. Thus, alterations in the proteome(s) present within the blood plasma in response to nickel will provide insight into the overall health of the fish. Moreover, our lab recently

established the survival and healing of rainbow trout after using non-lethal blood sampling techniques in laboratory and field settings (Pollard et al., 2022).

Epidermal mucus, on the other hand, is produced on the external surface of fish skin, and plays an important role as a protective mechanical barrier due to the presence of glycoproteins called mucins. Mucus is produced and sloughed off regularly, which facilitates the removal of pathogens and external particles such as bioavailable metals that are absorbed within it. Mucus also provides immunity against pathogens by producing antibacterial enzymes, lysozymes, immunoglobulins, lectins, and proteolytic enzymes (Dash et al., 2018). Previous literature has demonstrated a link between environmental contamination and occurrence of increased pathogenic disease in fish (Austin, 1998). Exposure to heavy metals such as arsenic, cadmium, and mercury altered skin mucosal immune activity by increasing enzymes related to immune protection (Guardiola et al., 2015). Therefore, studying the proteome of the epidermal mucus of fish exposed to metals can provide insight into their overall status of health.

1.9. Research Objectives

The overarching goal of my thesis was *to identify protein biomarkers that can be sampled from fish non-lethally, and that indicate exposure and/or adverse effects at environmentally*

relevant concentrations of waterborne nickel. To achieve this, I proposed the following objectives:

Objective 1: To investigate effects of nickel exposure in rainbow trout blood and plasma. The blood plasma of fish contains an array of proteins circulating from various organs of the body, and will provide a wealth of information about the biological response of fish to nickel exposure. Additionally, to establish the genotoxicity of nickel at the cellular level, I conducted a micronucleus assay on red blood cells. Moreover, since blood plasma is known to be a sink for Ni (Pane et al., 2004a, Chowdhury et al. 2008), Ni burden in rainbow trout plasma will also be measured.

Objective 2: To examine changes in the skin mucus proteome of rainbow trout at different times during a waterborne Ni^{2+} exposure. The epidermal mucus of fish can be sampled with minimal impact to fish health, and is secreted and undergoing constant change. I studied temporal changes in the protein profiles in mucus from rainbow trout exposed to nickel to determine if fish mucus responds to Ni.

Objective 3: To identify potential biomarkers of chronic waterborne nickel exposure. Using data obtained for objectives 1 and 2, I examined differentially abundant proteins among the protein profiles in both plasma and epidermal mucus to identify potential biomarkers of nickel exposure which could be used for future biomonitoring programs.

Chapter 2. Methodology

2.1 Fish housing and acclimation

Rainbow trout (25cm-35cm; 200-450g) were procured from Linwood Acre Trout Farms (Izumi Aquaculture Inc., Campbellcroft, Ontario) and allowed to acclimate in 1000L

fiberglass holding tanks (10 tanks, 15 fish each) for at least 3 weeks. Municipal water was supplied to the tanks from the City of Oshawa, drawn from Lake Ontario (hardness = 108-125 mg/L $CaCO_3$, pH = 7.5, Cl-= 0 ppm, DO = 11 mg/L, Ni = 0.5 µg/L). It is filtered, dechlorinated and maintained at 12±2°C by a chiller. Trout were maintained in flow-through systems receiving water at 4 turnovers per day, with a photoperiod of 16h light:8h dark. Fish were fed 1.6 % of their weight on alternate days with Corey Aquafeed Optimum™ 4mm trout food. Tanks were cleaned and drained daily to remove waste accumulated from uneaten food or fecal matter. No mortalities were observed during the acclimation and experimental period.

2.2 Experimental design and exposures

2.2.1 Nickel treatments

Concentrations of nickel (Ni) were selected based on levels present in the OROF (detected average of 0.2 µg/L; PWQMN, 2021), Canadian Water Quality Guidelines for Ni (25 µg/L; CCME 1987) and previous Ni toxicology studies conducted on rainbow trout (~24-2000 µg/L). For this experiment, 3 Ni treatment concentrations were chosen. Solutions were prepared by dissolving nickel sulphate hexahydrate salts ($NiSO_4.6H_2O$, CAS# 10101-97-0, Fisher Scientific, 99.97%) in distilled water. To study the impacts of Ni at the level of the proteome, which is more sensitive to changes in the environment, much lower, environmentally relevant, levels of Ni were used. Nominally, the Ni treatments were chosen to be 0 (control), 0.45, 4.5 and 44.5 ppb (or µg/L). These concentrations are approximately 2x, 20x and 200x the detected levels of Ni in the OROF. However, upon measuring the dissolved and total nickel concentrations (by SGS, Lakefield, ON), the Ni levels were determined to be 0.5 (control), 1.5, 4.9 and 45.7 ppb respectively (see section

2.9 for more details; Table 2.1). Therefore, throughout the rest of the paper, the Ni treatments will be referred to by their measured amounts.

2.2.2 Stock concentration preparation

Each of the experimental treatment was comprised of two replicate 1000L cylindrical tanks with 15 fish each, containing a total of 30 fish dosed with the same Ni treatment. The fish were exposed for a duration of 30 days. Housing tanks were maintained at 4 turnovers per day, with an inflow rate of 166.67 L/hr or 2.78 L/min. These flow rates were manually verified before the experiment by measuring flow rates every 10 seconds. Additionally, a water flow meter (Dewenwils, ASIN #B08TC4QYC2) was also used to ensure that the flow rates were maintained between 2.7-2.8 L/min. The direction of flow of water was circularly maintained. Each tank was supplied stock Ni concentrations using a peristaltic pump (205U/CA multi-channel cartridge pump; Watson-Marlow Bredel Pumps). A flow rate of 0.088 mL/min at 1.1 rpm (5.28 mL/hr) with tubing of bore size 1.42 mm was selected to dose the tanks with the pump. The pump flow rate was manually validated by running water through the pump to monitor hourly flow rates for each tank. The flow rate of water being pumped to each tank was calculated as the mean of measurements taken on 5 separate days (Table 2.2). The peristaltic pump flow rates and inflow rates of water to the tank were used to calculate the dilution factor to make stock concentrations.

$$D = \frac{P_f}{P_f + W_i}$$

where, *D = Dilution factor,*

P_f *= Peristaltic pump flow rate to the tank,*

W_i = Rate of inflow of water to the tank, assumed to be a constant rate of 2.77L/min or 166.67 L/hr for all tanks

The stock concentrations were obtained by dividing the nominal Ni concentrations by the dilution factor for each tank, and then dividing it by the number of moles of Ni present in the nickel sulphate salt used (Table 2.2).

$$C = \frac{N}{D} \times \frac{1}{n}$$

where, *N = nominal Ni concentration of each tank*

D = dilution factor of each tank

n = number of moles of nickel in $NiSO_4.6H_20$

$$n = \frac{mass\ of\ nickel}{molar\ mass\ of\ NiSO4.6H20}$$

$$n = \frac{58.69}{262.85} = 0.223$$

Nickel stock concentrations were prepared by first dissolving the salt in 500mL of distilled water. The salt was stirred for approximately 15 minutes before the solution was transferred to a 1L volumetric flask. The solution was diluted to 1L, inverted 5-10 times, and then transferred to Nalgene™ amber high-density polyethylene (HDPE) bottles. The HDPE bottles were then connected to the peristaltic pump for tank dosing. Based on flow rates of the pump, each bottle would last approximately 8 days before running out. However, the stock bottles were replaced every 6 days, and were freshly prepared prior to dosing. All experiments were conducted under Animal Utilization Protocol (AUP) #16421 as approved by the animal care committee at Ontario Tech University.

2.3 Mucus sampling

Prior to the initiation of the exposures (day=0), rainbow trout were netted from their holding tanks and transferred to a solution containing 80 mg/L tricaine methanesulfonate or MS-222 (Syncaine®, Syndel) to anesthetize them. This solution was changed after every 5 fish, with 3 changes for every 15 fish. The anesthetized fish were moved to a flat surface to measure their fork lengths and weights. Skin mucus was sampled from the lateral sides of the fish using a stainless-steel spatula. The mucus was then transferred to a pre-rinsed (150 µL of 0.1 M NaOH at 14,000g for 1 min, followed by 150 µL of Milli-Q water at 14,000g) 0.5mL amicon ultracentrifuge tube with a 10,000 kDa filter (Amicon® Ultra, Sigma Aldrich). The amicon was then moved to an ice bath until all the fish were sampled for mucus. After mucus sampling, the fish were then floy tagged (Floy Tags Inc.) just below their dorsal fin, transferred to a recovery tank receiving constant flow of water, before they were returned to their respective holding tanks. These steps were repeated on day 15 and day 30. Fish were individually identified by recording the unique identification numbers on their floy tags.

After sampling, the amicon tubes were centrifuged for 30 minutes at 14,000g to separate the mucus proteins from the filtrate. The tubes were then turned upside-down in a new collection tube and then re-centrifuged for 2 minutes at 1,000g to collect the concentrated proteins. Protein concentrates were then stored in -80°C until further protein digestion and extraction.

2.4 Blood plasma and tissue sampling

On day 30 of the exposure and after conducting mucus sampling, fish were euthanized via exsanguination followed by cervical dislocation. Approximately 4 mL of blood was

collected using a heparinized vacutainer with a 22-gauge needle. The vacutainers were then placed on an ice bath until all fish were sampled for blood. A drop of blood was immediately pipetted from the vacutainer after blood sample was taken, and transferred to a glass microscope slide for the micronucleus assay (See section 2.5. for more details). Dissections were conducted to sample trout livers and head kidneys. Liver weight was recorded to calculate the hepatosomatic index. All cryovials containing the tissues were immediately flash frozen and stored at -80°C. The liver and head kidneys were not analyzed in this study; however, they will be examined in later studies.

The vacutainers containing blood samples were centrifuged at 2,400 rpm for 15 minutes to separate the plasma. Plasma (~2mL) was then pipetted into two 1mL cryovials, flash frozen and stored at -80°C until protein extraction and metal burden analysis.

2.5 Micronucleus assay

Once the blood was collected in a vacutainer, a drop of blood was pipetted and transferred to the edge of a glass microscope slide. Two replicate slides were prepared for each fish. The drop of blood was smeared across the slide using a spare slide and left to air dry for 5 minutes. The slides were fixed in methanol for 5 minutes and air dried for 5 minutes before they were stained with Giemsa for 20 minutes. Once stained, the slides were rinsed with distilled water and left to air dry. Red blood cell imaging was performed with a Leica DME compound microscope at 100x magnification. Images of 5 different sections of the slide of each of the 2 replicate slides prepared from one individual fish (~1000 RBCs per fish). Frequencies of nuclear abnormalities and micronuclei were manually scanned and documented. Only the first 7 and 8 fish from tank replicates 1 and 2 respectively of each treatment were analyzed.

2.6. Protein digestion and extraction

Only 7 fish from the first tank replicate and 8 from the second replicate for each Ni treatment were processed, since a total of 15 fish was determined to be statistically sufficient to conduct proteomic analysis (Simmons et al., 2015).

Mucus and plasma samples were allowed to thaw completely after they were removed from -80°C. The tubes containing mucus protein concentrates and blood plasma were vortexed to get a uniform sample mixture. 50 µL of mucus from the amicon collection tube and 15 µL of plasma from the cryovials were transferred to new low retention microcentrifuge tube. 35 µL of 200 mM ammonium bicarbonate (AB) buffer was added to the tubes containing plasma to obtain a final volume of 50 µL. The tubes containing both plasma and mucus were vortexed, and 2.65 µL of 100 mM tris(2-carboxyethyl) phosphine hydrochloride (TCEP) in 200 mM of AB was added to the tubes, vortexed and allowed to incubate for 45 minutes to reduce the proteins. Following this, 2.8 µL of 200 mM iodoacetamide (IAA) in 200 mM AB buffer was added to the solutions, vortexed, and allowed to incubate for 45 minutes in the dark to alkylate the proteins. Digestion of the proteins was performed by adding 50 µL of 20% (v/v) formic acid in Milli-Q water to the tubes. The samples were then allowed to incubate at 115°C on a heating block for 30 minutes. Once cooled, the samples were evaporated to near dryness in SpeedVac™ SPD 1030/2030. Dried samples were reconstituted with 20 µL HPLC buffer containing 95% water, 5% acetonitrile and 0.1% formic acid (v/v). The reconstituted samples were centrifuged to separate the pellet and supernatant, the latter of which 20 µL was pipetted into 250 µL inserts of 2 mL screw thread HPLC vials capped with 9 mm blue

PFTE/silicone/PFTE screw caps. The final peptide solutions were stored in 4°C for immediate LC-MS instrumental analysis.

2.7 Liquid chromatography mass spectrometry analysis

The prepared HPLC vials were placed in the temperature regulated autosampler, where 2 µL of the digested protein solutions were injected and separated by reverse phase liquid chromatography using a Zorbax, 300SB-C18, 1.0 × 50 mm 3.5 µm column (Agilent Technologies Canada Inc., Mississauga, ON) with an Agilent 1260 Infinity Binary Liquid Chromatogram. Samples were separated with a gradient using solvent A (95% H2O, 5% acetonitrile and 0.1% formic acid) and Solvent B (5% H2O 95% acetonitrile and 0.1% formic acid). The separated peptides were detected and sequenced using the Agilent 6545 Accurate-Mass Quadrupole Time-of- Flight (Q-TOF) mass spectrometer in tandem to the Agilent 1200 series liquid chromatography system. Each analytical run included a solvent blank and a BSA (bovine serum albumin) digest standard (Agilent Technologies Canada Inc., Mississauga, ON) injection every 12 samples in order to monitor baseline, carry-over, drift, and sensitivity during the runtime. The samples were injected once per each individual fish. Detailed instrumental methods are provided in Appendix A. All mucus and plasma samples collected from fish exposed to Ni treatments were randomized and analyzed together, and the control samples were randomized and separately analyzed.

2.8 Protein identification and quantification

Spectral files obtained for each sample from the LC-MS/MS run were analyzed using the Spectrum Mill Software (Agilent Technologies, Version B.04.01.141) to identify detected peptides. Uniprot Reference Proteome for rainbow trout (ID: UP000193380, downloaded September 2021) was used to prepare a database of peptides using an *in-silico* digestion

method of the proteome based on formic acid amino-acid cleavage on the C and N terminus at aspartic acid, serine, leucine and proline. Proteins were then manually validated and accepted when at least one peptide had a peptide score (quality of the raw match between the observed spectrum and theoretical database spectrum) greater than 6 and a %SPI (scored peak intensity; the percentage of spectral peak-detected ion current explained by the search interpretation) of greater than 70%.

Peptides identified by Spectrum Mill at the MS/MS level were imported into Skyline 20.2 (MacCoss Lab Software) to perform MS1 filtering to quantify protein abundances based on chromatogram peak intensities. Quantification at the MS1 level was performed by creating a spectral library using the DDA (data dependent acquisition) workflow, with a cut-off score of 0.9, retention time window of 2 minutes, and 5 missed cleavages with transition settings for Q-TOF (Pino et al., 2020).

The Uniprot accession numbers of the identified proteins were mapped to orthologous human gene symbols using a custom Python script, which used the Basic Local Alignment Search Tool (BLAST) to identify the top sequence match to a protein query. Proteins that weren't matched using the script were mapped manually. Redundancies in gene symbols were consolidated on excel by choosing the row containing the gene symbol with the maximum value. Lastly, a visual basic for applications language (VBA) script was used to remove protein abundances (peak areas) with mean intensity values <2000.

2.9 Metal burden analysis

Water samples were collected at two separate times; once during the experiment, and then after the experiment. The samples collected during the experiment were pooled between

tank replicates using equal volumes to obtain 60 mL of sample for measuring dissolved Ni. Unfortunately, not enough water was collected during the experiment to measure total Ni. However, after the experiment, water samples were collected in 60 mL bottles lined with HNO_3 for measuring dissolved Ni, and in 125 mL bottles for measuring total Ni. For each tank replicate belonging to a particular treatment, water samples were collected on 2 separate days. Samples collected during the experiment were stored in the refrigerator until they were shipped to SGS (Lakefield, ON) in ice, along with the samples collected after the experiment. The samples were analyzed for dissolved and total Ni concentration using inductively-coupled plasma mass spectrometry (ICP-MS) (Table 2.1). A summary of the report by SGS is in Appendix B-I.

Blood plasma samples were also measured for Ni levels (Table 2.3, Figure 2.1). They were first thawed, and plasma samples from 5 fish were pooled to obtain 5mL of plasma, giving us 3 pooled replicates for each tank, and 6 replicates for each nickel treatment. The samples were pooled in cryovials, and stored in -80°C until the day they were shipped to SGS in ice for analysis. The limit of quantification (LOQ) for Ni was 0.05 µg/g. A pooled sample from the control treatment with Ni levels below the LOQ was removed prior to statistical analysis, leaving 5 samples. A summary of the report by SGS is in Appendix B-II.

2.10 Statistical analysis and data visualization

Proteins in mucus and plasma were analyzed using the *limma* package in Rstudio Version 4.2.0 (Ritchie et al., 2015). *Limma* (Linear Models for Microarray and RNA-seq Data analysis) uses an Empirical Bayes approach to fit the model. Proteins with missing values were removed. Pre-processing involved normalization between and within samples, and computing variation of samples by estimating the sample-specific weights. The functions

used for the above steps were ‘backgroundCorrect’, ‘normalizeBetweenArrays’ and ‘arrayWeights’ respectively (Ritchie et al., 2007; Ritchie et al., 2006). The fit of the model was assessed by estimating the mean-variance trend using the ‘voomWithQualityWeights’ function (Appendix C, Figures C1&C2). This function was also used to compute the weights for each observation or protein. The model was corrected for batch effects due to tank replicates using the function ‘duplicateCorrelation’ (Symth et al., 2005). Using the ‘matvec’ function, combined weights of the samples and proteins were computed and the coefficients of the model were fit by calling the function ‘lmFit’ (Philipson et al., 2016). Finally, the function ‘eBays’ was used to calculate the t-statistics. To obtain protein lists significantly affected due to either nickel treatment or time (main effects) as well as nickel treatment and time (interaction effect), the function ‘makeContrasts’ was used to specify the coefficients that are to be extracted from the fit to make appropriate comparisons. A Benjamini-Hochberg FDR correction of < 0.05 was used for multiple testing. Heatmaps of abundance of proteins obtained due to main and interaction effects were created using the pheatmap function (Kolde, 2019). Pairwise comparisons for the mucus data set were done using a p-value of < 0.01 to obtain an adequate list of proteins, which could not be accomplished using an FDR of 0.05. Volcano plots were made using the EnhancedVolcano package in R to visualize significant proteins and their fold change (Blighe et al., 2022).

Ni burden in the blood plasma of rainbow trout was tested for significance. This data did not pass the Shapiro-Wilk test for normality with raw and transformed data. Significance was tested using a Kruskal-Wallis test with a Dunn’s multiple comparison (alpha=0.05 Table 2.3, Figure 2.1).

Rainbow trout hepatosomatic indices (HSI) and condition factors (K) were calculated using liver weights and whole-body weights on day 30 and fork lengths and weight on day 0, 15 and 30 respectively.

$$\text{HSI} = \frac{Weight\ of\ liver\ (grams)}{Whole\ body\ weight\ of\ fish (grams)}$$

$$\text{K} = \frac{Whole\ body\ weight\ (grams)}{Fork\ Length\ (cm)^3} \times 100$$

Data was analyzed for normality using a Shapiro-Wilk test. The HSI data did not pass for normality with raw and transformed data, and was thus tested for significance using a Kruskal-Wallis test, with a Dunn's multiple comparison test with an alpha value of 0.05 (Appendix D, Figure D1). The data set for condition factor was only normal when transformed using a natural logarithm. A two-way ANOVA was performed along with Tukey's test for multiple comparisons with an alpha value of 0.05 (Appendix D, Figure D2).

2.11 Pathway and network analysis

Overrepresentation analysis of protein lists obtained from main effects of nickel treatment for both mucus and plasma was performed on ConsensusPathDB-human (CPDB). For this analysis, we used orthologous human gene symbols and selected human as the species. No background protein lists were used. All pathways and Gene Ontology (GO) biological processes with a p-value cut-off of 0.01 were selected and manually re-arranged to create a network based on the overlap between pathways and processes due to shared genes. Protein lists obtained from pairwise comparisons for mucus were analyzed using GO enrichment with no multiple test correction and a p-value cut-off of < 0.05. GO terms were

manually selected based primarily on significance and uniqueness to eliminate redundancy. For plasma, Enrich R (Xie et al., 2021), a GO enrichment analysis tool, was used to obtain adequate number of processes, which wasn't achievable using GO enrichment alone. The top 20 most significantly enriched processes were selected ($p < 0.05$). For both mucus and plasma, the selected significant GO terms were plotted using GraphPad Prism 9.3.1.

Table 2.1. Nominal and measured nickel concentrations. The dissolved and total nickel concentrations were measured using an ICP-MS by SGS. Dissolved nickel is the most bioavailable form of nickel. Columns a and b refer to measurements on two separate days respectively for each tank. Text highlighted in **blue** are measurements of pooled water samples from tank replicates I and II for each nickel treatment collected during the experiment. There is only one value for pooled water samples since the volume of sample pooled during the experiment was sufficient to be measured only once. All other measurements in black font were performed on water samples collected after the experiment.

Nominal Nickel (ppb or µg/L)	Tank replicates	Measured Nickel (ppb or µg/L)							
		Dissolved Nickel				Total Nickel			
		a	b	Mean ± St. Er*	Mean ± St. Er#	a	b	Mean ± St. Er*	Mean ± St. Er#
Control	I	0.5	0.5	0.5 ± 0	***0.5 ± 0***	0.5	0.5	0.5 ± 0	***0.5 ± 0***
	II	0.5	0.5	0.5 ± 0		0.5	0.5	0.5 ± 0	
0.45	I	1.2	1.2	1.2 ± 0	***1.52 ± 2.4***	1.2	1.2	1.2 ± 0	***1.58 ± 0.22***
	II	2.2	2	2.1 ± 0.07		2	1.9	1.95 ± 0.05	
	I and II	1	*NA*	*NA*		*NA*	*NA*	*NA*	
4.5	I	4.2	4.2	4.2 ± 0	***4.86 ± 0.79***	4.4	4.5	4.45 ± 0.05	***4.85 ± 0.24***
	II	8	3.6	5.8 ± 1.6		5.4	5.1	5.26 ± 0.15	
	I and II	4.3	*NA*	*NA*		*NA*	*NA*	*NA*	
44.6	I	38.5	36.6	37.55 ± 0.67	***45.68 ± 4.92***	39.3	37.7	38.5 ± 0.8	***52.33 ± 8.07***
	II	54.2	60.7	57.45 ± 2.3		64.5	67.8	66.15± 1.65	
	I and II	38.4	*NA*	*NA*		*NA*	*NA*	*NA*	

* mean and standard error calculated within each replicate tank

over all mean and standard error of a treatment calculated using measured values from both replicates and pooled samples

Table 2.2. **Nickel sulphate stock concentration calculations.**

Nominal Nickel Concentrations *N* (ug/L)	**Tank Replicate**	**Mean peristaltic pump flow rate** [a] P_f (L/hr)	**Inflow rate of tank water** [b] W_i (L/hr)	**Dilution factor** [c] *D*	**Stock concentrations of $NiSO_4.6H_2O$** [d] *C* (mg/L)
0	I	0.00425	166.67	2.54988E-05	0
	II	0.00491	166.67	2.94585E-05	0
0.45	I	0.0051	166.67	3.05985E-05	65.949
	II	0.00501	166.67	3.00585E-05	67.13367
4.5	I	0.00513	166.67	3.07784E-05	655.6334
	II	0.00511	166.67	3.06584E-05	658.1994
44.5	I	0.00521	166.67	3.12584E-05	6383.935
	II	0.00508	166.67	3.04785E-05	6547.298

[a] Calculated by taking the average of the measured flow rates on 5 different days

[b] Measured manually and using a water flow meter

[c] Calculated using the formula $D = \frac{P_f}{P_f + W_i}$

[d] Calculated using the formula $C = \frac{N}{D} \times \frac{1}{n} \times \frac{1}{1000}$ mg/L;

where $n = \frac{mass\ of\ nickel}{molar\ mass\ of\ NiSO4.6H20}$; $n = \frac{58.69}{262.85} = 0.223$

Table 2.3: Descriptive statistics of Ni burden (µg/g) in blood plasma rainbow trout

Nickel treatment (ppb)	Control (0.5)	1.5	4.9	45.7
N	5	6	6	6
Mean (ug/g)	0.07600	0.07500	0.1367	0.5117
Standard deviation	0.005477	0.02258	0.01211	0.1196
Standard error	0.002449	0.009220	0.004944	0.04881

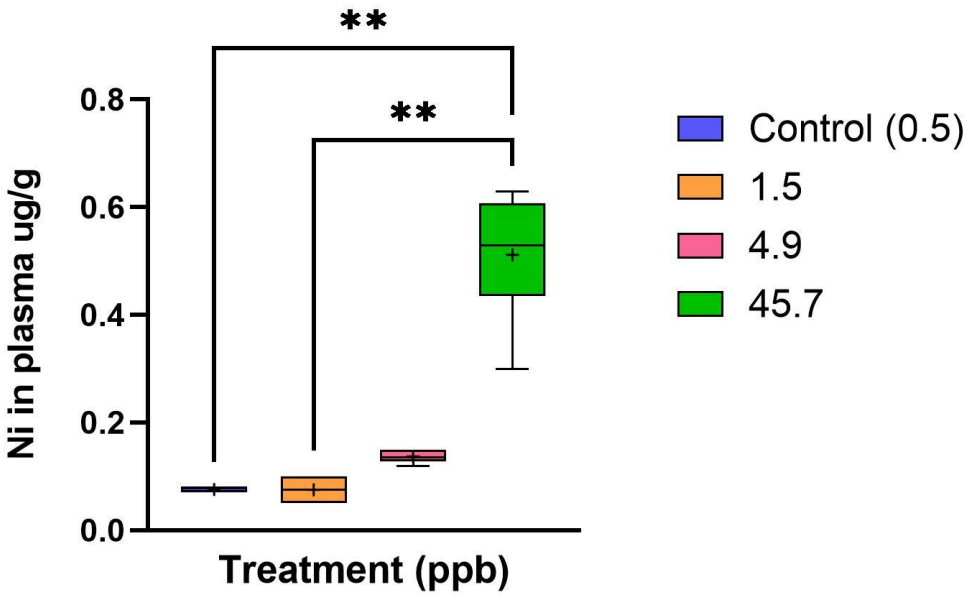

Figure 2.1. Nickel burden (µg/g) in blood plasma of rainbow trout. Nickel was measured in blood plasma by SGS using an ICP-MS. Blood plasma was pooled from 5 individual fish into one cryovial, with 3 cryovials per replicate tank and a total of 6 for each nickel treatment (N=6, except for control, N=5). Boxplot represents the 25th, 50th (median) and 75th quantiles with outliers. Mean of group is represented by a '+' sign. Kruskal-Wallis test followed by a Dunn's multiple comparison test ($p < 0.05$) revealed that accumulated Ni was significantly different in fish exposed to 45.7 ppb vs controls, and 45.7 ppb vs 1.5 ppb of Ni. Plots were created using GraphPad 9.3.1.

Chapter 3. Results

3.1 Dissolved and total nickel in water samples

Fish were exposed to 3 nickel treatments and a control as described in Table 2.1. Mean and standard error was calculated for each replicate tank with water samples collected after the experiment. As well, the overall mean and standard error for each treatment group was calculated by considering measured nickel in samples collected during and after the experiment.

Control water received by the tanks was the municipal water, which when measured for both dissolved and total nickel had a consistent concentration of 0.5 ppb (Table 2.1). The first nickel treatment, with a nominal nickel value of 0.45 ppb group, had a mean dissolved nickel concentration of 1.52 ±2.4 ppb and a mean total nickel concentration of 1.575 ± 0.22ppb (Table 2.1). These nickel levels are more than 3-fold the nominal amount. The dissolved nickel and total nickel concentrations in replicate tank 1 for the 0.45 ppb group remained constant at 1.2 ppb. However, the replicate tank 2 had a measured dissolved and total nickel values of about 2.1 ±0.07 ppb and 1.95 ± 0.05 ppb. This is twice the amount than tank replicate 1 (Table 2.1). On the other hand, pooled water samples from tank replicates 1 and 2 during the experiment had measured dissolved nickel concentration of 1 ppb. This value is closer to the mean of dissolved nickel concentration measured in water samples of tank replicate 1 collected after the experiment.

Dissolved and total nickel in the second nickel treatment, nominally 4.5 ppb, had a mean of 4.86 ±0.79 and 4.85±0.24 ppb respectively, which is about 8% higher than the nominal amount (Table 2.1). The dissolved nickel and total nickel concentrations in replicate tank 1 were 4.2 ppb and 4.45 ± 0.05 ppb, respectively. Similar to the first nickel treatment,

replicate tank 2 in this case had mean dissolved and total nickel concentrations of 5.8 ± 1.6 ppb and 5.26 ± 0.15 ppb that were 38% and 18% higher than the measured amounts in tank replicate 1 (Table 2.1). Pooled water samples from tank replicates 1 and 2 during the experiment had measured dissolved nickel concentration of 4.3 ppb. This value is closer to the mean of dissolved nickel concentration measured in water samples of tank replicate 1 collected after the experiment.

The third nickel treatment, nominally 44.6 ppb, had mean measured dissolved and total nickel concentrations of about 45.68±4.92 ppb and 52.325±8.07 ppb respectively (Table 2.1). This is about 2% and 17% higher than the nominal amount. The dissolved nickel and total nickel concentrations in replicate tank 1 were 37.55 ± 0.67 ppb and 38.5 ± 0.8 ppb, respectively. The second replicate tank measured higher dissolved and total nickel concentration values of 57.45±2.3 ppb and 66.15±1.65 ppb, which is about 2X and 3X higher respectively than tank replicate 1. Pooled water samples from tank replicates 1 and 2 during the experiment had measured dissolved nickel concentration of 38.4 ppb. This value is closer to the mean of dissolved nickel concentration measured in water samples of tank replicate 1 collected after the experiment (Table 2.1).

Principal Component Analysis (PCA) plots (Appendix E, Figure E1 and E2) for mucus samples and blood plasma samples collected from fish belonging to different treatment groups show that fish belonging to the control treatments cluster well together, regardless of the tank replicate they belong to. Additionally, there is no clustering observed for the nickel treatment groups, and their respective tank replicates. For blood plasma samples, there is considerable variation within samples belonging to the control treatment, but these samples were not removed from analyses.

Overall, we observe a trend that one of the tank replicates have higher measured nickel concentrations compared to the other replicate for water samples collected after the experiment. Additionally, pooled water samples during the experiment from tank replicates 1 and 2 during the experiment have measured dissolved nickel concentrations that are more similar to the values of dissolved nickel in water samples collected from tank replicate 1 after the experiment.

3.2 Nickel burden in blood plasma of trout

Fish exposed to different experimental treatments were also measured for nickel burden in their blood plasma. Blood plasma was pooled among 5 fish to obtain a volume of 5mL in one vial, with 3 vials of blood plasma for each treatment replicate and a total of 6 vials within each treatment group. Figure 2.1 shows the nickel burden in the blood plasma of trout. The accumulation of nickel was the highest in the fish exposed to 45.7 ppb Ni treatment (mean ± st. error = 0.51 ± 0.05 µg/g), followed by the fish exposed to 4.9 ppb (0.13 ± 0.004 µg/g), control (0.076 ± 0.002 µg/g) and finally 1.5 ppb (0.075 ± 0.009 µg/g) (Table 2.3). The mean of nickel burden of fish exposed to 45.7 ppb of Ni was approximately x6.7, x6.8 and x3.9 fold the mean of the nickel accumulated in the fish exposed to control, 1.5 and 4.9 ppb Ni treatments. Statistical analysis revealed that treatment had a significant effect on the accumulation of Ni in blood plasma ($p=0.0003$, Kruskal-Wallis test). Multiple comparison using Dunn's multiple comparison revealed that Ni burden of fish exposed to the highest Ni treatment, 45.7 ppb, were significantly different from the Ni burden of fish exposed to control and 1.5 ppb of waterborne Ni (adjusted p-value<0.01).

3.3 Micronucleus assay

There were no micronuclei observed in the RBCs of rainbow trout exposed to the nickel treatments. Additionally, nuclear abnormalities were too rare to be mentioned (1-2 per 1000 RBCs per fish) and did not have a concentration-effect. Thus, the data was negligible for this measure and not presented.

3.4 Mucus proteomics

3.4.1 Main and interaction effects

Data-dependent acquisition using liquid chromatography high resolution tandem mass-spectrometry analysis (DDA LC-HR-MS/MS) was able to identify a total of 6934 proteins in the mucus proteome of fish. Proteins with missing values were removed, leaving a total of 5776 proteins before statistical analysis. Statistical analysis revealed that 51, 1552 and 206 proteins that were significant for nickel treatment effect, time effect and interaction effect respectively (FDR <0.05, Figure 3.1). All of the proteins significantly affected by nickel treatment were overlapped by the list of proteins affected by time and also partially with proteins with interaction effects of both time and nickel (Figure 3.1). 36 proteins significantly affected by nickel treatment were overlapped with proteins significantly affected by time and 15 with proteins significantly affected by the interaction effect. 170 proteins had significant interaction for both nickel and time effect.

A heatmap was plotted to visualize the abundance of the 51 proteins significant for nickel treatment effect (Figure 3.2.). Clusters represent groups of proteins demonstrating similar expression profiles on different days and nickel treatments. Abundances of all 51 proteins were relatively lower in the control group for all sampling days, i.e., day 0, 15 and 30, compared to their abundances in treatments containing nickel (Figure 3.2). Protein

abundances on day 0 for the nickel treatments were low in clusters 1 and 6 compared to their abundances on day 15 and day 30. Clusters 2 and 3 had lower protein abundances on day 15 in samples exposed to nickel, in comparison to their abundances on day 0 and day 30. Clusters 1 and 6 had relatively higher protein abundances on day 15 compared to day 0 for samples exposed to nickel, however, protein abundances in cluster 1 decreased again on day 30 to values similar to the controls on day 0 for samples exposed to nickel; whereas the protein abundances in cluster 6 remained high in all nickel treatments except 45.7 ppb on day 30 (Figure 3.2). Clusters 2,3,4 and 5 had higher protein abundances on day 30 in comparison to abundances on day 0 and 15 for samples exposed to nickel, except for the treatment containing 45.7 ppb.

Additionally, an over-representation analysis of the 51 proteins significantly affected by nickel treatment was conducted using CPDB, and revealed many biological networks that were significant ($p < 0.01$) (Figure 3.3(A-B); Appendix F, Tables F1 & F2). These included cell morphogenesis and neuron projection development, sensory perception of sound, interleukin-12 signaling, RAS and RAF signaling, JAK-STAT cascade, response to growth factor and chemical stimulus, smooth muscle cell proliferation, type II interferon signaling, pathways in clear cell carcinoma, retina vasculature development in camera-type eye and other signaling pathways (Figure 3.3 (A-B); Appendix F, Tables F1 & F2). Interleukin-12 pathways were the most significant observed.

3.4.2 Temporal changes in protein abundance

To understand the influence of time on protein abundance, pairwise comparisons between day 0 and day 15, and day 0 and day 30 for all 3 nickel treatments were conducted. Volcano plots represent the proteins significantly increasing and decreasing in abundance based on

a log2 fold-change of 1.5 ($p < 0.01$) (Appendix G, Figures G1 & G2). Venn diagrams were created to visualize the number of proteins shared between nickel treatments that either all increased or all decreased in abundance on day 15 and day 30 in comparison to control (Figure 3.4 (B,D), Figure 3.5 (B,D)).

For pairwise comparisons of protein abundances on day 0 vs day 15, a greater percentage of proteins decreased than increased in abundance in all treatments compared to the controls (Figure 3.4 (A)). In general, number of significant proteins that increased or decreased in treatment 45.7 ppb were lower than the other 2 nickel treatments (Figure 3.4 (A)).

A total of 52, 105, and 40 proteins increased in abundance in the 1.5, 4.9 and 45.7 ppb nickel treatments, respectively, on day 15 vs the controls (Figure 3.4 (B)). Only 5 proteins increased in abundance in all nickel treatments on day 15 compared to the controls on day 0 (Figure 3.4 (B)). GO enrichment analysis revealed that these proteins can be broadly classified into the following GO biological process categories; protein catabolic process, thyroid hormone metabolism, stem cell division and differentiation, and regulation of transcription in response to stress (p-value < 0.05, Figure 3.4 (C), Table 3.1). GO terms were manually selected based on uniqueness and p-value.

Similarly, a total of 206, 178 and 69 proteins decreased in abundance in the 1.5, 4.9 and 45.7 ppb nickel treatments, respectively, on day 15 vs the controls (Figure 3.4 (D)). From these, 26 proteins decreased in abundance in all nickel treatments on day 15 compared to day 0 (Figure 3.4 (D)). GO enrichment analysis revealed that these proteins can be broadly classified into the following GO biological process categories; regulation of transcription and chromatin assembly, actin cytoskeleton, RNA transport and localization, renal system

development, vesicle mediated transport and signaling, skeletal system morphogenesis, histidine biosynthetic process and glutamatergic neuron differentiation (p-value < 0.05, Figure 3.4 (E), Table 3.2).

Proteins abundances on day 0 vs day 30 revealed that approximately an equal amount of proteins increased and decreased in abundance for all nickel treatments (Figure 3.5 (A)). A total of 71, 150 and 56 proteins increased in abundance in all nickel treatments 1.5, 4.9 and 45.7 ppb, respectively, on day 30 vs their controls (Figure 3.5 (B)). The Venn diagram revealed that all nickel treatments shared 11 proteins in common that had increased in abundance on day 30 when compared to day 0 (Figure 3.5 (B)). A GO enrichment analysis revealed that these proteins can be broadly classified into the following GO biological process categories: Peptide and pentose metabolism, fatty-acid metabolism, DNA damage and telomere maintenance, protein catabolic processes, vesicle tethering involved in exocytosis, positive regulation of cellular senescence, negative regulation of cell growth involved in cardiac muscle cell development, nerve factor signaling pathway, erythrocyte maturation and thyroid hormone generation (p-value<0.05, Figure 3.5 (C), Table 3.3)

94, 119, and 62 proteins decreased in abundance in 1.5, 4.9 and 45.7 Ni ppb, respectively, on day 30 vs their controls (Figure 3.5 (D)). 15 of these proteins were decreased in abundance in all the 3 nickel treatments (Figure 3.5 (D)). GO enrichment analysis revealed that these proteins can be broadly classified into the following GO biological process categories: Endothelial cell migration, sensory and nervous system development, renal system development, positive regulation of cytokine activity and negative regulation of hepatic stellate cell activation (p-value < 0.05, Figure 3.5 (E), Table 3.4).

3.5 Blood plasma proteomics

Unlike skin mucus, blood plasma of the rainbow trout was only sampled on the last day of the exposures. Therefore, only the impact of nickel treatment, and not time, could be tested for proteomics. We identified a total of 2840 proteins in the blood plasma proteome of fish. Proteins with missing values were removed, leaving a total of 2705 proteins before statistical analysis. Statistical analysis revealed 1240 proteins that were significant for nickel treatment effect (FDR <0.05).

A heatmap was created to visualize the abundance of the 1240 plasma proteins significantly affected by nickel treatment in the blood plasma of trout (Figure 3.6 (A)). There were 5 clusters formed based on the expression profiles of the abundance of proteins in all 4 treatments. Clusters 1, 2 and 3 formed the largest clusters, whereas clusters 4 and 5 had much fewer proteins. The proteins in cluster 1 had low abundances in all treatments except the highest nickel treatment, i.e. 45.7 ppb. In cluster 2, protein abundances were highest in the controls, with a big dip in abundance in treatment 1.5 ppb of nickel, and then a slight increase in abundances in the 4.9 and 45.7 ppb of nickel treatments. Cluster 3 had highest protein abundances in the control and 4.9 ppb nickel treatment, with protein abundances in treatment 45.7 ppb being the lowest among them all (Figure 3.6 (A)). Additionally, a subset of the proteins of interest were used to create a separate heatmap with their abundance (Figure 3.6 (B)). This allows a closer look at the concentration-dependent response of the protein abundances when subject to different nickel treatments.

An over-representation analysis of the 1240 plasma proteins significantly affected by nickel treatment was conducted using CPDB, and revealed many biological networks that were significant ($p < 0.01$) (Figure 3.7 (A-C); Appendix F, Tables F3 & F4). These

networks included vesicle mediated transport, cell projection and cilium assembly, interleukin signaling, cell migration, kidney development, nucleotide metabolism, striated muscle contraction, extracellular matrix organization, lipid and ion transport, apoptosis, Rho GTPases and RAS signaling, peptide transport, organelle and actin cytoskeleton organization, neuron projection development, eye development, phosphatidylinositol metabolism, and sensory processing of sound (Figure 3.7 (A-C). Of these networks, neuron projection development was the most significant, followed by cell projection and cilium assembly, Rho GTPase and RAS signaling, and extracellular matrix organization.

Pairwise comparisons of protein abundances between nickel treatments and controls were conducted to obtain protein lists that were increasing and decreasing in abundances. Volcano plots represent the proteins significantly increasing and decreasing in abundance based on a log2 fold-change of 2 (FDR<0.05, Appendix G, Figure G3) The proportion of proteins that increased and decreased in abundance in the nickel treatments compared to the control treatment were relatively equal in number (Figure 3.8 (A)). 680, 515 and 660 proteins increased in abundance in the 1.5, 4.9 and 45.7 ppb nickel treatments in comparison to the control treatment (Figure 3.8 (B)). From these proteins, 403 proteins increased in abundance in all nickel treatments (Figure 3.8 (B)). A GO enrichment analysis using an online tool Enrich R (Xie et al., 2021) revealed that these 403 proteins can be broadly classified into the following GO biological process categories: phosphatidylinositol-mediated signaling, nervous system organization and signaling, histone H3-K9 demethylation, glycolysis, protein localization and transport, regulation of angiogenesis, and apoptotic mitochondrial changes ($p<0.05$, Figure 3.8 (C), Table 3.5).

Similarly, 597, 503 and 547 proteins decreased in abundance in the 1.5, 4.9 and 45.7 ppb nickel treatments, respectively, in comparison to the control (Figure 3.8 (D)). 364 proteins were commonly decreased in abundance in all nickel treatments (Figure 3.8 (D)). GO enrichment analysis using an online tool Enrich R (Xie et al., 2021) revealed that these 364 proteins can be broadly classified into the following GO biological process categories: Renal system development, actin cytoskeleton depolymerization, phospholipid transport, neuron differentiation and development, MAPK signaling, wound healing, spreading of cells, spliceosomal tri-snRNP complex assembly, plasma membrane bounded cell projection organization and cellular response to growth factor stimulus (p-value < 0.05, Figure 3.8 (E), Table 3.6).

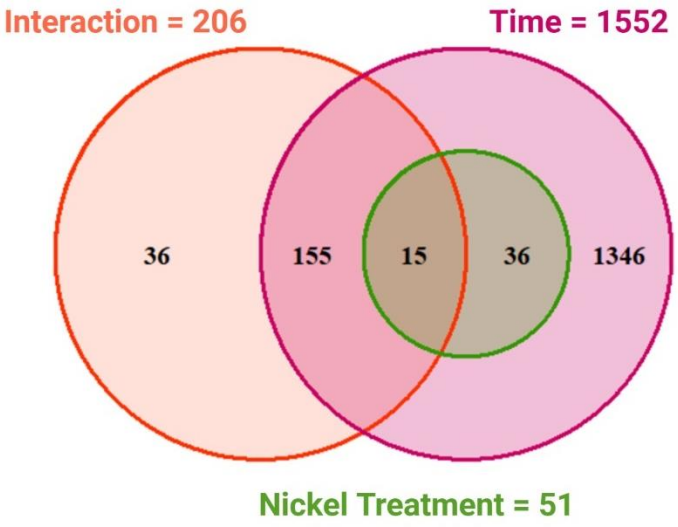

Figure 3.1. ***Limma*** **model summary of main and interaction effects in the mucus proteome following exposure of rainbow trout to nickel**. The model had 2 factors, nickel treatment and time**.** Main effect of nickel treatment impacted the abundance of 51 proteins, main effect of time affected the abundance of 1552 proteins, and the interaction effect of nickel treatment and time together impacted the abundance of 206 proteins in the epidermal mucus proteome of rainbow trout. Time had the strongest effect on the abundance of proteins. A Benjamini-Hochberg value or FDR value of 0.05 was selected to obtain protein lists. Statistical analysis was conducted on R using the *limma* package.

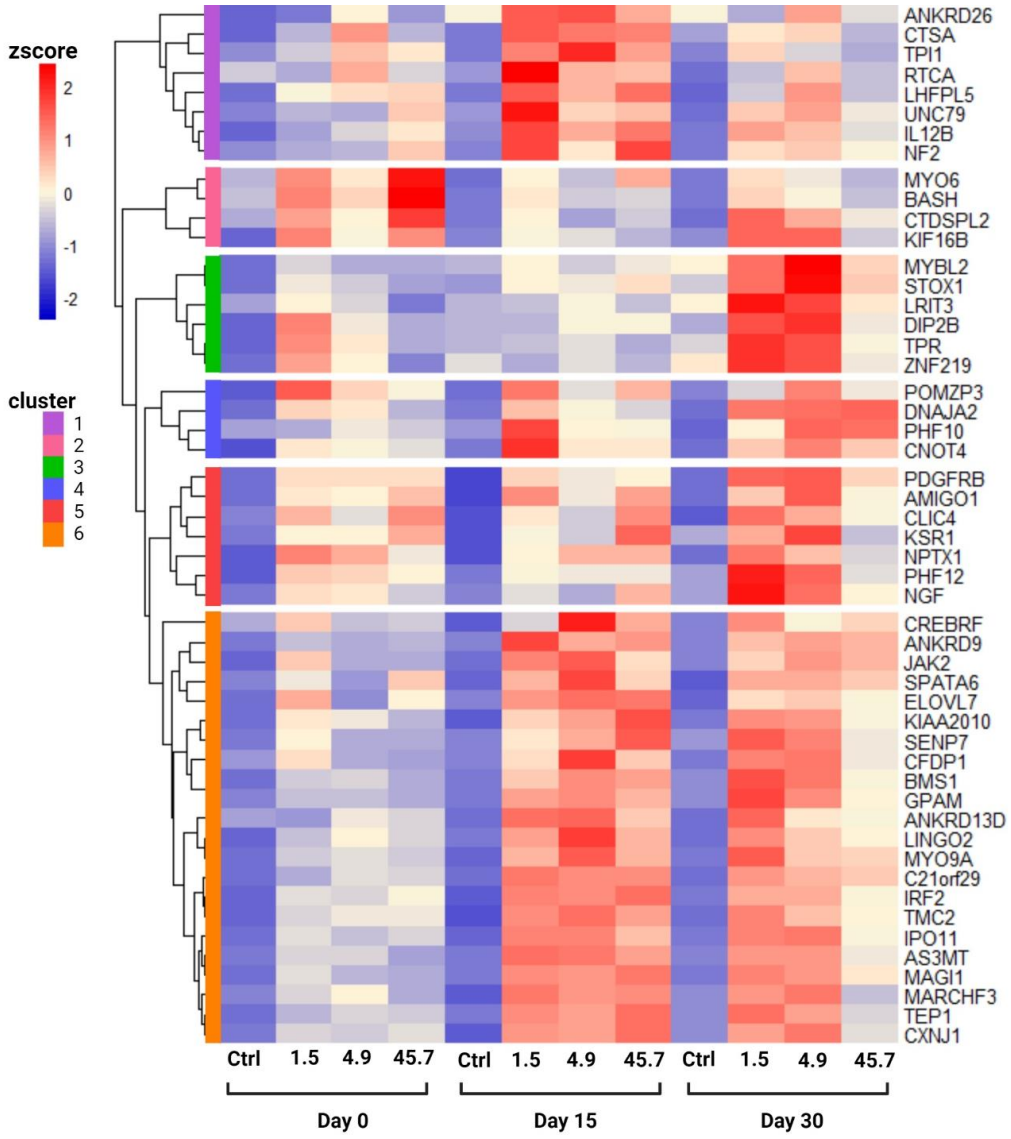

<u>Figure 3.2.</u> Heatmap of the abundance of the proteins significantly affected by nickel treatment in the mucus proteome of rainbow trout. 51 proteins were affected by nickel treatment (main effect of treatment) using *limma* analysis (FDR < 0.05). Abundances are represented by z-scores (standard scaling), while the clustered rows represent the different expression profiles among the 51 proteins; clusters were obtained using Euclidean distance calculation in the 'pheatmap' function. Each column is labelled by first the nickel treatment (ppb), and then the day the mucus was collected

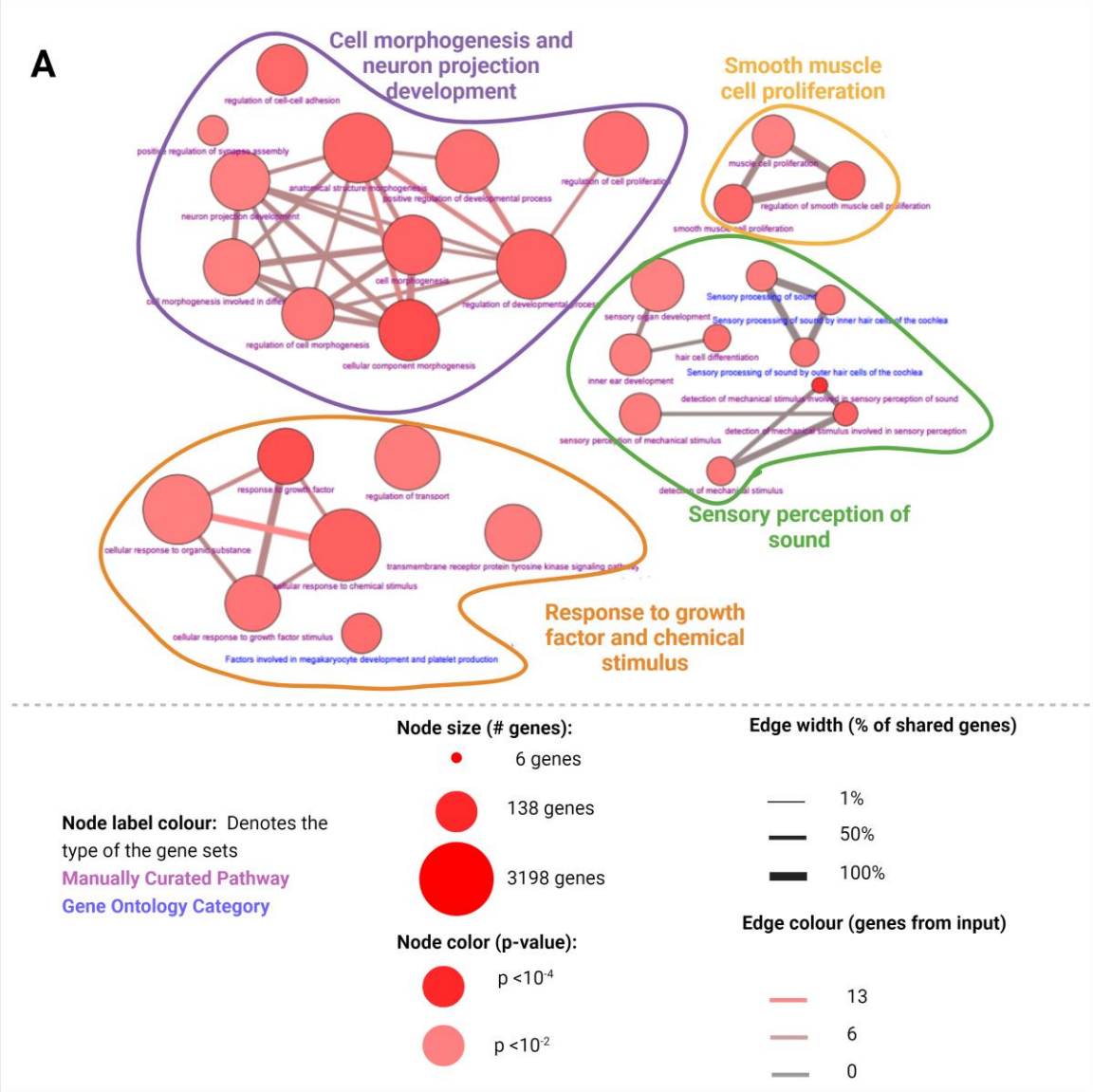

Figure 3.3 (A) – description below

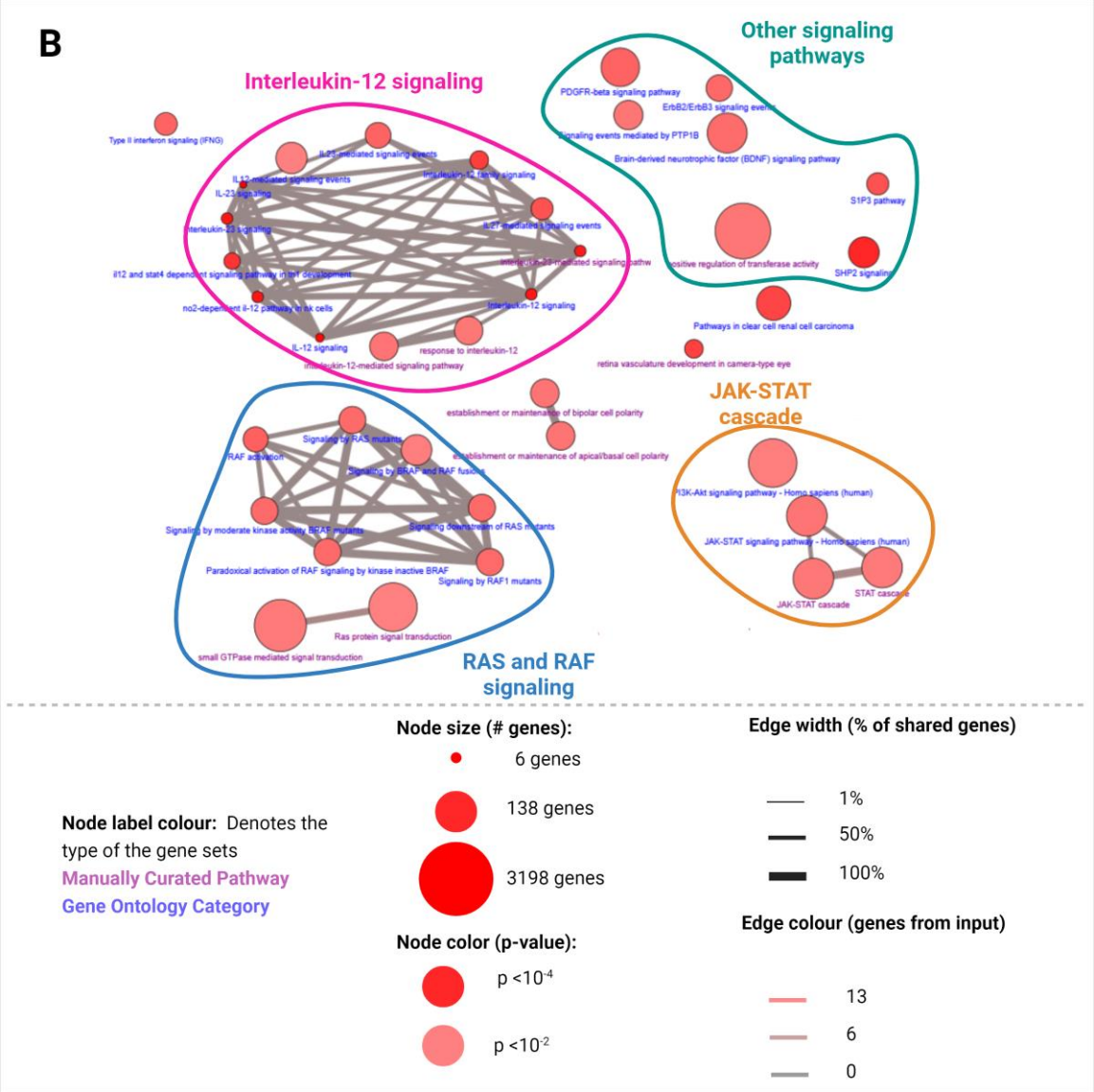

Figure 3.3 (B) – description below

Figure 3.3 (A-B): Network of over-represented biological pathways and processes in the mucus proteome of rainbow trout affected by nickel treatment. The list of 51 proteins significantly affected by nickel treatment were searched against the Consensus Pathway database (CPDB) to find over-represented pathways from different databases as well as gene ontology (GO) biological processes involved in response to nickel exposure ($p < 0.01$). Each node represents a pathway/process, where the greater the intensity of red, more significant the process and the larger nodes represent processes with larger gene sets. The nodes are connected with edges, where the width of the edge represents the percentage of shared genes between the nodes, and the intensity of the edge color represents the proteins shared between the nodes from the input list. A relative minimum overlap filter of 40% was applied to the edges. A background protein list was not used

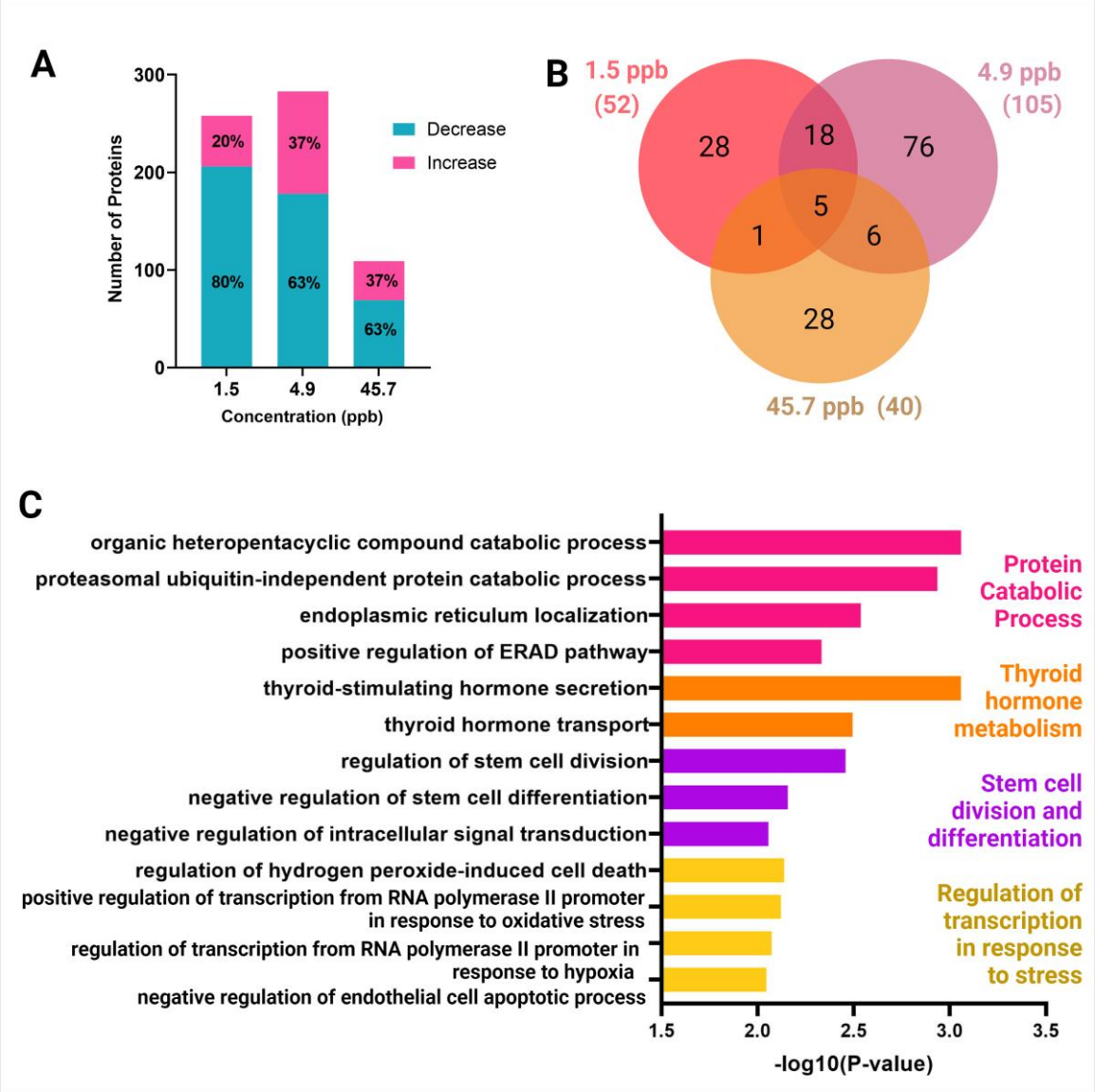

Figure 3.4 (A, B, C) - description below

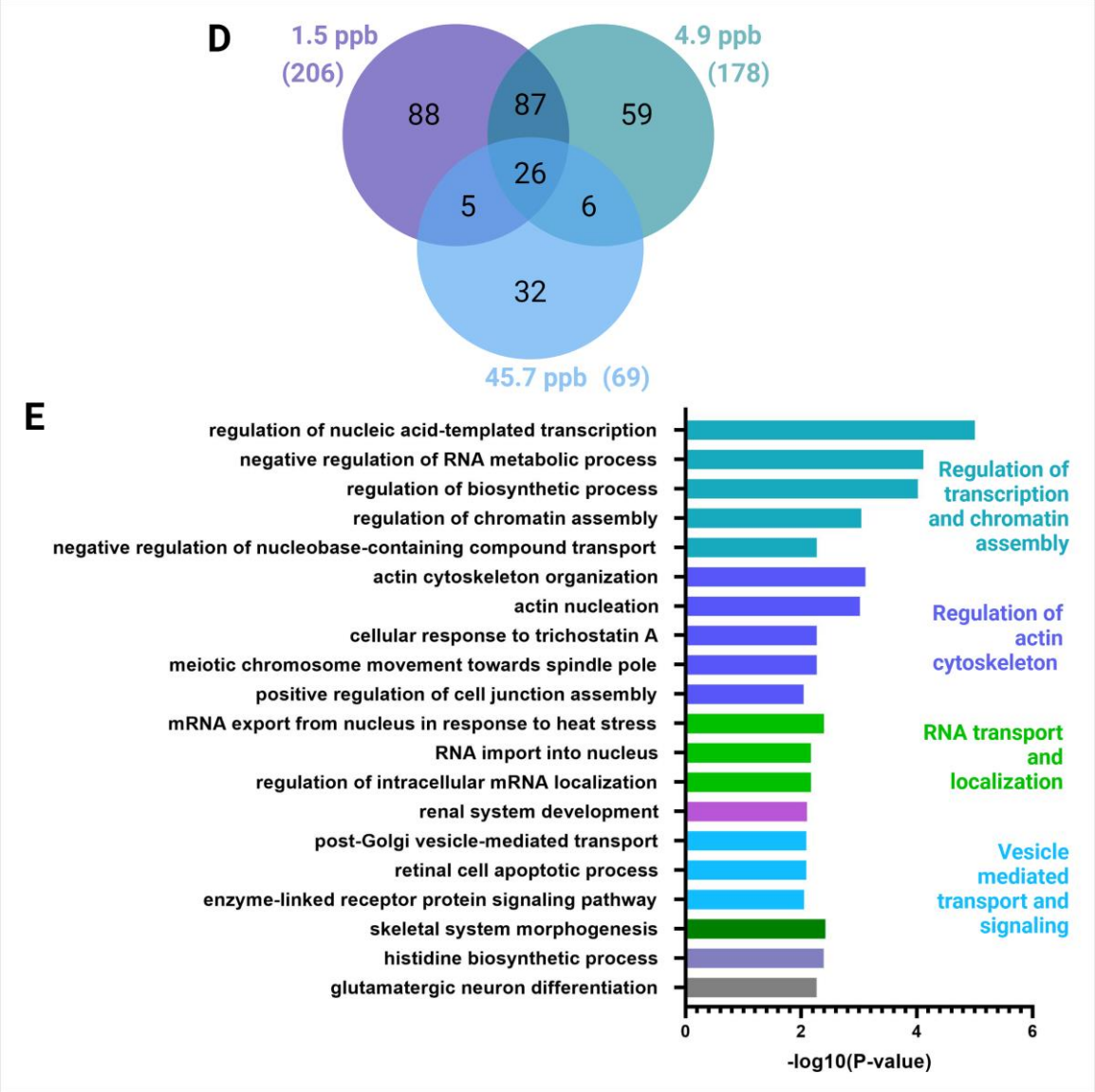

Figure 3.4 (D, E) – description below

Figure 3.4. GO enrichment analysis of the mucus proteins increasing and decreasing in abundance in rainbow trout exposed to nickel on day 15 compared to control. (A) Bar plot representing the number and percentage of proteins increasing or decreasing in abundance on day 15 in the 3 nickel treatments in comparison to the control (pairwise comparisons, $p < 0.01$) , **(B)** Venn diagram of number of proteins increasing in abundance on day 15 in the 3 nickel treatments in comparison to their controls (pairwise comparisons, $p < 0.01$), **(C)** GO enrichment analysis displaying the top biological processes of the 5 proteins that are increasing in abundance in all nickel treatments on day 15 in comparison to their controls on day 0 (GO terms manually selected based on uniqueness and p-value < 0.05), **(D)** Venn diagram of number of proteins decreasing in abundance on day 15 in all the 3 nickel treatments in comparison to their controls (pairwise comparisons, $p < 0.01$), **(E)** GO enrichment analysis displaying the top biological processes of the 26 proteins decreasing in abundance in all nickel treatments on day 15 in comparison to their controls on day 0 (GO terms manually selected based on uniqueness and p-value < 0.05).

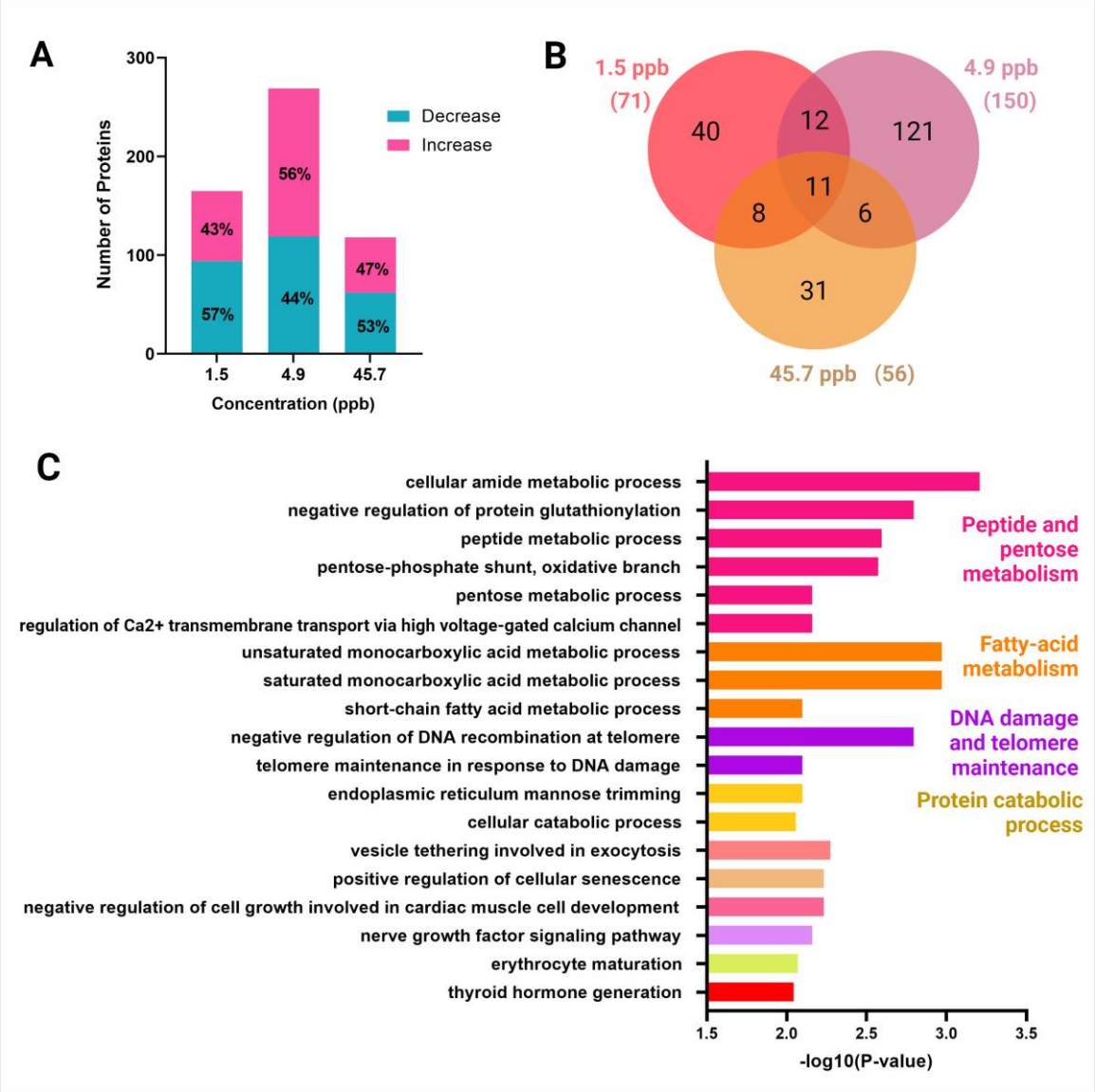

Figure 3.5 (A, B, C) – description below

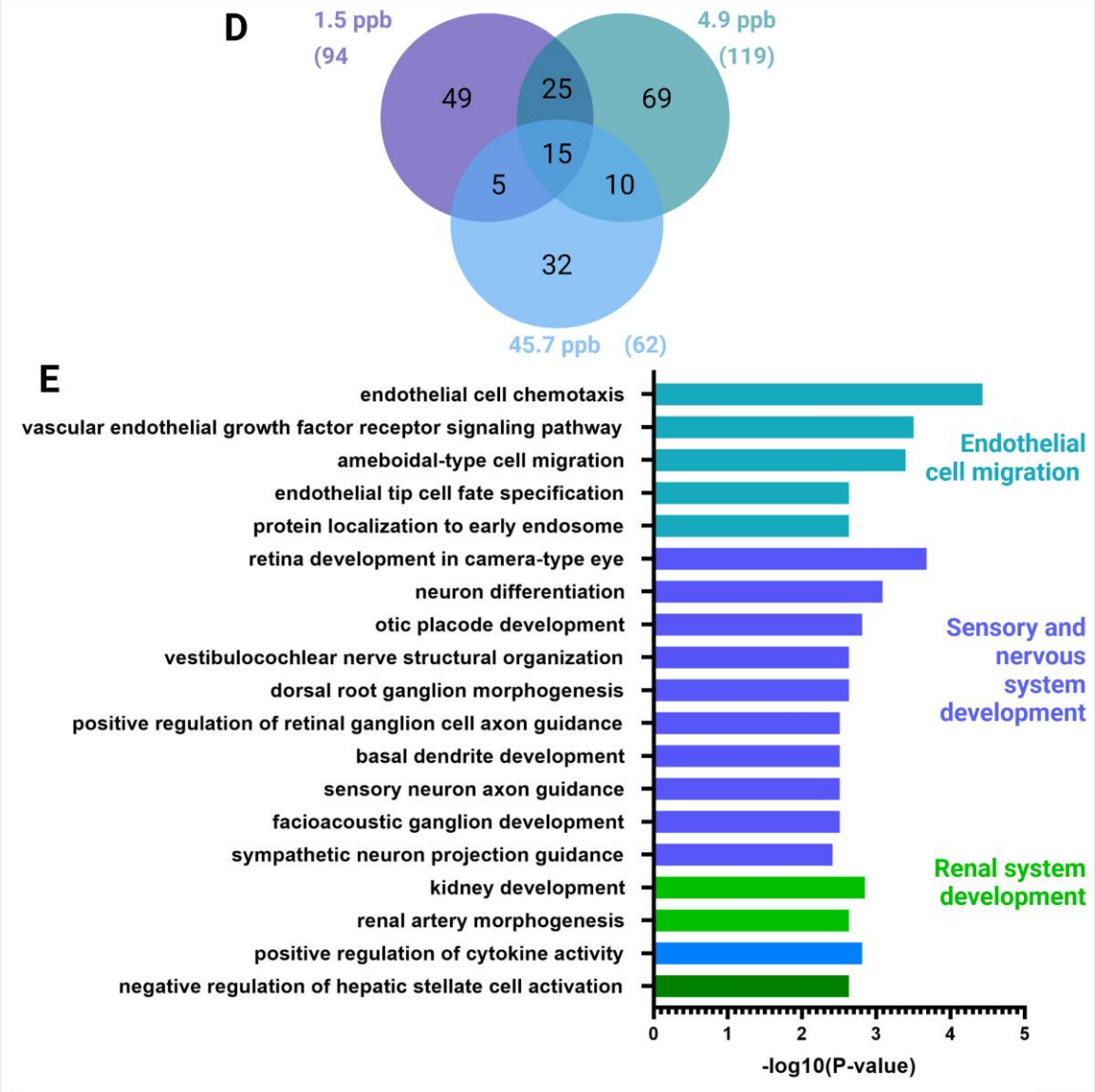

Figure 3.5 (D, E) – description below

<u>Figure 3.5.</u> GO enrichment analysis of the mucus proteins increasing and decreasing in abundance in rainbow trout exposed to nickel on day 30 compared to control. (A) Bar plot representing the number and percentage of proteins increasing or decreasing in abundance on day 30 in the 3 nickel treatments in comparison to the control (pairwise comparisons, $p < 0.01$), **(B)** Venn diagram of number of proteins increasing in abundance on day 30 in the 3 nickel treatments in comparison to their controls, **(C)** GO enrichment analysis displaying the top biological processes of the 11 proteins that are increasing in abundance in all nickel treatments on day 30 in comparison to their controls on day 0 (GO terms manually selected based on uniqueness and p-value < 0.05), **(D)** Venn diagram of number of proteins decreasing in abundance on day 30 in all the 3 nickel treatments in comparison to their controls (pairwise comparisons, $p < 0.01$), **(E)** GO enrichment analysis displaying the top biological processes of the 15 proteins decreasing in abundance in all nickel treatments on day 30 in comparison to their controls on day 0 (GO terms manually selected based on uniqueness and p-value < 0.05).

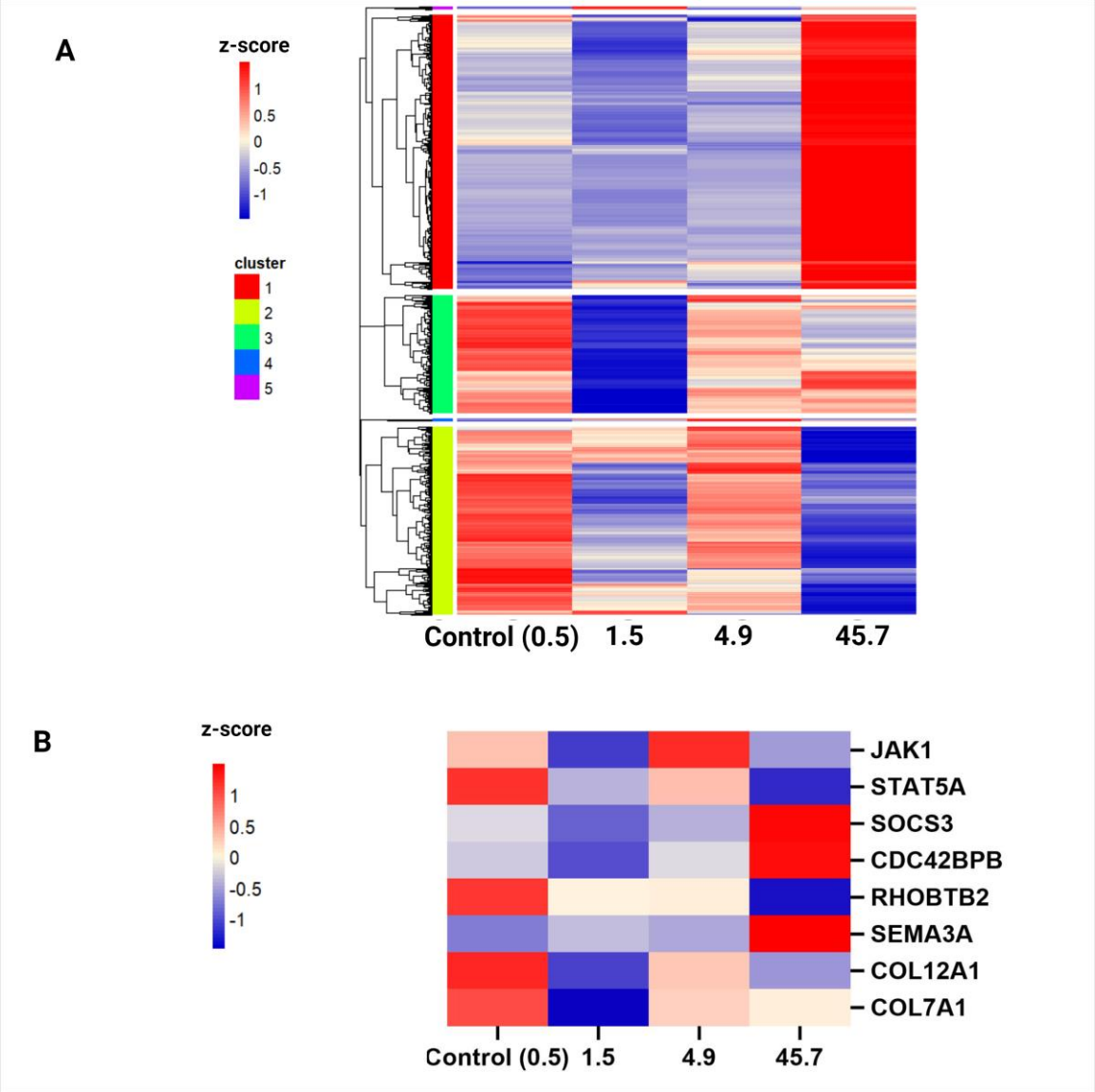

Figure 3.6. Heatmap of the abundance of plasma proteins significantly affected by nickel treatment in rainbow trout. (A) 1240 proteins were significantly affected by nickel treatment in blood plasma using *limma* analysis (FDR < 0.05) Abundances are represented by z-scores, while the clustered rows represent the different expression profiles of the proteins; clusters were obtained using Euclidean distance calculation in the 'pheatmap' function. Each column is labelled by the nickel treatment (ppb), **(B)** Subset of heatmap A showing the abundances of proteins of interest. Abundances are represented by z-scores and each column is labelled by the nickel treatment (ppb).

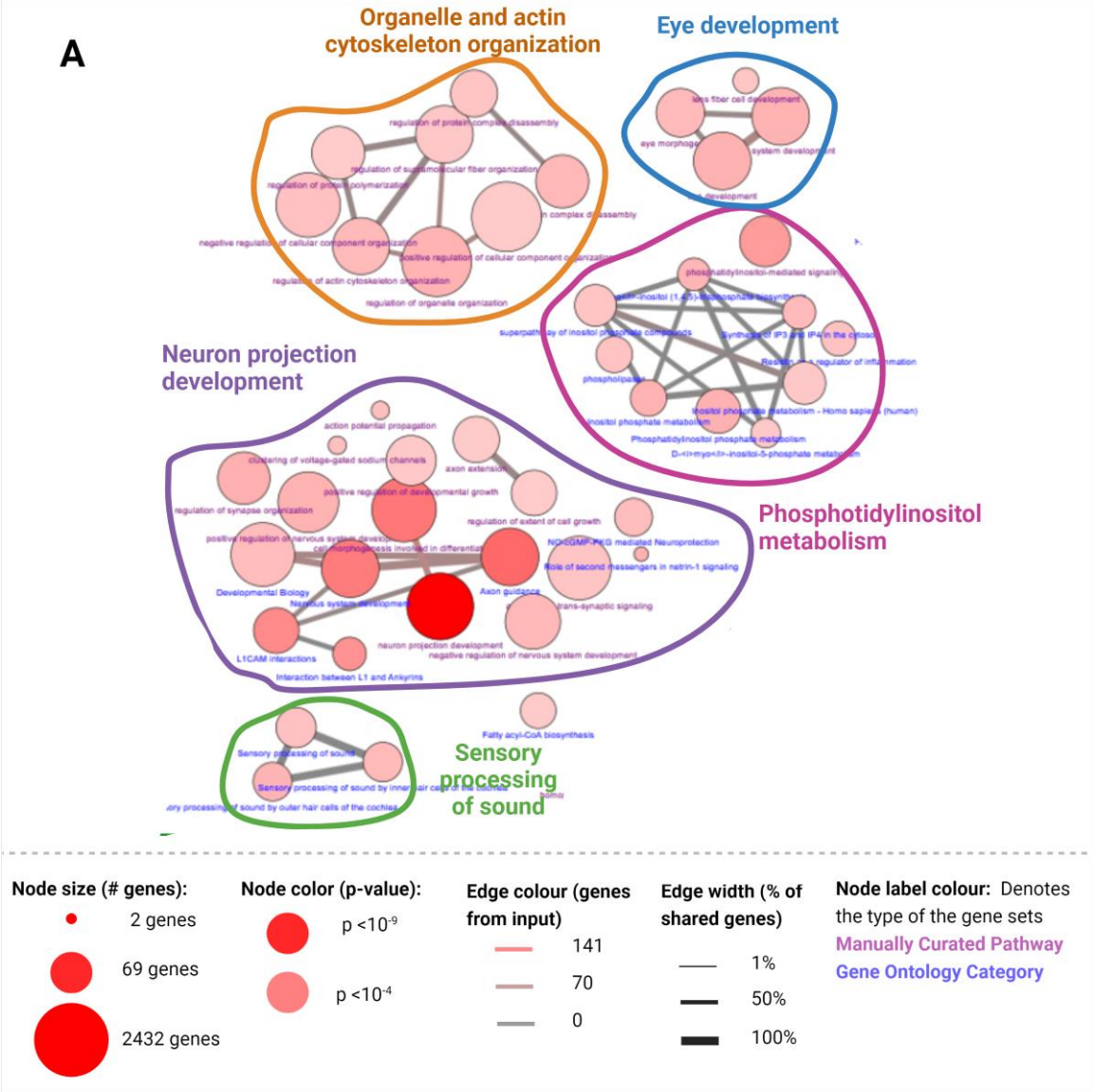

Figure 3.7 (A) – description below

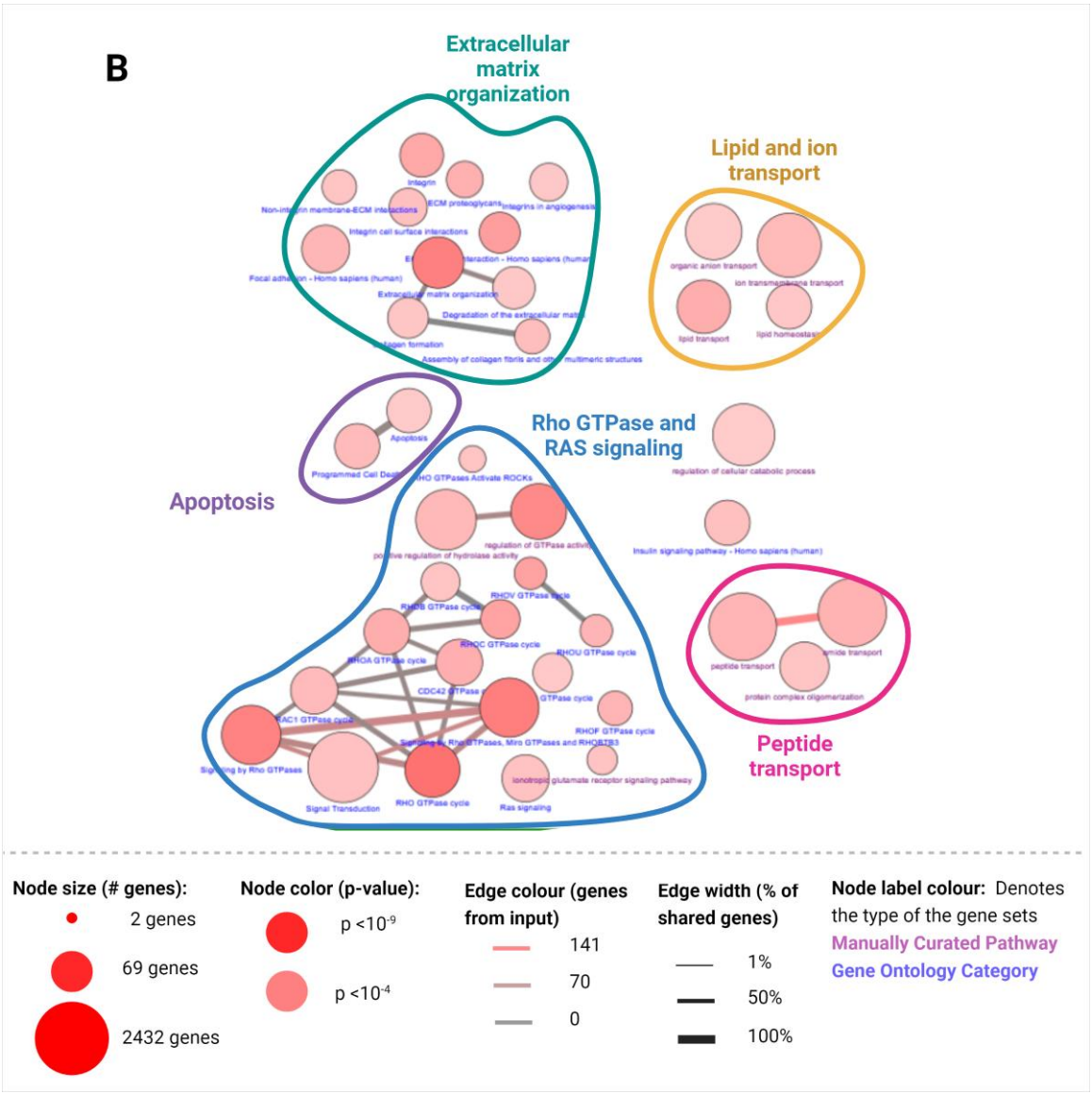

Figure 3.7 (B) – description below

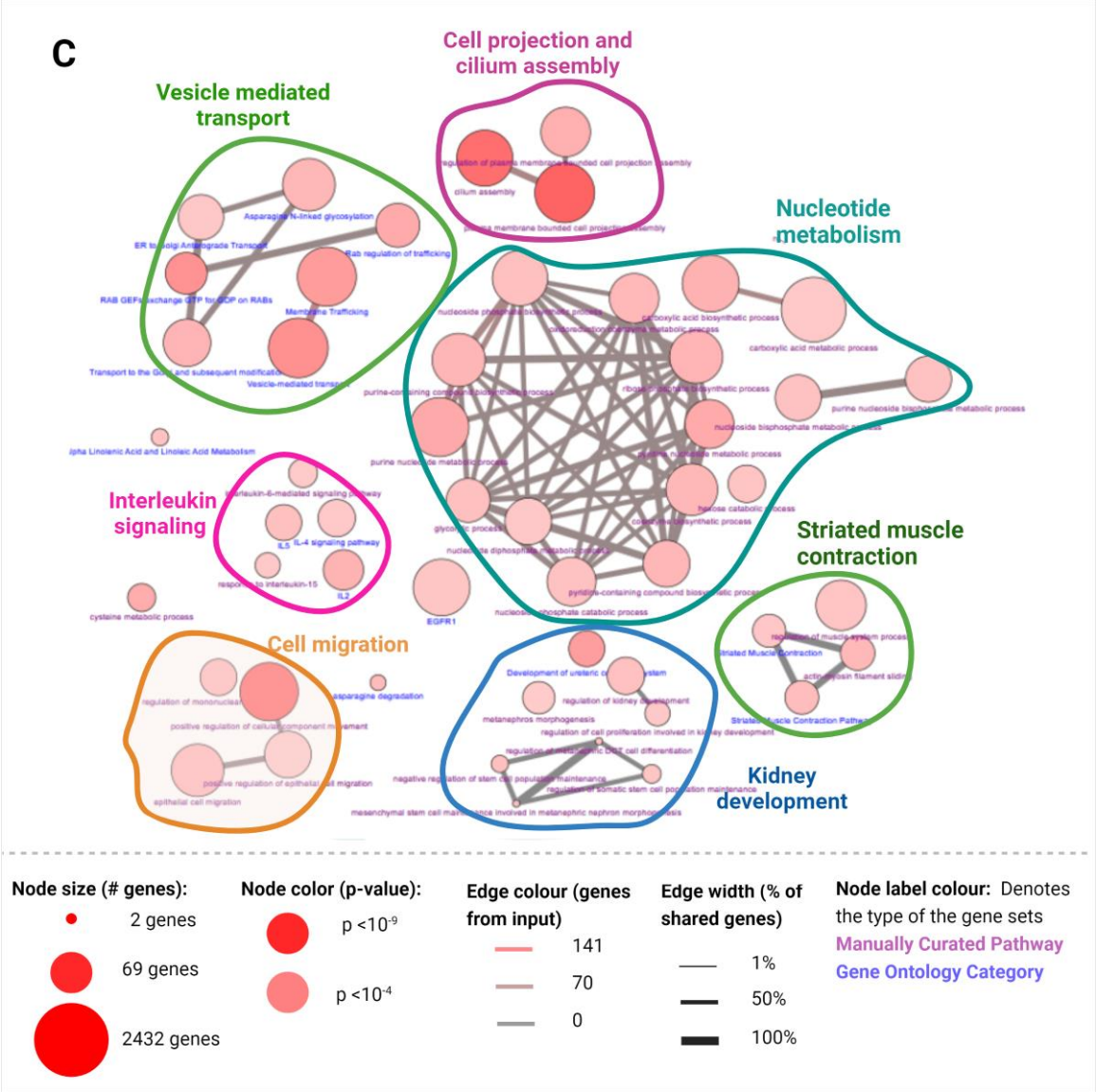

Figure 3.7 (C) – description below

Figure 3.7 (A-C). Network of over-represented biological pathways and processes in the blood plasma proteome of rainbow trout affected by nickel treatment. The list of 1240 proteins significantly affected by nickel treatment were searched against the Consensus Pathway database (CPDB) to find over-represented pathways from different databases as well as gene ontology (GO) biological processes involved in response to nickel exposure ($p < 0.01$). Each node represents a pathway/process, where the greater the intensity of red, more significant the process and the larger nodes represent processes with larger gene sets. The nodes are connected with edges, where the width of the edge represents the percentage of shared genes between the nodes, and the intensity of the edge color represents the proteins shared between the nodes from the input list. A relative minimum overlap filter of 50% was applied to the edges. A background protein list was not used

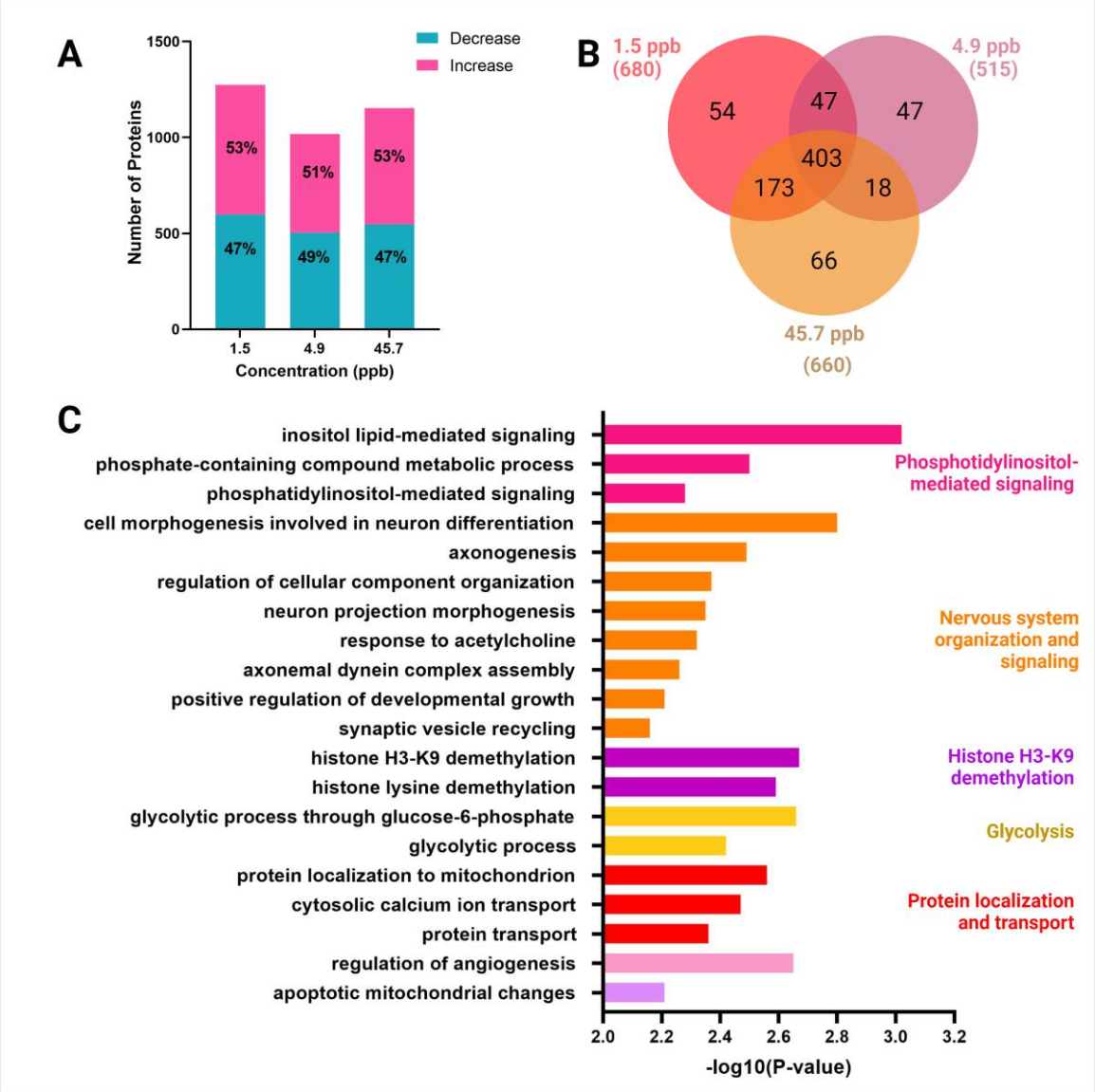

Figure 3.8 (A, B, C) – description below

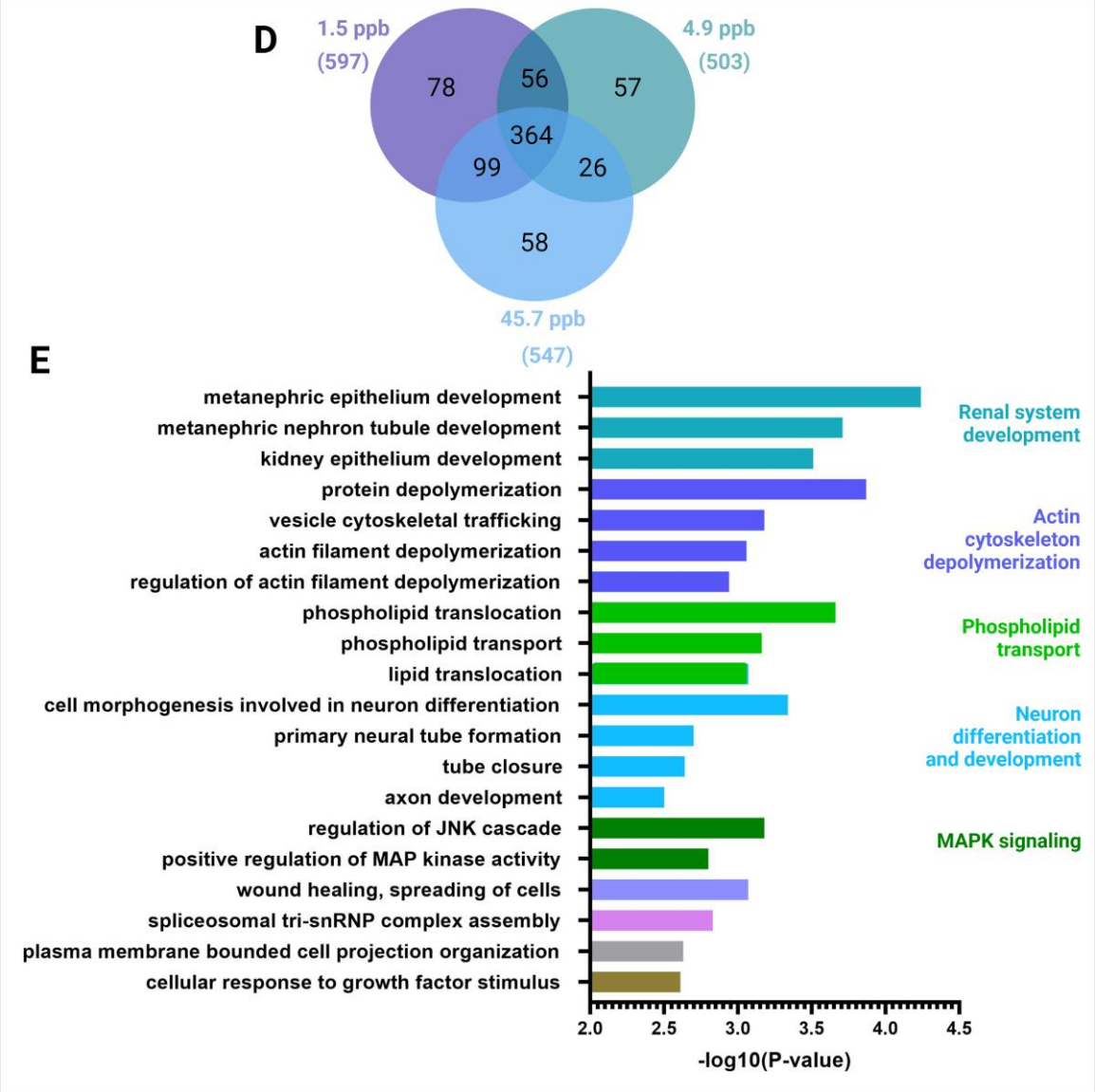

Figure 3.8 (D, E) – description below

Figure 3.8. GO enrichment analysis of the plasma proteins increasing and decreasing in abundance in rainbow trout exposed to nickel. (A) Bar plot representing the number and percentage of proteins increasing or decreasing in abundance in the 3 nickel treatments in comparison to the control treatment (pairwise comparisons, $p < 0.01$), **(B)** Venn diagram of number of proteins increasing in abundance in the 3 nickel treatments in comparison to the control treatment, **(C)** GO enrichment analysis using Enrich R displaying the top biological processes of the 403 proteins that are increasing in abundance in all nickel treatments in comparison to the control treatment (p-value < 0.05), **(D)** Venn diagram of number of proteins decreasing in abundance in all the 3 nickel treatments in comparison to the control treatment (pairwise comparisons, $p < 0.01$), **(E)** GO enrichment analysis using Enrich R displaying the top biological processes of the 364 proteins decreasing in abundance in all nickel treatments in comparison to the control treatment (p-value < 0.05).

Table 3.1. Top GO terms of biological processes of proteins increasing in abundance on day 15 in the mucus proteome of rainbow trout exposed to nickel. GO enrichment results of the top biological processes of the 5 proteins increasing in abundance in all nickel treatments on day 15 in comparison to their controls on day 0. Proteins were searched against the reference list of *Homo sapiens* using a Fisher's exact test, with no correction. GO terms were manually selected based on uniqueness and p-value.

GO Term ID	GO Term	Proteins from Input List	Fold-Enrichment	P-value
GO:1901377	organic heteropentacyclic compound catabolic process	Hebp1	> 100	8.74E-04
GO:0010499	proteasomal ubiquitin-independent protein catabolic process	Hebp1	> 100	1.16E-03
GO:0051643	endoplasmic reticulum localization	Esyt2	> 100	2.91E-03
GO:1904294	positive regulation of ERAD pathway	Hebp1	> 100	4.65E-03
GO:0070460	thyroid-stimulating hormone secretion	Slc16a2	> 100	8.74E-04
GO:0070327	thyroid hormone transport	Slc16a2	> 100	3.20E-03
GO:2000035	regulation of stem cell division	Prdm15	> 100	3.49E-03
GO:2000737	negative regulation of stem cell differentiation	Hebp1	> 100	6.97E-03
GO:1902532	negative regulation of intracellular signal transduction	Hebp1, Prdm15	13.35	8.79E-03

GO:1903205	regulation of hydrogen peroxide-induced cell death	Hebp1	> 100	7.26E-03
GO:1901522	positive regulation of transcription from RNA polymerase II promoter in response to oxidative stress	Hebp1	> 100	7.55E-03
GO:0061418	regulation of transcription from RNA polymerase II promoter in response to hypoxia	Hebp1	> 100	8.42E-03
GO:2000352	negative regulation of endothelial cell apoptotic process	Hebp1	> 100	9.00E-03

Table 3.2. Top GO terms of biological processes of proteins decreasing in abundance on day 15 in the mucus proteome of rainbow trout exposed to nickel. GO enrichment results of the top biological processes of the 26 proteins decreasing in abundance in all nickel treatments on day 15 in comparison to their controls on day 0. Proteins were searched against the reference list of *Homo sapiens* using a Fisher's exact test, with no correction. GO terms were manually selected based on uniqueness and p-value.

GO Term ID	GO Term	Proteins from Input List	Fold-Enrichment	P-value
GO:1903506	regulation of nucleic acid-templated transcription	Zhx2, Hnrnpab, Mphosph8, Tpr, Actr2, Magee1, Arid5b, Atp1b4, Mybl2, Znf234, Phf12, Gdf6, Trappc9	3.19	9.87E-06
GO:0051253	negative regulation of RNA metabolic process	Zhx2, Hnrnpab, Mphosph8, Tpr, Magee1, Arid5b, Arid5b	4.64	7.72E-05
GO:0009889	regulation of biosynthetic process	Zhx2, Hnrnpab, Mphosph8, Tpr, Actr2, Magee1, Arid5b, Atp1b4, Mybl2, Mybl2, Phf12, Gdf6, Trappc9	2.65	9.50E-05
GO:0010847	regulation of chromatin assembly	Mphosph8, Tpr	47.44	9.15E-04
GO:0032240	negative regulation of nucleobase-containing compound transport	Zhx2, Hnrnpab, Mphosph8, Tpr,Magee1, Arid5b, Phf12	> 100	5.42E-03
GO:0030036	actin cytoskeleton organization	Gdpd2, Actr2, Sptbn1, Sptbn1, Sptbn1	6.76	7.78E-04

GO:0045010	actin nucleation	Fmn1	45.96	9.71E-04
GO:0035984	cellular response to trichostatin A	Actr2	> 100	5.42E-03
GO:0016344	meiotic chromosome movement towards spindle pole	Actr2	> 100	5.42E-03
GO:1901890	positive regulation of cell junction assembly	Nphp4, Fmn1	14.14	9.07E-03
GO:0031990	mRNA export from nucleus in response to heat stress	Tpr	> 100	4.07E-03
GO:0006404	RNA import into nucleus	Tpr	> 100	6.77E-03
GO:1904580	regulation of intracellular mRNA localization	Hnrnpab	> 100	6.77E-03
GO:0072001	renal system development	Arid5b, Gdf6, Fmn1	7.33	7.92E-03
GO:0006892	post-Golgi vesicle-mediated transport	Kif16b, Sptbn1	15.01	8.11E-03
GO:1990009	retinal cell apoptotic process	Gdf6	> 100	8.12E-03
GO:0007167	enzyme-linked receptor protein signaling pathway	Kif16b, Sptbn1, Arid5b, Gdf6	4.84	8.94E-03
GO:0048705	skeletal system morphogenesis	Mthfd1, Arid5b, Fmn1	9.59	3.79E-03
GO:0000105	histidine biosynthetic process	Mthfd1	> 100	4.07E-03
GO:1905962	glutamatergic neuron differentiation	Zhx2	> 100	5.42E-03

Table 3.3. Top GO terms of biological processes of proteins increasing in abundance on day 30 in the mucus proteome of rainbow trout exposed to nickel. GO enrichment results of the top biological processes of the 11 proteins increasing in abundance in all nickel treatments on day 30 in comparison to their controls on day 0. Proteins were searched against the reference list of *Homo sapiens* using a Fisher's exact test, with no correction. GO terms were manually selected based on uniqueness and p-value

GO Term ID	GO Term	Proteins from Input List	Fold-Enrichment	P-value
GO:0043603	cellular amide metabolic process	Acot4, Cpq, G6pd, Eef1e1	9.32	6.19E-04
GO:0010734	negative regulation of protein glutathionylation	G6pd	> 100	1.60E-03
GO:0006518	peptide metabolic process	G6pd,Cpq, Eef1e1	10.44	2.54E-03
GO:0009051	pentose-phosphate shunt, oxidative branch	G6pd	> 100	2.67E-03
GO:0019321	pentose metabolic process	G6pd	> 100	6.92E-03
GO:1902514	regulation of calcium ion transmembrane transport via high voltage-gated calcium channel	G6pd	> 100	6.92E-03
GO:0032789	unsaturated monocarboxylic acid metabolic process	Acot4	> 100	1.07E-03
GO:0032788	saturated monocarboxylic acid metabolic process	Acot4	> 100	1.07E-03
GO:0046459	Short-Chain Fatty Acid Metabolic Process	Acot4	> 100	7.98E-03

GO:0048239	negative regulation of DNA recombination at telomere	Terf2ip	> 100	1.60E-03
GO:0043247	telomere maintenance in response to DNA damage	Terf2ip	> 100	7.98E-03
GO:1904380	endoplasmic reticulum mannose trimming	Marchf6	> 100	7.98E-03
GO:0044248	cellular catabolic process	Marchf6, Ppp2r5c, Acot4, Cpq	4.52	8.78E-03
GO:0090522	vesicle tethering involved in exocytosis	Exoc1	> 100	5.33E-03
GO:2000774	positive regulation of cellular senescence	Eef1e1	> 100	5.86E-03
GO:0061052	negative regulation of cell growth involved in cardiac muscle cell development	G6pd	> 100	5.86E-03
GO:0038180	nerve growth factor signaling pathway	Kidins220	> 100	6.92E-03
GO:0043249	erythrocyte maturation	Acot4	> 100	8.51E-03
GO:0006590	thyroid hormone generation	Cpq	> 100	9.04E-03

Table 3.4. Top GO terms of biological processes of proteins decreasing in abundance on day 30 in the mucus proteome of rainbow trout exposed to nickel. GO enrichment results of the top biological processes of the 15 proteins decreasing in abundance in all nickel treatments on day 30 in comparison to their controls on day 0. Proteins were searched against the reference list of *Homo sapiens* using a Fisher's exact test, with no correction. GO terms were manually selected based on uniqueness and p-value.

GO Term ID	GO Term	Proteins from Input List	Fold-Enrichment	P-value
GO:0035767	endothelial cell chemotaxis	Nrp1	> 100	3.71E-05
GO:0048010	vascular endothelial growth factor receptor signaling pathway	Nrp1	80.43	3.13E-04
GO:0001667	ameboidal-type cell migration	Arid5b, Nrp1	20.53	4.02E-04
GO:0097102	endothelial tip cell fate specification	Nrp1	> 100	2.33E-03
GO:1902946	protein localization to early endosome	Nrp1	> 100	2.33E-03
GO:0060041	retina development in camera-type eye	Zhx2, Nrp1, Nphp4	25.74	2.09E-04
GO:0030182	neuron differentiation	Zhx2, Nrp1, Nphp4, Trappc9	6.32	8.24E-04
GO:1905040	otic placode development	Nrp1	> 100	1.55E-03
GO:0021649	vestibulocochlear nerve structural organization	Nrp1	> 100	2.33E-03
GO:1904835	dorsal root ganglion morphogenesis	Nrp1	> 100	2.33E-03
GO:1902336	positive regulation of retinal ganglion cell axon guidance	Nrp1	> 100	3.10E-03

GO:0150018	basal dendrite development	Nrp1	> 100	3.10E-03
GO:0097374	sensory neuron axon guidance	Nrp1	> 100	3.10E-03
GO:1903375	facioacoustic ganglion development	Nrp1	> 100	3.10E-03
GO:0097491	sympathetic neuron projection guidance	Nrp1	> 100	3.88E-03
GO:0001822	kidney development	Arid5b, Nrp1, Gdf6	13.22	1.42E-03
GO:0061441	renal artery morphogenesis	Nrp1	> 100	2.33E-03
GO:0060301	positive regulation of cytokine activity	Nrp1	> 100	1.55E-03
GO:2000490	negative regulation of hepatic stellate cell activation	Cygb	> 100	2.33E-03

Table 3.5. Top 20 GO terms of biological processes of proteins increasing in abundance in the blood plasma proteome of rainbow trout exposed to nickel. GO enrichment results of the top biological processes of the 403 proteins increasing in abundance in all nickel treatments in comparison to the control treatment were performed using Enrich R (Xie et al., 2021). The list shows the top 20 GO terms were selected based on their p-value.

GO Term ID	GO Term	Proteins From Input List	P-value
GO:0048017	inositol lipid-mediated signaling	Pitpnm2;Plce1;Plcb1;Plcd3;Plcd4;Muc5ac	9.59E-04
GO:0006796	phosphate-containing compound metabolic process	Plppr4;Hkdc1;Angptl3;Plce1;Pla2g4a;Nudt5;Plcb1;Plcd3;Plpp2;Plcd4;Hk2;Hk1	0.003197
GO:0048015	phosphatidylinositol-mediated signaling	Pitpnm2;Plce1;Plcb1;Plcd3;Plcd4;Muc5ac	0.00524
GO:0048667	cell morphogenesis involved in neuron differentiation	Sptbn4;Ntng2;Rab3a;Dcc;Plppr4;Tmem106b;Nrcam	0.001601
GO:0007409	axonogenesis	Sptbn4;Ntng2;Sptbn5;Rab3a;plx4d;Usp9x;Dcc;Plppr4;Lama3;Prkca;Dab1;Nrcam;Sptbn1	0.003209
GO:0051128	regulation of cellular component organization	Itch;Rab5c;Ncln;Sema4d;Rock2;Plce1;Atf5;Rasgrp2;Rab5a	0.004264
GO:0048812	neuron projection morphogenesis	Sptbn4;Ntng2;Cntnap1;Rab3a;Tnn;Dcc;Plppr4;Tmem106b;Nrcam	0.004469
GO:1905144	response to acetylcholine	Chrna3;Rock2	0.004829
GO:0070286	axonemal dynein complex assembly	Dnah17;Dnah8;Lrrc49;Ccdc40	0.005523

GO:0048639	positive regulation of developmental growth	Unc13a;Sema4d;Ghrl;Plcb1;Ntn1	0.006149
GO:0036465	synaptic vesicle recycling	Rab3a;Tbc1d24;Cel;Rab5a	0.006876
GO:0033169	histone H3-K9 demethylation	Kdm3b;Jmjd1c;Kdm7a	0.00214
GO:0070076	histone lysine demethylation	Kdm5a;Kdm3b;Jmjd1c;Kdm7a	0.002553
GO:0061620	glycolytic process through glucose-6-phosphate	Adpgk;Gapdh;Hk2;Hk1	0.002199
GO:0006096	glycolytic process	Hkdc1;Gapdh;Hk2;Hk1	0.003846
GO:0070585	protein localization to mitochondrion	Maip1;Hk2;Hk1	0.002735
GO:0015031	protein transport	Arf3;Arf1;Rab3a;Rab5c;Lrp1;Arrdc1;Arrdc3;Cltc;Tbc1d2b;Snx33;Dnajc27;Rab20;Tbc1d5;Atp6v1b2;Rab5a;Sptbn1;Arf5	0.004405
GO:0045765	regulation of angiogenesis	Flt1;Adgra2;Rock2;Adam12;Angptl3;Prkca;Ghrl;Hspg2;Hoxa5;Hk2;Mtdh;Amot	0.002241
GO:0060401	cytosolic calcium ion transport	Jph2;Micu3;Slc35g1;Maip1	0.003375
GO:0008637	apoptotic mitochondrial changes	Ggct;Bax;Ndufs1;Hk2	0.006175

Table 3.6. Top 20 GO terms of biological processes of proteins decreasing in abundance in the blood plasma proteome of rainbow trout exposed to nickel. GO enrichment results of the top biological processes of the 364 proteins decreasing in abundance in all nickel treatments in comparison to the control treatment were performed using Enrich R (Xie et al., 2021). The list shows the top 20 GO terms were selected based on their p-value.

GO Term ID	GO Term	Proteins from Input List	P-value
GO:0072207	metanephric epithelium development	Pax8;Wnt7b;Pax2	5.77E-05
GO:0072234	metanephric nephron tubule development	Pax8;Wnt7b;Pax2	1.97E-04
GO:0072073	kidney epithelium development	Pax8;Wnt7b;Pax2	3.10E-04
GO:0051261	protein depolymerization	Vil1;Cfl2;Nckap5l;Twf2;Ckap5	1.34E-04
GO:0099518	vesicle cytoskeletal trafficking	Kif1a;Fnbp1l;Trak1;Myo19;Tanc2	6.64E-04
GO:0030042	actin filament depolymerization	Vil1;Cfl2;Twf2	8.78E-04
GO:0030834	regulation of actin filament depolymerization	Vil1;Lima1;Cfl2	0.001155
GO:0045332	phospholipid translocation	Abca1;Plscr1;Tmem30b;Atp10d;Atp11c	2.21E-04
GO:0015914	phospholipid transport	Abca1;Tmem30b;Pitpna;Atp10d;Osbpl2;Atp11c	6.87E-04
GO:0034204	lipid translocation	Abca1;Tmem30b;Atp10d;Atp11c	8.51E-04
GO:0048667	cell morphogenesis involved in neuron differentiation	Farp1;Slitrk4;Wnt7a;Ank3;Cntn4;Celsr2;Pax2	4.57E-04

GO:0014020	primary neural tube formation	Vangl2;Cobl;Plxnb2;Pax2	0.002014
GO:0060606	tube closure	Vangl2;Cobl;Plxnb2;Pax2	0.00228
GO:0061564	axon development	Slitrk4;Vash2;Wnt7a;Ank3;Cntn4;Pax2	0.003133
GO:0046328	regulation of JNK cascade	Sdcbp;Cops5;Ncor1;Wnt7b;Serpinf2;Wnt7a;Map3k11;Egfr	6.59E-04
GO:0043406	positive regulation of MAP kinase activity	Pdcd10;Kit;Adam8;Pik3cg;Egfr;Map3k11	0.001571
GO:0044319	wound healing, spreading of cells	Pdcd10;Wnt7a;Flna;Itga5	8.51E-04
GO:0000244	spliceosomal tri-snRNP complex assembly	Prpf3;Cd2bp2;Prpf8	0.001481
GO:0120036	plasma membrane bounded cell projection organization	Lgi1;Csf1r;Lima1;Fam161a;Prdm12;Cntn4;Mark4;Manf	0.00236
GO:0071363	cellular response to growth factor stimulus	Vil1;Ntrk2;Acap2;Wnt10a;Cilp;Pde2a;Twf2;Wnt7a;Egfr	0.002432

Chapter 4. Discussion

4.1. Nickel water chemistry

Nickel concentrations detected in the control treatments were consistent at 0.5 µg/L. This concentration, which is almost twice as high as the amount measured in the rivers near the Ontario Ring of Fire (0.2 µg/L), might be due to the leaching of nickel in the water system delivering the water to the tanks. There are no drinking water quality guidelines for Ni in Canada. However, considering the guideline for nickel in drinking water set by WHO at 70 µg/L, the levels of Ni found in our control samples are likely safe for consumption (WHO, 2021).

The first nickel treatment had a mean dissolved concentration of 1.52 ±2.4 ppb, which is more than 3-fold its nominal concentration of 0.45 ppb. With our aquatic facility control water already containing 0.5 µg/L of Ni, it suggests that our stock solution of Ni was about 2x greater than our nominal calculations, which at such low levels, could easily be due to error during stock solution preparation.

Mean dissolved Ni concentrations in the other two higher concentration nickel treatments were much closer to the nominal values, suggesting that the largest source of error was from baseline concentrations present in our system. Additionally, the PCA plots of proteome profiles from all of the fish in our study (Appendix E, Figures E1 and E2) show that there is no clustering among tank replicates belonging to the same treatment, further supporting that differences between tank water samples collected during the experiment had a negligible effect, and that tank replicates within a nickel treatment group could reasonably be pooled together for subsequent statistical and bioinformatic analyses.

4.2 Nickel burden in blood plasma

Previous studies have established that blood plasma is a sink for Ni (Pane et al., 2004a, Chowdhury et al., 2008). These studies observed significant nickel accumulation in the blood plasma of rainbow trout at much higher Ni exposure concentrations of ~380-2000 µg/L (Pane et al., 2004a, Chowdhury et al., 2008). Our study is the first to present findings of Ni accumulation in blood plasma at lower, environmentally relevant concentrations. Ni accumulated significantly in fish exposed to 45.7 ppb of Ni, with an increasing trend of accumulation seen in fish exposed to 4.9 ppb of Ni compared to the control. The empirical findings in the present study suggests that rainbow trout are able to actively regulate levels of Ni in their blood plasma when exposed to the lower concentrations of 1.5 ppb, but not at 45.7 ppb. Additionally, proteomic analysis revealed that 1240 proteins in blood plasma were differentially abundant in fish exposed to the nickel treatments. This is evidence that at concentrations below which accumulation of Ni occurs, and likely below the traditional lowest observed adverse effects level (LOAEL), there are changes in molecular function in the proteome of trout. This is relevant because conventional methods employ the use of concentration of accumulated metals and higher-level endpoints such as behavior, hatching time and even mortality to monitor biological effects. However, as shown in this study, molecular changes occur at much lower concentrations, and thus could be used to improve environmental monitoring guidelines to prevent higher level effects from occurring at more chronic or higher exposures.

4.3 Genotoxicity of nickel

Nickel is a well-known genotoxic agent in humans (Cameron et al., 2011), and was found to be genotoxic in freshwater fish such as spotted snakehead (Singh et al., 2019) and Nile

tilapia (Oliveira-Filho et al., 2010). We expected to see genotoxicity in the RBCs of rainbow trout, especially at the highest concentration of 45.7 ppb which resulted in the accumulation of significant levels of Ni. However, we did not observe any nuclear damage in the RBCs of rainbow trout in the present study. In contrast, Singh et al. (2019) observed a significant increase of micronuclei in RBCs from Spotted snakehead exposed for 30 days to comparable levels of 50 ppb of Ni compared to controls. The disparity between the two studies could be due to differences in sensitivity of the two different species of fish. Longer exposure durations may also be required for lower exposure concentrations to impact RBC nuclei in rainbow trout.

4.4 Sensory perception of sound and neuron projection development in the mucus proteome

The epidermis of fish includes a lateral line that runs across both lateral sides of the fish. This lateral line is a sensory system, allowing fish to detect water currents, pressure, and movements which are integral to prey and predator interaction. The lateral line is made up of many neuromasts, which are the functional unit of the sensory system. The neuromasts are lined by ciliated hair cell epithelium (Bleckmann and Zelick, 2009). This system is analogous to the hair cells present in the inner ears of vertebrates, and thus the over-representation of pathways involved in sensory perception of sound among differentially abundant epidermal mucus proteins could be explained by the dysregulation of proteins present in these hair cells. We did not expect to observe the over-representation of pathways related to sensory perception of sound when fish were exposed to a metal, however, this is the advantage that non-targeted proteomics offers; it is able to identify several pathways that are affected due to exposure to contaminants.

The hair cells of the lateral line each contain up to 150 stereocilia, forming a hair bundle (Bleckmann and Zelick, 2009). In mice, these hair cells contain an assembly of proteins and lipids known as the mechano-electrical transduction (MET) complex. Proteins identified in this complex include pore-forming subunits transmembrane channel-like proteins TMC1 and TMC2 (Pan et al., 2013, 2018), and lipoma HMGIC fusion partner-like 5 (LHFPL5) (Cunningham and Muller, 2019). In zebrafish, *tmc2b and lhpl5a* were found to be expressed in hair cells of the lateral line (Chou et al., 2017, Erickson et al., 2020), and are both integral to the functioning of the MET complex. Of these, proteins Lhfpl5 and Tmc2 were differentially abundant in the mucus of rainbow trout in the present study. Studies have demonstrated a reduction in the number of neuromasts of zebrafish embryos when exposed to copper and silver salts, ultimately reducing their ability to maintain equilibrium (Hernandez et al., 2006; McNeil et al., 2014). Another study on larval zebrafish and Coho salmon found that exposure to sub-lethal levels of stormwater damaged the lateral line hair cells and reduced the number of neuromasts and hair cells per neuromast, and impaired their growth (Young et al., 2018). In our study, we initially see the increase in abundance of proteins Lhfpl5 and Tmc2 on day 15 in all Ni treatments. This could be a compensatory response to maintain the sensory function of the MET complex when there is a reduction of hair cells. On day 30 we see a decline in abundance of the proteins Lhfpl5 and Tmc2 of fish exposed to 45.7 ppb of Ni could be due to the disruption of the number of neuromasts on the rainbow trout exposed to nickel. Dysregulation of proteins in the hair cells of the lateral line could suggest negative impacts on the rainbow trout sensory system, and thus the fitness of the fish. Behavioral studies in conjunction with

expression analysis of proteins in the hair cells should be conducted at environmentally relevant concentrations of nickel to understand whole-level organismal impacts on fish.

Since the lateral line is part of the sensory system of the fish, it is innervated by nerve fibers at the hair cells (Bleckmann and Zelick, 2009). Therefore, the observed decrease in proteins involved in neuron generation, particularly neuropilin-1 (Nrp1), on day 30 of exposures could be potentially linked to the disruption of either the number of neuromasts or hair cells of fish. Nrp1 expression has been studied in the development of cochlea of mice (Salehi et al., 2017), but not in the hair cells of the lateral line in fish. Future studies should closely examine the impact of nickel exposure on the neuromasts as well the neuronal networks of the lateral line of fish.

Proteins involved in processes such as actin cytoskeleton organization and actin nucleation were observed to have decreased in abundance in mucus on day 15 of exposures. These proteins included glycerophosphodiester phosphodiesterase domain containing 2 (Gdpd2), Actin-related protein 2 (Actr2), Formin 1 (Fmn1), and Spectrin beta non-erythrocytic (Sptbn1). Actin is a cytoskeletal protein and is involved in axon development and growth. Actin regulates the morphology of axons and dendrites in neurons (Dogterom and Koenderink, 2019). A decrease in abundance of proteins involved in actin organization could be linked to a decrease in proteins involved in neuron generation, such as Nrp-1, which are speculated to be involved in the neuronal connections present on the neuromasts of trout.

Additionally, in mucus we see the activation of RAS and RAF signaling, in particular by the protein Jak2. This is a non-receptor tyrosine kinase important in cytokine signaling

pathways, as mentioned earlier. However, it was recently observed in mice embryonic stem cells that the gene JAK2 might negatively regulate neuronal differentiation (Oh et al., 2021). Thus, the increase in abundance of Jak2 protein in comparison to the controls could explain the decrease in processes involved in sensory nervous system development.

4.5 Rho GTPases and neuron projection development in the plasma proteome

Processes involved in extracellular matrix (ECM) organization such as integrin cell surface interactions, and focal adhesion were over-represented among the differentially abundant proteins in the plasma. The extracellular matrix consists of collagen, and glycoproteins such as proteoglycans. Cell adhesion, migration, and cell-to-cell communication are performed via the extracellular matrix. Many collagen proteins were identified in the present study, including Collagen Type XII Alpha 1 Chain (Col12a1) and Collagen Type VII Alpha 1 Chain (Col7a1). A previous study demonstrated that exposing human lung fibroblasts to $NiCl_2$ suppressed collagen matrix contraction and cell migration (Ciubăr et al., 2006). Collagens interact with surface integrins, which form transmembrane links between the ECM and internal cell contents. Collagens also bind to Rho GTPases to initiate a signaling cascade. Several integrins were identified in the present study, including Integrin subunit alpha 1 (Itga1), which is a well-known collagen binding integrin (Gullberg and Lundgren-Akerlund, 2002). It can be speculated that dysregulation of collagen proteins identified in our study would have led to the activation of Rho GTPases via integrin interaction.

In plasma, we observed over-representation of differentially abundant proteins involved in the RAS and Rho-GTPase signaling pathways. The Ras superfamily of small GTPases are guanine nucleotide binding proteins and include Rho, Ras and Rab, among many others

and (Hall and Lalli, 2010). The Rho GTPases can be further divided into subfamilies, which are Cdc42 and RhoBTB (Stankiewicz and Linseman, 2014). In our study, we identified differentially abundant proteins from these families: CDC42 Binding Protein Kinase Beta (Cdc42bpb), Rho associated coiled-coil containing protein kinase 2 (Rock2) and Rho related BTB domain containing 2 (Rhobtb2). Rho GTPases regulate axon growth and guidance, as well as neuronal survival and death (Stankiewicz and Linseman, 2014). Moreover, studies have demonstrated that Rac/Cdc42 and Rho GTPases have an antagonistic relationship in regulating neuronal morphology. Rac/Cdc42 usually promotes the survival of neurons, whereas Rho activation can lead to neuronal death (Stankiewicz and Linseman, 2014). Rho activates its downstream effector, Rho kinase (ROCK), which leads to neuronal death. A previous study showed that ROCK2 levels are significantly increased prior to neuronal death (Kitaoka et al., 2004). In our study, Rock2 increased in abundance in all nickel treatments, and thus would have led to a decrease in abundance of proteins involved in axon development and neuron differentiation. Therefore, the increase and decrease in abundance of proteins involved in biological processes such as neuron differentiation and development in plasma proteins could be explained by the antagonistic interactions of the Rho and Rac GTPases.

Rho GTPases also regulate the assembly and dynamics of actin cytoskeletons, which play an important role in neuronal morphology and polarization. In our study, we saw a decrease in abundance of proteins involved in actin depolymerization in plasma, including cofilin 2 (Cfl2), which is important for continual growth of the actin cytoskeleton. Therefore, a decrease in abundance of proteins involved in actin depolymerization may be in part due

to an increase in abundance of proteins involved in neuronal death, thereby reducing neuron projection and axon guidance activity in rainbow trout.

In plasma, we identified several semaphorins, including semaphorin-4D (Sema4d), which increased in abundance in all nickel treatments. Additionally, the cell surface receptor of Sema4d, a protein known as Plexin-B2 (Plxnb2) was decreasing in abundance in all nickel treatments. These proteins are directly involved in neurite growth and development via Rho GTPase signaling. In the present study, there was an increase in abundance of Sema4d in plasma, which induces growth cone collapse of axons via RAS activity (Ito et al., 2006). *PLXNB2* can also stimulate the activity of RhoA signaling (Perrot et al., 2002), which can inhibit axon regeneration (Hu et al., 2017). Thus, these interactions altogether could explain the dysregulation of processes involving neuron projection and axon guidance.

We also identified semaphorin-3a (Sema3a) in plasma increasing in abundance. A study on mice suggests that semaphorins are involved in immune response and modulation. Researchers showed that the deletion of *Sema3a* in the keratinocytes of mice alleviated Ni allergy and inflammatory reaction (Liu et al., 2021). This suggests that these proteins are involved in the modulation of both the immune and nervous system, and thus there is an interconnectedness between these systems, which can be regulated by master signaling pathways like the Rho GTPases.

In general, nickel is a documented neurotoxin. Mice exposed to 10 mg/L of nickel chloride in drinking water showed signs of learning and memory impairment, caused due to reduced dendrite length and number and reduced levels of histone acetylation in their hippocampi (Zhou et al., 2021). In an annelid worm *Enchytraeus crypticus*, exposure to nickel nitrate

interfered with the functioning of the nervous system, with negative impacts seen on signal conduction (Gomes et al., 2019). Thus, the over-represented pathways due to differentially abundant proteins involved in neuron development provide a better understanding of the probable mechanism of neurotoxicity observed in rainbow trout, and other fish exposed to Ni.

4.6 Interleukin signaling pathways

Both mucus and plasma contained over-represented proteins belonging to interleukin pathways. In particular, the interleukin-12 signaling pathway was over-represented among the differentially abundant mucus proteins, and the interleukin 2, 4, 5, 6 and 15 pathways were over-represented among the significantly altered plasma proteins. Interleukin-12 subunit beta (Il12b) was increased in abundance on day 15 of exposures. Il12b is a subunit of the family of interleukin-12 cytokines. Cytokines belonging to this family were previously implicated in human skin allergic reactions to nickel sulphate via the activation of CD4+ T cells (Bechara et al., 2017). Previous research has shown that Interleukin 6 was upregulated in a human lung epithelial cell line exposed to nickel (Ge et al., 2016). The observation of Il12b increasing in abundance on day 15 in the present study might suggest that exposure to waterborne Ni in rainbow trout elicits an immune response at the mucosal or epidermal layer, similar to the one seen in humans. Although visible external impacts on the skin were not observed, analysis of the skin tissue using a histology approach with a small skin tissue plug might confirm inflammatory responses, if any, due to epidermal allergies. Additionally, interleukin 12 activates the JAK-STAT pathway by phosphorylating JAK2, leading to downstream signaling (Watford et al, 2003). Janus kinase 2 (Jak2) was increased in the mucus and both the interleukin-12 signaling and the

JAK-STAT pathways were over-represented in mucus, suggesting that phosphorylation of Jak2 occurred.

Although interleukins themselves were not detected in plasma, downstream proteins such as janus kinase 1 (Jak1), signal transducer and activator of transcription factor 5a (Stat5a), and suppressor of cytokine signaling 3 (Socs3) were dysregulated and are involved in many of the previously mentioned over-represented interleukin pathways. These findings suggest that an immune response towards nickel was also reflected in the blood plasma of rainbow trout.

4.7 Kidney and thyroid development

In mucus and plasma, we observed the over-representation of pathways involved in clear cell renal carcinoma, and kidney ureteric system development respectively. Additionally, we also observed proteins enriched in renal system development were decreasing in abundance in both mucus and plasma. It is well established that nickel accumulates primarily in the kidney of trout (Pane et al., 2004 a,b), and thus can induce tissue damage. The kidney filters the blood, and thus proteins expressed within the kidney can be transported in the blood. In our study we identified two proteins of interest in the plasma that are linked to kidney development, namely Paired-box 2 (Pax2) and Paired-box 8 (Pax8). Both of these decreased in abundance in nickel treatments compared to control. Pax2 is a transcription factor and has an important role in the development of the kidney, eyes, and nervous system. Normal renal development requires the PAX2 gene, expressed and detected in the mesenchymal derived epithelium during the embryonic stages (Dressler and Woolf, 1999). *Pax2* was found to be expressed in the eye field, brain, and pronephric mesoderm of zebrafish larvae (Xu et al., 2017). This suggests that there is

a link between the regulation of kidney, eye, and nervous system development, all of which were among the overrepresented pathways of the differentially abundant plasma proteins. Although most research on the dysregulation of these genes has been conducted during developmental stages, impacts are not well understood in adulthood. Pax8 is involved in regulation of thyroid-specific genes. It is also implicated as a potential biomarker of renal cell carcinoma (Bleu et al., 2019). *Pax2* and *Pax8* deletions induced severe polyuria, or increased amount and frequency of urination (Laszczyk et al., 2020). This suggests that Pax2 and Pax8 are important for regulating urine secretion and concentration. Nickel is known to be secreted via urine in fish, with previous studies in rainbow trout showing a reduction in glomerular filtration rate with no change in urine flow rate, which suggests a reduction in water reabsorption to main urine flow rate (Pane et al., 2005). Thus, it can be inferred that dysregulation of these genes in the present study may have occurred to regulate the elimination of nickel via urine.

We also observed an increase in abundance of proteins involved in thyroid hormone metabolism in the mucus, on day 15 and day 30. Notably, solute carrier family 16 member 2 (Slc16a2) is an important and highly active thyroid hormone membrane transporter. In zebrafish, a study demonstrated that Slc16a2 facilitates the uptake of thyroid hormone T3 (Arjona et al., 2011). Studies in mice have shown that there was a decrease in levels of T3 when they were exposed to $NiSO_4$ and $NiCl_2$ (Cheng and Yin, 1992; Liu et al., 2020). Since this gene in zebrafish shares a high sequence homology with human SLC16A2, it is thought that it has similar functions to that of mammals. Uptake of T3 is important for neuronal processes because it plays an important role in neuron development and differentiation (Noda, 2018), which may be another contributing reason for the

dysregulation of sensory and neuron projection pathways observed in the mucus proteome of trout in this study.

4.8 Epigenetic modifications via histone H3K9 demethylation

In the present study, Jumonji domain containing 1C (Jmjd1c), Lysine demethylase 7a (Kdm7a), and lysine demethylase 3b (Kdm3b), were increased in abundance in rainbow trout plasma from Ni treatments compared to controls. All three of these proteins demethylate histone lysine 9 of histone H3 (H3K9). Histone demethylation regulates gene expression by activation. An increase in abundance of H3K9 demethylases suggests an increased activation of transcription. In contrast, previous studies have shown that nickel exposure in a transgenic cell model silenced gene expression via increasing H3K9 methylation (Chen et al., 2006). It was shown in that study that JMD1A demethylates H3K9 (Chen et al., 2006), and functions as a transcriptional coactivator of many metabolic processes. An increase in H3K9 demethylase abundance seen in plasma proteins collected from rainbow trout on day 30 may be a response to the decrease in abundance of proteins involved in the regulation of transcription and chromatin assembly observed on day 15 in the mucus proteome.

4.9 Energy metabolism

In mucus, we observed an increase in abundance of proteins involved in endoplasmic reticulum associated degradation (ERAD) on both day 15 and day 30 in comparison to the proteins from the control fish. ERAD results in the catabolism of proteins that are misfolded. This was also observed in annelid worms exposed to nickel nitrate and nickel nanoparticles (Gomes et al., 2019). Previous studies reported an increase in protease activities in common carp exposed to nickel (Sreedevi et al., 1991). Catabolism of proteins

is thought to occur in response to increased stress. This could suggest that there is an increase in elimination of misfolded or damaged proteins in response to nickel stress. Additionally, on day 30 in mucus, we observed an increase in proteins involved in peptide and pentose metabolism, as well as fatty-acid metabolism, and in plasma there was an increase in the abundance of proteins involved in glycolysis. These proteins included hexokinase 1 (Hk1), hexokinase 2 (Hk2) and glyceraldehyde-3-phosphate dehydrogenase (Gapdh). Hexokinases are enzymes that phosphorylate glucose into glucose-6-phosphate, and Gapdh converts D-glyceraldehyde 3-phosphate (G3P) into 3-phospho-D-glycerol phosphate in the glycolysis pathway. An increase in abundance of these enzymes indicates an increase in processes involved in energy metabolism and consumption. These proteins are also involved in the synthesis of pentoses and peptides, which could be occurring to compensate for the loss of proteins via catabolism. Previous studies have seen a decrease in total serum protein and protein in the gills and kidneys, with an increase in proteolytic activity of common carp exposed to nickel (Sreedevi et al., 1991; Gopal et al., 1997). Energy metabolism may be increased in demand to maintain normal biological conditions in response to the disruption of many regulatory processes such as the loss of neurons, regulation of transcription and chromatin assembly, elimination of Ni and regulation of the immune system occurring due to nickel stress.

Chapter 5. Conclusion

Canada is the world's 8th largest exporter and 5th largest producer of nickel, with the province of Ontario being Canada's largest nickel producer (Workman, 2019; NRC 2019). Although nickel is of economic importance and increasing in commercial demand, very little research has been conducted to analyze its toxic effects on freshwater fish. Additionally, the mechanism behind the observed toxic effects of nickel remains elusive.

In our study, we subjected adult rainbow trout to environmentally relevant concentrations of nickel that are much lower than had typically been studied in the past. We show that at these concentrations the rainbow trout mucus and blood plasma proteome is sensitive to nickel exposure. The differentially expressed proteins in the blood plasma and skin mucus of rainbow trout were largely involved in regulation of the immune system, the sensory nervous system, kidney function, and Rho and RAS signaling. The dysregulation of the Rho and RAS GTPase pathways due to nickel stress could control the modulation of many other downstream pathways. These responses don't necessarily indicate toxicity, since higher level impacts like genotoxicity were not observed. However, they provide insight into the mechanisms involved to acclimate to low levels of waterborne nickel and also early signs of nickel exposure at concentrations that begin to accumulate in plasma.

The findings of this study support what is known by expanding on current knowledge, reveals novel biological processes regulated in fish exposed to nickel, and suggest new avenues of research to corroborate other findings. Targeted studies are required to confirm some of the observed protein changes and to fill in the knowledge gaps surrounding the mechanism of toxicity of nickel in fish; for instance, the inflammatory responses of

trout and impacts on lateral line sensory neuromasts could be confirmed using traditional blood cell count endpoints, histology, and behavioral approaches.

We also demonstrate that blood plasma, in conjunction with skin mucus, can provide a wealth of information about the health status of fish. Proteins in blood plasma and skin mucus could be used to develop targeted, non-lethal bioassays useful for diagnosing wild fish health in environmental effects monitoring programs. Protecting aquatic ecosystems and ensuring their vitality can greatly contribute towards economic development by safeguarding the fisheries industry and sport fishing activities. Ultimately, early detection and prediction of nickel toxicity through the identification of biomarkers that are strongly linked to molecular initiating events of a well-established adverse outcome pathway could protect fish populations.

References

Alsop, D., & Wood, C. M. (2011). Metal uptake and acute toxicity in zebrafish: common mechanisms across multiple metals. *Aquatic toxicology*, 105(3-4), 385-393.

Alsop, D., Lall, S. P., & Wood, C. M. (2014). Reproductive impacts and physiological adaptations of zebrafish to elevated dietary nickel. *Comparative Biochemistry and Physiology Part C: Toxicology& Pharmacology*, 165, 67-75.

Arjona, F. J., de Vrieze, E., Visser, T. J., Flik, G., & Klaren, P. H. (2011). Identification and functional characterization of zebrafish solute carrier Slc16a2 (Mct8) as a thyroid hormone membrane transporter. *Endocrinology*, *152*(12), 5065-5073

Athikesavan, S., Vincent, S., Ambrose, T., & Velmurugan, B. (2006). Nickel induced histopathological changes in the different tissues of freshwater fish, *Hypophthalmichthys molitrix (Valenciennes*). *Journal of Environmental Biology*, 37(2), 391-395.

Austin, B. (1998). The effects of pollution on fish health. *Journal of applied microbiology*, *85*(S1), 234S-242S.

Baylock, B. G., Frank, M. L. (1979). A comparison of the toxicity of the developing eggs and larvae of carp (*Cyprinus carpio). Bull, Environ. Contain. Toxicol*. 21, 604-611

Bechara, R., Antonios, D., Azouri, H., & Pallardy, M. (2017). Nickel sulfate promotes IL-17A producing CD4+ T cells by an IL-23-dependent mechanism regulated by TLR4 and Jak-STAT pathways. *Journal of Investigative Dermatology*, *137*(10), 2140-2148.

Bleckmann, H., & Zelick, R. (2009). Lateral line system of fish. *Integrative zoology*, *4*(1), 13-25.

Bleu, M., Gaulis, S., Lopes, R., Sprouffske, K., Apfel, V., Holwerda, S., Pregnolato, M., Yildiz, U., Cordo', V., Dost, A. F. M., Knehr, J., Carbone, W., Lohmann, F., Lin, C. Y., Bradner, J. E., Kauffman, A., Tordella, L., Roma, G., & Galli, G. G. (2019). PAX8 activates metabolic genes via enhancer elements in Renal Cell Carcinoma. *Nature communications*, *10*(1), 1-10.

Blighe K, Rana S, Lewis M (2022). *EnhancedVolcano:* Publication-ready volcano plots with enhanced colouring and labeling. R package version 1.14.0, https://github.com/kevinblighe/EnhancedVolcano

Bougas, B., Normandeau, E., Pierron, F., Campbell, P. G., Bernatchez, L., & Couture, P. (2013). How does exposure to nickel and cadmium affect the transcriptome of yellow perch (*Perca flavescens*)–results from a 1000 candidate-gene microarray. *Aquatic toxicology*, 142, 355-364.

Brix, K. V., Keithly, J., DeForest, D. K., & Laughlin, J. (2004). Acute and chronic toxicity of nickel to rainbow trout (*Oncorhynchus mykiss*). *Environmental Toxicology and Chemistry: An International Journal*, 23(9), 2221-2228.

Cameron, K. S., Buchner, V., & Tchounwou, P. B. (2011). Exploring the molecular mechanisms of nickel-induced genotoxicity and carcinogenicity: a literature review.

Canadian Environmental Protection Act: Priority Substances List. (1989). CEPA Priority Substances List. [online] Available at:
https://www.canada.ca/en/environment-climate-change/services/canadianenvironmental-protection-act-registry/substances-list/priority-list.html

CCME. (1987). Canadian water quality guidelines for the protection of aquatic wildlife. Canadian Council of the Ministers of the Environment. Available at: http://stts.ccme.ca/en/index.html?lang=en&factsheet=139

Chau, Y. K., & Kulikovsky-Cordeiro, O. T. R. (1995). Occurrence of nickel in the Canadian environment. *Environmental Reviews*, 3(1), 95-120.

Chen, H.; Ke, Q.; Kluz, T.; Yan, Y.; Costa, M. (2006). Nickel Ions Increase Histone H3 Lysine 9 Dimethylation and Induce Transgene Silencing. *Molecular and Cellular Biology*, 26(10), 3728–3737. doi:10.1128/MCB.26.10.3728-3737.2006

Cheng, W. Z., & Yin, C. F. (1992). Effects of nickel chloride (NiCl2) and nickel sulfate (NiSO4) on T3, T4, TSH content in rat serum. *J Shijiazhuang Med Coll*, *3*, 4-7.

Chou, S. W., Chen, Z., Zhu, S., Davis, R. W., Hu, J., Liu, L., Fernando, C. A., Kindig, K., Brown, W. C., Stepanyan, R., & McDermott, B. M. (2017). A molecular basis for water motion detection by the mechanosensory lateral line of zebrafish. *Nature communications*, *8*(1), 1-16.

Chowdhury, M. J., Bucking, C., & Wood, C. M. (2008). Pre-exposure to waterborne nickel downregulates gastrointestinal nickel uptake in rainbow trout: indirect evidence for nickel essentiality. *Environmental science & technology*, 42(4), 1359-1364.

Ciubăr, R., Mitran, V., Bonoiu, A., Cimpean, A., & Iordăchescu, D. (2006). The effect of nickel on the fibroblast-mediated collagen matrix contraction. *Rom. J. Biophys*, *16*(2), 125-133.

Cunningham, C. L., and Müller, U. (2019). Molecular structure of the hair cell mechanoelectrical transduction complex. *Cold Spring Harb. Perspect. Med.*9:a033167. doi: 10.1101/cshperspect.a033167

Dash, S., Das, S. K., Samal, J., & Thatoi, H. N. (2018). Epidermal mucus, a major determinant in fish health: a review. *Iranian Journal of Veterinary Research*, 19(2), 72.

Dave, G., & Xiu, R. (1991). Toxicity of mercury, copper, nickel, lead, and cobalt to embryos and larvae of zebrafish, *Brachydanio rerio*. *Archives of Environmental Contamination and Toxicology*, *21*(1), 126-134.

Deleebeeck, N. M., De Schamphelaere, K. A., & Janssen, C. R. (2007). A bioavailability model predicting the toxicity of nickel to rainbow trout (*Oncorhynchus mykiss*) and fathead minnow (*Pimephales promelas*) in synthetic and natural waters. *Ecotoxicology and Environmental Safety*, 67(1), 1-13.

Denkhaus, E. and K. Salnikow, 2002. Nickel essentially, toxicity and carcinogenity. *Critical Reviews in Oncology/Hematology*, 42 (2002) 35-56

Dixit, S.S., Dixit, A.S., and Smol, J.P. (1992). Assessment of changes in lake water chemistry in Sudbury area lakes since preindustrial times. *Can. J. Fish. Aquat. Sci*. 49, 8-16.

Dogterom, M., & Koenderink, G. H. (2019). Actin–microtubule crosstalk in cell biology. *Nature Reviews Molecular Cell Biology*, *20*(1), 38-54.

Dressler, G. R., & Woolf, A. S. (2003). Pax2 in development and renal disease. *International Journal of Developmental Biology*, *43*(5), 463-468.

Driessnack, M. K., Jamwal, A., & Niyogi, S. (2017). Effects of chronic exposure to waterborne copper and nickel in binary mixture on tissue-specific metal accumulation and reproduction in fathead minnow (*Pimephales promelas*). *Chemosphere*, 185, 964-974.

Eisler, R., 1998. Nickel hazards to fish, wildlife, and invertebrates: a synoptic review. U.S. Geological Survey, Biological Resources Division, Biological Science Report 1998-0001

Erickson, T., Pacentine, I. V., Venuto, A., Clemens, R., & Nicolson, T. (2020). The lhfpl5 Ohnologs lhfpl5a and lhfpl 5b Are Required for Mechanotransduction in Distinct Populations of Sensory Hair Cells in Zebrafish. *Frontiers in molecular neuroscience*, *12*, 320.

Ge, Y., Bruno, M., Haykal-Coates, N., Wallace, K., Andrews, D., Swank, A., Winnik, W., & Ross, J. A. (2016). Proteomic assessment of biochemical pathways that are critical to nickel-induced toxicity responses in human epithelial cells. *PLoS One*, *11*(9), e0162522.

Ghazaly, K.S., 1992. Sublethal effects of nickel on carbohydrate metabolism, blood, and mineral contents of *Tilapia nilotica*. *Water, Air, Soil Pollut*. 64, 525-532

Gomes, S. I., Roca, C. P., Scott-Fordsmand, J. J., & Amorim, M. J. (2019). High-throughput transcriptomics: insights into the pathways involved in (nano) nickel toxicity in a key invertebrate test species. *Environmental Pollution*, *245*, 131-140.

Gopal, V., Parvathy, S., & Balasubramanian, P. R. (1997). Effect of heavy metals on the blood protein biochemistry of the fish *Cyprinus carpio* and its use as a bio-indicator of pollution stress. *Environmental monitoring and assessment*, 48(2), 117-124.

Goytain, A., Quamme, G. A. (2005) Identification and characterization of a novel mammalian Mg2+ transporter with channel-like properties. *BMC Genom*., 6, 48.

Grande, M., Andersen, S. (1983). Lethal effects of hexavalent chromium, lead, and nickel on young stages of Atlantic salmon (*Salmo salar L*.) in soft water. *Vatten (Lund)*. 39,405-416

Guardiola, F. A., Dioguardi, M., Parisi, M. G., Trapani, M. R., Meseguer, J., Cuesta, A., Cammarata, M., & Esteban, M. A. (2015). Evaluation of waterborne exposure to heavy metals in innate immune defences present on skin mucus of gilthead seabream (*Sparus aurata*). *Fish & shellfish immunology*, 45(1), 112-123.

Gullberg, D. E., & Lundgren-Åkerlund, E. (2002). Collagen-binding I domain integrins—what do they do?. *Progress in histochemistry and cytochemistry*, *37*(1), 3-54.

Gunshin, H.; Mackenzie, B.; Berger, U. V.; Gunshin, Y.; Romero, M. F.; Boron, W. F.; Nussberger, S.;Golan, J. L.; Hediger, M. A. (1997). Cloning and characterization of a mammalian proton-coupled metal-ion transporter. *Nature*, 388, 482–488

Hall, A., & Lalli, G. (2010). Rho and Ras GTPases in axon growth, guidance, and branching. *Cold Spring Harbor perspectives in biology*, *2*(2), a001818.

Hernández, P. P., Moreno, V., Olivari, F. A., & Allende, M. L. (2006). Sub-lethal concentrations of waterborne copper are toxic to lateral line neuromasts in zebrafish (Danio rerio). *Hearing research*, *213*(1-2), 1-10.

Hoang, T. C., Tomasso, J. R., & Klaine, S. J. (2004). Influence of water quality and age on nickel toxicity to fathead minnows (*Pimephales promelas*). *Environmental Toxicology and Chemistry*: *An International Journal*, 23(1), 86-92

Hu, J., & Selzer, M. E. (2017). RhoA as a target to promote neuronal survival and axon regeneration. *Neural regeneration research*, *12*(4), 525–528. https://doi.org/10.4103/1673-5374.205080

Ito, Y., Oinuma, I., Katoh, H., Kaibuchi, K., & Negishi, M. (2006). Sema4D/plexin-B1 activates GSK-3beta through R-Ras GAP activity, inducing growth cone collapse. *EMBO reports*, *7*(7), 704–709. https://doi.org/10.1038/sj.embor.7400737

Kienle, C., Köhler, H. R., & Gerhardt, A. (2009). Behavioural and developmental toxicity of chlorpyrifos and nickel chloride to zebrafish (*Danio rerio*) embryos and larvae. *Ecotoxicology and Environmental Safety*, 72(6), 1740-1747.

Kitaoka, Y., Kitaoka, Y., Kumai, T., Lam, T. T., Kuribayashi, K., Isenoumi, K., Munemasa, Y., Motoki, M., Kobayashi, S., & Ueno, S. (2004). Involvement of RhoA and possible neuroprotective effect of fasudil, a Rho kinase inhibitor, in NMDA-induced neurotoxicity in the rat retina. *Brain research*, *1018*(1), 111-118.

Kolde, R. (2019). pheatmap: Pretty Heatmaps. R package version 1.0. 12. *CRAN. R-project. org/package= pheatmap*.

Kubrak OI, Poigner H, Husak VV, Rovenko BM, Meyer S, Abele D, Lushchak VI .(2014). Goldfish brain and heart are well protected from Ni2+-induced oxidative stress. *Comp Biochem Physiol C Toxicol Pharmaco,l* 162:43–50

Kubrak, O. I., Husak, V. V., Rovenko, B. M., Poigner, H., Mazepa, M. A., Kriews, M., Abele, D. & Lushchak, V. I. (2012). Tissue specificity in nickel uptake and induction of oxidative stress in kidney and spleen of goldfish *Carassius auratus*, exposed to waterborne nickel. *Aquatic toxicology*, 118, 88-96

Laszczyk, A. M., Higashi, A. Y., Patel, S. R., Johnson, C. N., Soofi, A., Abraham, S., & Dressler, G. R. (2020). Pax2 and Pax8 proteins regulate urea transporters and aquaporins to control urine concentration in the adult kidney. *Journal of the American Society of Nephrology*, *31*(6), 1212-1225.

Léger, J. A., Athanasio, C. G., Zhera, A., Chauhan, M. F., & Simmons, D. B. (2021). Hypoxic responses in *Oncorhynchus mykiss* involve angiogenesis, lipid, and lactate metabolism, which may be triggered by the cortisol stress response and epigenetic methylation. *Comparative Biochemistry and Physiology Part D: Genomics and Proteomics*, *39*, 100860.

Liang, X., Martyniuk, C. J., & Simmons, D. B. (2020). Are we forgetting the "proteomics" in multi-omics ecotoxicology?.*Comparative Biochemistry and Physiology Part D: Genomics and Proteomics*, *36*, 100751.

Liu, L., Watanabe, M., Minami, N., Yunizar, M., & Ichikawa, T. (2021). Semaphorin3A Promotes the Development of Nickel Allergy. https://doi.org/10.21203/rs.3.rs-598449/v1

Liu, Y., Chen, H., Zhang, L., Zhang, T., & Ren, X. (2020). The association between thyroid injury and apoptosis, and alterations of Bax, Bcl-2, and caspase-3 mRNA/protein expression induced by nickel sulfate in Wistar rats. *Biological trace element research*, *195*(1), 159-168.

Martyniuk, C. J., Kroll, K. J., Doperalski, N. J., Barber, D. S., & Denslow, N. D. (2010). Environmentally relevant exposure to 17α-ethinylestradiol affects the telencephalic proteome of male fathead minnows. *Aquatic toxicology*, *98*(4), 344-353.

McNeil, P. L., Boyle, D., Henry, T. B., Handy, R. D., & Sloman, K. A. (2014). Effects of metal nanoparticles on the lateral line system and behaviour in early life stages of zebrafish (*Danio rerio*). *Aquatic toxicology*, *152*, 318-323.

Muyssen, B. T., Brix, K. V., DeForest, D. K., & Janssen, C. R. (2004). Nickel essentiality and homeostasisin aquatic organisms. *Environmental reviews*, 12(2), 113-131.

National Wetlands Working Group. (1997). The Canadian Wetland Classification System, 2nd Edition. Warner, B.G. and C.D.A. Rubec (eds.), Wetlands Research Centre, University of Waterloo, Waterloo, ON, Canada. 68 p.

Nickel Institute. (2020). Nickel In Batteries. Available at: https://nickelinstitute.org/about-nickel/nickelin-batteries/

Niyogi, S., Wood, C.M., (2004). Biotic ligand model, a flexible tool for developing site-specific waterquality guidelines for metals. *Environ. Sci. Technol*. 38, 6177–6192.

Noda, M. (2018). Thyroid hormone in the CNS: contribution of neuron–glia interaction. *Vitamins and hormones*, *106*, 313-331.

NRC. (2019). Nickel Facts. Natural Resources Government of Canada. https://www.nrcan.gc.ca/sciencedata/science-research/earth-sciences/earth-sciences-resources/earth-sciences-federalprograms/nickel-facts/20519

Oh, M., Kim, S. Y., Byun, J. S., Lee, S., Kim, W. K., Oh, K. J., Lee, E. W., Bae, K. H., Lee, S. C., & Han, B. S. (2021). Depletion of Janus kinase-2 promotes neuronal differentiation of mouse embryonic stem cells. *BMB reports*, *54*(12), 626.

Oliveira-Filho, E. C., de Freitas Muniz, D. H., Ferreira, M. F. N., & Grisolia, C. K. (2010). Evaluation of acute toxicity, cytotoxicity and genotoxicity of a nickel mining waste to

Oreochromis niloticus. *Bulletin of Environmental Contamination and Toxicology*, *85*(5), 467-471.

Olson, K. R. (1992). 3 Blood and Extracellular Fluid Volume Regulation: Role of the Renin-Angiotensin System, Kallikrein-Kinin System, and Atrial Natriuretic Peptides. In *Fish physiology* (Vol. 12, pp. 135-254). Academic Press.

Pan, B., Akyuz, N., Liu, X. P., Asai, Y., Nist-Lund, C., Kurima, K., Derfler, B. H., Gyorgy, B., Limapichat, W., Walujkar, S., Wimalasena, L. N., Sotomayor, M., Corey, D. P., & Holt, J. R. (2018). TMC1 forms the pore of mechanosensory transduction channels in vertebrate inner ear hair cells. Neuron, 99(4), 736-753.

Pan, B., Géléoc, G. S., Asai, Y., Horwitz, G. C., Kurima, K., Ishikawa, K., Kawashima, Y., Griffith, A. J., & Holt, J. R. (2013). TMC1 and TMC2 are components of the mechanotransduction channel in hair cells of the mammalian inner ear. *Neuron*, *79*(3), 504-515.

Pane, E. F., Bucking, C., Patel, M., & Wood, C. M. (2005). Renal function in the freshwater rainbow trout (*Oncorhynchus mykiss*) following acute and prolonged exposure to waterborne nickel. *Aquatic toxicology*, 72(1-2), 119-133.

Pane, E. F., Glover, C. N., Patel, M., & Wood, C. M. (2006). Characterization of Ni transport into brush border membrane vesicles (BBMVs) isolated from the kidney of the freshwater rainbow trout (*Oncorhynchus mykiss*). *Biochimica et Biophysica Acta (BBA)-Biomembranes*, 1758(1), 74-84.

Pane, E. F., Haque, A., & Wood, C. M. (2004b). Mechanistic analysis of acute, Ni-induced respiratory toxicity in the rainbow trout (*Oncorhynchus mykiss*): an exclusively branchial phenomenon. *Aquatic Toxicology*, 69(1), 11-24.

Pane, E. F., Haque, A., Goss, G. G., & Wood, C. M. (2004a). The physiological consequences of exposure to chronic, sublethal waterborne nickel in rainbow trout (*Oncorhynchus mykiss*): exercise vs resting physiology. *Journal of Experimental Biology*, 207(7), 1249-1261.

Pane, E. F., Patel, M., & Wood, C. M. (2006). Chronic, sublethal nickel acclimation alters the diffusive properties of renal brush border membrane vesicles (BBMVs) prepared from the freshwater rainbow trout. *Comparative Biochemistry and Physiology Part C: Toxicology & Pharmacology*, 143(1), 78-85.

Pane, E. F., Richards, J. G., & Wood, C. M. (2003). Acute waterborne nickel toxicity in the rainbow trout (*Oncorhynchus mykiss*) occurs by a respiratory rather than ionoregulatory mechanism. *Aquatic toxicology*, 63(1), 65-82.

Perrot, V., Vázquez-Prado, J., & Gutkind, J. S. (2002). Plexin B regulates Rho through the guanine nucleotide exchange factors leukemia-associated Rho GEF (LARG) and PDZ-RhoGEF. *Journal of Biological Chemistry*, *277*(45), 43115-43120.

Philipson, B, Lee, S, Majewski, IJ, Alexander, WS, and Smyth, GK (2016). Robust hyperparameter estimation protects against hypervariable genes and improves power to detect differential expression. *Annals of Applied Statistics* 10(2), 946-963.

Pickering, Q. H. (1974). Chronic toxicity of nickel to the fathead minnow. *J. Water Pollut Control Fed*.,46,760-765

Pollard, S., Anderson, J. C., Bah, F., Mateus, M., Sidhu, M., & Simmons, D. (2022). Non-Lethal Blood Sampling of Fish in the lab and Field With Methods for Dried Blood Plasma Spot Omic Analyses. *Frontiers in genetics*, *13*, 795348-795348.

Ptashynski, M. D., & Klaverkamp, J. F. (2002). Accumulation and distribution of dietary nickel in lake whitefish (*Coregonus clupeaformis*). *Aquatic toxicology*, 58(3-4), 249-264.

Ptashynski, M. D., Pedlar, R. M., Evans, R. E., Wautier, K. G., Baron, C. L., & Klaverkamp, J. F. (2001). Accumulation, distribution and toxicology of dietary nickel in lake whitefish (*Coregonus clupeaformis*) and lake trout (*Salvelinus namaycush*). *Comparative Biochemistry and Physiology Part C: Toxicology & Pharmacology*, 130(2), 145-162.

PWQMN. (2021). Provincial (Stream) Water Quality Monitoring Network - Ontario Data Catalogue. Government of Canada. Available at: <https://data.ontario.ca/dataset/provincial-stream-waterquality-monitoring-network>.

Pyle, G. G., Swanson, S. M., & Lehmkuhl, D. M. (2002). The influence of water hardness, pH, and suspended solids on nickel toxicity to larval fathead minnows (*Pimephales promelas*). *Water, Air, and Soil Pollution*, 133(1-4), 215-226

Pyle, G.G., Couture, P., 2012. Homeostasis and toxicology of essential metals. In: Wood, C.M., Farrell, A.P., Brauner, C.J. (Eds.), *Fish Physiology*, vol. 31A. Elsevier Inc. pp. 253-289.

Ritchie ME, Phipson B, Wu D, Hu Y, Law CW, Shi W, Smyth GK (2015). Limma powers differential expression analyses for RNA-sequencing and microarray studies. *Nucleic Acids Research*, **43**(7), e47. doi: 10.1093/nar/gkv007.

Ritchie, M. E., Diyagama, D., Neilson, van Laar, R., J., Dobrovic, A., Holloway, A., and Smyth, G. K. (2006). Empirical array quality weights in the analysis of microarray data. *BMC Bioinformatics* **7**, 261.

Ritchie, M. E., Silver, J., Oshlack, A., Silver, J., Holmes, M., Diyagama, D., Holloway, A., and Smyth, G. K. (2007). A comparison of background correction methods for two-colour microarrays. *Bioinformatics* 23, 2700-2707.

Roskill. (2021). Study on future demand and supply security of nickel for electric vehicle batteries. European Union

Salehi, P., Ge, M. X., Gundimeda, U., Michelle Baum, L., Lael Cantu, H., Lavinsky, J., Tao, L., Myint, A., Cruz, C., Wang, J., Nikolakopoulou, A. M., Abdala, C., Kelley, M. W., Ohyama, T., Coate, T. M., & Friedman, R. A. (2017). Role of Neuropilin-1/Semaphorin-3A signaling in the functional and morphological integrity of the cochlea. *PLoS genetics*, *13*(10), e1007048. https://doi.org/10.1371/journal.pgen.1007048

Simmons, D. B., Benskin, J. P., Cosgrove, J. R., Duncker, B. P., Ekman, D. R., Martyniuk, C. J., & Sherry, J. P. (2015). Omics for aquatic ecotoxicology: Control of extraneous variability to enhance the analysis of environmental effects. Environmental Toxicology and Chemistry, 34(8), 1693-1704.

Singh, M., Khan, H., Verma, Y., & Rana, S. V. S. (2019). Distinctive fingerprints of genotoxicity induced by As, Cr, Cd, and Ni in a freshwater fish. *Environmental Science and Pollution Research*, 26(19), 19445-19452

Smyth, G. K., Michaud, J., and Scott, H. (2005). The use of within-array replicate spots for assessing differential expression in microarray experiments. *Bioinformatics* **21**, 2067-2075

Sobsey, C. A., Ibrahim, S., Richard, V. R., Gaspar, V., Mitsa, G., Lacasse, V., Zahedi, R. P., Batist, G., & Borchers, C. H. (2020). Targeted and untargeted proteomics approaches in biomarker development. *Proteomics*, *20*(9), 1900029.

Sreedevi, P., Sivaramakrishna, B., Suresh, A., & Radhakrishnaiah, K. (1992). Effect of nickel on some aspects of protein metabolism in the gill and kidney of the freshwater fish, *Cyprinus carpio L*. *Environmental Pollution*, 77(1), 59-63.

Stankiewicz, T. R., & Linseman, D. A. (2014). Rho family GTPases: key players in neuronal development, neuronal survival, and neurodegeneration. *Frontiers in cellular neuroscience*, *8*, 314.

Tallkvist, J.; Bowlus, C. L.; Lunnerdal, B. (2003). Effect of iron treatment on nickel absorption and gene expression of the divalent metal transporter (DMT1) by human intestinal caco-2 cells. *Pharmacol. Toxicol*., 92, 121–124

Tannouri, N. (2021). Characterizing Blood Plasma Proteins from Organ Tissue in Rainbow Trout (*Oncorhynchus mykiss*) Using a Non-Targeted Proteomics Approach. [Unpublished master's thesis]. Ontario Tech University

Thorstensen, M. J., Vandervelde, C. A., Bugg, W. S., Michaleski, S., Vo, L., Mackey, T. E., Lawrence, M. J., & Jeffries, K. M. (2022). Non-Lethal Sampling Supports Integrative Movement Research in Freshwater Fish. *Frontiers in Genetics*, *13*, 795355-795355.

Tjälve, H., Gottofrey, J., & Borg, K. (1988). Bioaccumulation, distribution and retention of 63Ni2+ in the brown trout (*Salmo trutta*). *Water Research*, 22(9), 1129-1136.

Topal, A., Atamanalp, M., Oruç, E., & Erol, H. S. (2017). Physiological and biochemical effects of nickel on rainbow trout (*Oncorhynchus mykiss*) tissues: assessment of nuclear factor kappa B activation, oxidative stress and histopathological changes. *Chemosphere*, 166, 445-452.

Topal, A., Atamanalp, M., Oruç, E., Halıcı, M. B., Şişecioğlu, M., Erol, H. S., Gergit, A., Yılmaz, B. (2015). Neurotoxic effects of nickel chloride in the rainbow trout brain: assessment of c-Fos activity, antioxidant responses, acetylcholinesterase activity, and histopathological changes. *Fish Physiology and Biochemistry*, 41(3), 625-634.

Wasinger, V. C., Cordwell, S. J., Cerpa-Poljak, A., Yan, J. X., Gooley, A. A., Wilkins, M. R., Duncan, M. W., Harris, R., Williams, K. L., & Humphery-Smith, I. (1995). Progress with gene-product mapping of the Mollicutes: *Mycoplasma genitalium*. *Electrophoresis*, *16*(1), 1090-1094.

Watford, W. T., Moriguchi, M., Morinobu, A., & O'Shea, J. J. (2003). The biology of IL-12: coordinating innate and adaptive immune responses. *Cytokine & growth factor reviews*, *14*(5), 361-368.

World Health Organization (WHO). (2021). *Nickel in drinking-water. Background document for development of WHO Guidelines for drinking-water quality*. Geneva, World Health Organization.

Workman, D. (2019). Top Nickel Exporters by Country. World's Top exports. http://www.worldstopexports.com/top-nickel-exporters-by-country/

Xie, Z., Bailey, A., Kuleshov, M. V., Clarke, D. J., Evangelista, J. E., Jenkins, S. L., Lachmann, A., Wojciechowicz, M. L., Kropiwnicki, E., Jagodnik, K. M., Jeon, M., & Ma'ayan, A. (2021). Gene set knowledge discovery with enrichr. *Current protocols*, *1*(3), e90.

Xu, J., Zhang, Q., Li, X., Zhan, S., Wang, L., & Chen, D. (2017). The effects of copper oxide nanoparticles on dorsoventral patterning, convergent extension, and neural and cardiac development of zebrafish. *Aquatic Toxicology*, *188*, 130-137.

Young, A., Kochenkov, V., McIntyre, J. K., Stark, J. D., & Coffin, A. B. (2018). Urban stormwater runoff negatively impacts lateral line development in larval zebrafish and salmon embryos. *Scientific reports*, *8*(1), 1-14.

Zheng, G. H., Liu, C. M., Sun, J. M., Feng, Z. J., & Cheng, C. (2014). Nickel-induced oxidative stress and apoptosis in *Carassius auratus* liver by JNK pathway. *Aquatic toxicology*, 147, 105-111

Zhou, C., Liu, M., Mei, X., Li, Q., Zhang, W., Deng, P., He, Z., Xi, Y., Tong, T., Pi, H., Lu, Y., Chen, C., Zhang, L.,Yu, Z., Zhou, Z., & He, M. (2021). Histone hypoacetylation contributes to neurotoxicity induced by chronic nickel exposure in vivo and in vitro. *Science of The Total Environment*, *783*, 147014.

Appendices

Appendix A. Proteomics Acquisition methods

Acquisition Method Report

Agilent | Trusted Answers

Acquisition Method Info

Method Name	Agilent_training_peptides_slope4.m
Method Path	D:\MassHunter\Methods\peptides\Agilent_training_peptides_slope4.m
Method Description	

Device List

Multisampler
Binary Pump
Column Comp.
Q-TOF

TOF/Q-TOF Mass Spectrometer

Component Name	MS Q-TOF	**Component Model**	G6545A
Ion Source	Dual AJS ESI	**Stop Time (min)**	No Limit/As Pump
Can wait for temp.	Enable	**Fast Polarity**	False
MS Abs. threshold	500	**MS Rel. threshold(%)**	0.010
MS/MS Abs. threshold	5	**MS/MS Rel. threshold(%)**	0.010

Time Segments

Time Segment #	Start Time (min)	Diverter Valve State	Storage Mode	Ion Mode
1	0	MS	Both	Dual AJS ESI

Report generation date: 23-Aug-2021 07:28:26 PM

Page 1 of 6

Time Segment 1

Acquisition Mode AutoMS2

MS Min Range (m/z)	200
MS Max Range (m/z)	3000
MS Scan Rate (spectra/sec)	3.00
MS/MS Min Range (m/z)	50
MS/MS Max Range (m/z)	3000
MS/MS Scan Rate (spectra/sec)	2.00
Isolation Width MS/MS	Medium (~4 amu)
Decision Engine	Native

Ramped Collision Energy

Charge	Slope	Offset
All	4	2

Auto MS/MS Preferred/Exclude Table

Mass	Delta Mass (ppm)	Charge	Type	Retention Time (min)	Delta Ret. Time (min)	Isolation Width	Collision Energy
921.9686	100	1	Exclude	0		Narrow (~1.3 amu)	

Precursor Selection

Max Precursors Per Cycle	10
Threshold (Abs)	500
Threshold (Rel)(%)	0.010
Precursor abundance based scan speed	Yes
Target (counts/spectrum)	25000.000
Use MS/MS accumulation time limit	Yes
Use dynamic precursor rejection	No
Purity Stringency (%)	100.000
Purity Cutoff (%)	30.000
Isotope Model	Peptides
Active exclusion enabled	Yes
Active exclusion excluded after (spectra)	2
Active exclusion released after (min)	0.20
Sort precursors	By abundance only

Static Exclusion Ranges

StartMZ	EndMZ
25	300

Charge State Preference

Selected Charges
2
3
>3

Instrument Parameters

Parameter	Value
Gas Temp (°C)	325
Gas Flow (l/min)	8
Nebulizer (psig)	35
SheathGasTemp	350
SheathGasFlow	11

Scan Segments

Scan Seg #	Ion Polarity
1	Positive

Scan Segment 1

Scan Source Parameters

Parameter	Value
VCap	4500
Nozzle Voltage (V)	1000
Fragmentor	180
Skimmer1	65
OctopoleRFPeak	750

ReferenceMasses

Ref Mass Enabled	Disabled
Ref Nebulizer (psig)	

Chromatograms

Chrom Type	Label	Offset	Y-Range
TIC	TIC	15	10000000
TIC	TIC	15	10000000

Name: Multisampler **Module: G7167A**

Sampling Speed	
Draw Speed	100.0 µL/min
Eject Speed	400.0 µL/min
Wait Time After Drawing	1.2 s
Injection	
Needle Wash Mode	Standard Wash
Injection Volume	2.00 µL
Standard Needle Wash	
Needle Wash Mode	Flush Port
Duration	10 s
High Throughput	
Injection Valve to Bypass for Delay Volume Reduction	No
Sample Flush-Out Factor	5.0
Overlapped Injection	
Overlap Injection Enabled	No
Needle Height Position	
Draw Position Offset	-1.0 mm
Use Vial/Well Bottom Sensing	No
Stop Time	
Stoptime Mode	No Limit
Post Time	
Posttime Mode	Off

Name: Binary Pump **Module: G7112B**

Flow	0.000 mL/min
Use Solvent Types	Yes
Low Pressure Limit	0.00 bar
High Pressure Limit	400.00 bar
Maximum Flow Gradient	100.000 mL/min²
Stroke A	
Automatic Stroke Calculation A	Yes
Stroke B	
Automatic Stroke Calculation B	Yes
Stop Time	
Stoptime Mode	Time set
Stoptime	50.00 min
Post Time	
Posttime Mode	Off

Solvent Composition

	Channel	Solvent 1	Name 1	Solvent 2	Name 2	Selected	Used	Percent (%)
1	A	H20		H20		Ch. 1	Yes	98.0 %
2	B	premixed ACN(95%) - H2O(5%)		ACN		Ch. 1	Yes	2.0 %

Timetable

	Time (min)	A (%)	B (%)	Flow (mL/min)
1	0.00 min	98.0 %	2.0 %	0.100 mL/min
2	2.00 min	98.0 %	2.0 %	0.100 mL/min

	Pressure (bar)
1	400.00 bar
2	400.00 bar

	Time (min)	A (%)	B (%)	Flow (mL/min)
3	27.00 min	60.0 %	40.0 %	0.100 mL/min
4	32.00 min	40.0 %	60.0 %	0.100 mL/min
5	32.01 min	15.0 %	85.0 %	0.100 mL/min
6	37.00 min	15.0 %	85.0 %	0.100 mL/min
7	37.01 min	98.0 %	2.0 %	0.100 mL/min

Name: Column Comp. **Module:** G7116A

Left Temperature Control

Temperature Control Mode	Temperature Set
Temperature	40.0 °C
Enable Analysis Left Temperature	
Enable Analysis Left Temperature On	Yes
Enable Analysis Left Temperature Value	1.0 °C
Left Temp. Equilibration Time	0.0 min

Right Temperature Control

Right temperature Control Mode	Temperature Set
Right temperature	40.0 °C
Enable Analysis Right Temperature	
Enable Analysis Right Temperature On	Yes
Enable Analysis Right Temperature Value	0.8 °C
Right Temp. Equilibration Time	0.0 min

Enforce column for run

Enforce column for run enabled	No

Stop Time

Stoptime Mode	As pump/injector

Post Time

Posttime Mode	Off

Timetable

Valve Position	Position 2 (Port 1 -> 2)
Position Switch After Run	Do not switch

	Pressure (bar)
3	400.00 bar
4	400.00 bar
5	400.00 bar
6	400.00 bar
7	400.00 bar

Appendix B. SGS (Lakefield, ON) report summaries

B1. Nickel in water samples

CERTIFICATE OF ANALYSIS

Final Report

Sample ID	Sample Date & Time	Temperature Upon Receipt °C	Nickel (total) mg/L	Nickel (dissolved) mg/L
1: Analysis Start Date		---	06-Dec-21	06-Dec-21
2: Analysis Start Time		---	12:30	12:30
3: Analysis Completed Date		---	07-Dec-21	08-Dec-21
4: Analysis Completed Time		---	12:56	17:15
5: DN-2-1a	28-Nov-21	2.0	---	0.0012
6: DN-2-1b	29-Nov-21	2.0	---	0.0012
7: DN-CT-1a	28-Nov-21	2.0	---	0.0005
8: DN-CT-1b	29-Nov-21	2.0	---	0.0005
9: DN-2-2a	28-Nov-21	2.0	---	0.0022
10: DN-2-2b	29-Nov-21	2.0	---	0.0020
11: DN-0.2-2a	28-Nov-21	2.0	---	0.0011
12: DN-0.2-2b	29-Nov-21	2.0	---	0.0031
13: DN-20-1a	28-Nov-21	2.0	---	0.0042
14: DN-20-1b	29-Nov-21	2.0	---	0.0042
15: DN-CT-2a	28-Nov-21	2.0	---	0.0005
16: DN-CT-2b	29-Nov-21	2.0	---	0.0005
17: DN-200-2a	28-Nov-21	2.0	---	0.0542
18: DN-200-2b	29-Nov-21	2.0	---	0.0607
19: DN-200-1a	28-Nov-21	2.0	---	0.0385
20: DN-200-1b	29-Nov-21	2.0	---	0.0366
21: DN-20-2a	28-Nov-21	2.0	---	0.0080
22: DN-20-2b	29-Nov-21	2.0	---	0.0036
23: DN-0.2-1a	28-Nov-21	2.0	---	0.0006
24: DN-0.2-1b	29-Nov-21	2.0	---	0.0006
25: DN-2-3	28-Nov-21	2.0	---	0.0010
26: DN-20-3	29-Nov-21	2.0	---	0.0043
27: DN-200-3	28-Nov-21	2.0	---	0.0384
48: DN-0.2-3	28-Nov-21	2.0	---	0.0005
28: TN-2-1a	28-Nov-21	2.0	0.0012	---
29: TN-2-1b	29-Nov-21	2.0	0.0012	---
30: TN-CT-1a	28-Nov-21	2.0	0.0005	---
31: TN-CT-1b	29-Nov-21	2.0	0.0005	---

OnLine LIMS

0002743721

Sample ID	Sample Date & Time	Temperature Upon Receipt °C	Nickel (total) mg/L	Nickel (dissolved) mg/L
32: TN-2-2a	28-Nov-21	2.0	0.0020	---
33: TN-2-2b	29-Nov-21	2.0	0.0019	---
34: TN-0.2-2a	28-Nov-21	2.0	0.0009	---
35: TN-0.2-2b	29-Nov-21	2.0	0.0031	---
36: TN-20-1a	28-Nov-21	2.0	0.0044	---
37: TN-20-1b	29-Nov-21	2.0	0.0045	---
38: TN-CT-2a	28-Nov-21	2.0	0.0005	---
39: TN-CT-2b	29-Nov-21	2.0	0.0005	---
40: TN-200-2a	28-Nov-21	2.0	0.0645	---
41: TN-200-2b	29-Nov-21	2.0	0.0678	---
42: TN-200-1a	28-Nov-21	2.0	0.0393	---
43: TN-200-1b	29-Nov-21	2.0	0.0377	---
44: TN-20-2a	28-Nov-21	2.0	0.0054	---
45: TN-20-2b	29-Nov-21	2.0	0.0051	---
46: TN-0.2-1a	28-Nov-21	2.0	0.0006	---
47: TN-0.2-1b	29-Nov-21	2.0	0.0006	---

Method Descriptions

Parameter	SGS Method Code	Reference Method Code
Metals in aqueous samples - ICP-MS	ME-CA-[ENV]SPE-LAK-AN-006	SM 3030/EPA 200.8

Chris Sullivan

CHARTERED Christopher Sullivan CHEMIST

Chris Sullivan, B.Sc., C.Chem
Project Specialist,
Environment, Health & Safety

Online LIMS

0002743721

Quality Control Report

Inorganic Analysis													
Parameter	Reporting Limit	Unit	Method Blank	Duplicate				LCS / Spike Blank			Matrix Spike / Reference Material		
				Result 1	Result 2	RPD	Acceptance Criteria	Spike Recovery (%)	Recovery Limits (%)		Spike Recovery (%)	Recovery Limits (%)	
							%		Low	High		Low	High
Metals in aqueous samples - ICP-MS - QCBatchID: EMS0031-DEC21													
Nickel (total)	0.0001	mg/L	<0.0001			8	20	96	90	110	91	70	130

Online LIMS

0002743721

B2. Nickel in blood plasma

CERTIFICATE OF ANALYSIS

Final Report

Sample ID	Sample Date & Time	Nickel ug/g
1: Analysis Start Date		30-Dec-21
2: Analysis Start Time		00:59
3: Analysis Completed Date		10-Jan-22
4: Analysis Completed Time		12:16
5: P-CT-1a	09/17/21	0.07
6: P-CT-1b	09/17/21	0.08
7: P-CT-1c	09/17/21	0.07
8: P-CT-2a	09/17/21	0.08
9: P-CT-2b	09/17/21	0.08
10: P-CT-2c	09/17/21	< 0.05
11: P-0.2-1a	09/17/21	0.08
12: P-0.2-1b	09/17/21	0.07
13: P-0.2-1c	09/17/21	0.07
14: P-0.2-2a	09/17/21	0.10
15: P-0.2-2b	09/17/21	0.07
16: P-0.2-2c	09/17/21	0.09
17: P-2-1a	09/17/21	0.10
18: P-2-1b	09/17/21	0.05
19: P-2-1c	09/17/21	0.07
20: P-2-2a	09/17/21	0.05
21: P-2-2b	09/17/21	0.08
22: P-2-2c	09/17/21	0.10
23: P-20-1a	09/17/21	0.12
24: P-20-1b	09/17/21	0.13
25: P-20-1c	09/17/21	0.15
26: P-20-2a	09/17/21	0.14
27: P-20-2b	09/17/21	0.13
28: P-20-2c	09/17/21	0.15
29: P-200-1a	09/17/21	0.63
30: P-200-1b	09/17/21	0.48
31: P-200-1c	09/17/21	0.49
32: P-200-2a	09/17/21	0.60
33: P-200-2b	09/17/21	0.30
34: P-200-2c	09/17/21	0.57

Online LIMS

Nickel values reported to the Level of Quantification by ICP-MS
Report revised to report lower levels.

00025961208

Chris Sullivan, B.Sc., C.Chem
Project Specialist,
Environment, Health & Safety

Online UHS

Appendix C. Voom Diagnostic Plots

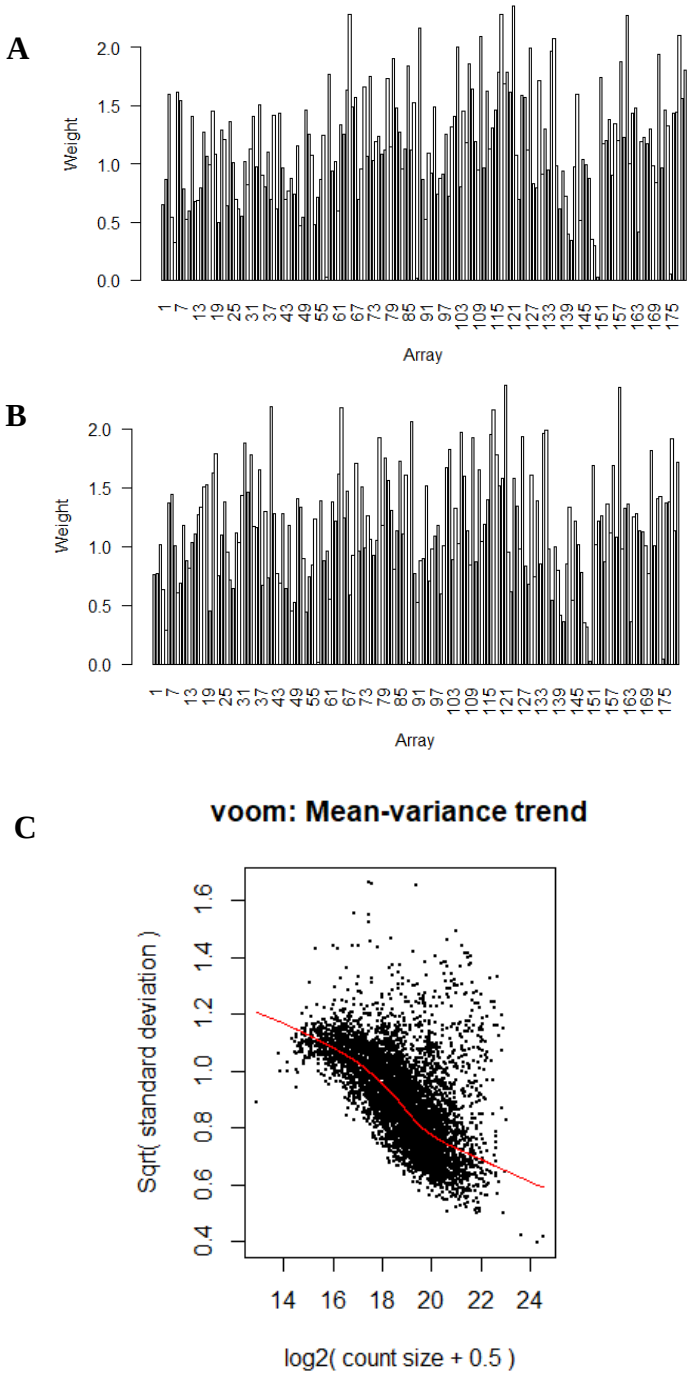

Figure C1: Pre-processing and mean-variance trend for model design with main and interaction effects for mucus proteomics. (A) Sample specific weights before adjustment and, (B) after adjustment for model design; N=180. (C) Mean-variance plot of model. Plots were created using the *limma* package in R.

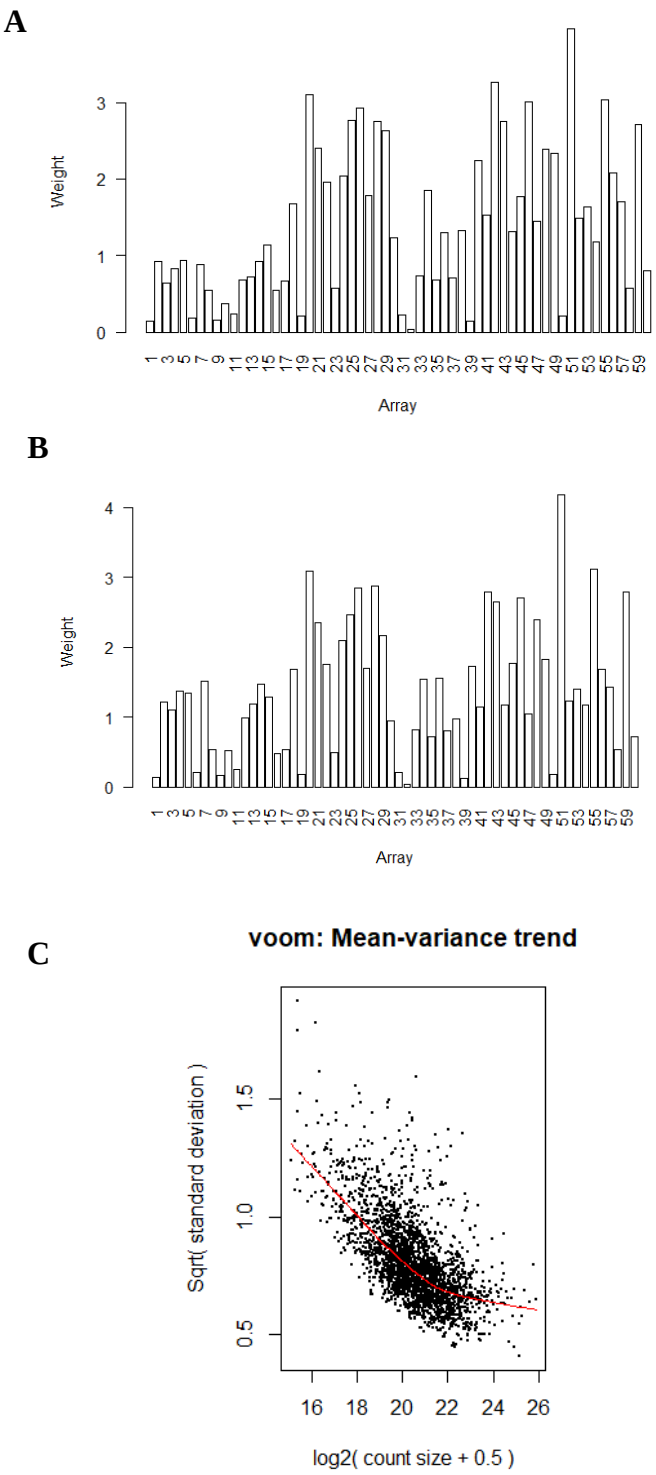

Figure C2: Pre-processing and mean-variance trend for model design with main effects for blood plasma proteomics. (A) Sample specific weights before adjustment and, (B) after adjustment for model design; N=60. (C) Mean-variance plot of model. Plots were created using the *limma* package in R.

Appendix D. HSI and Condition factor of rainbow trout

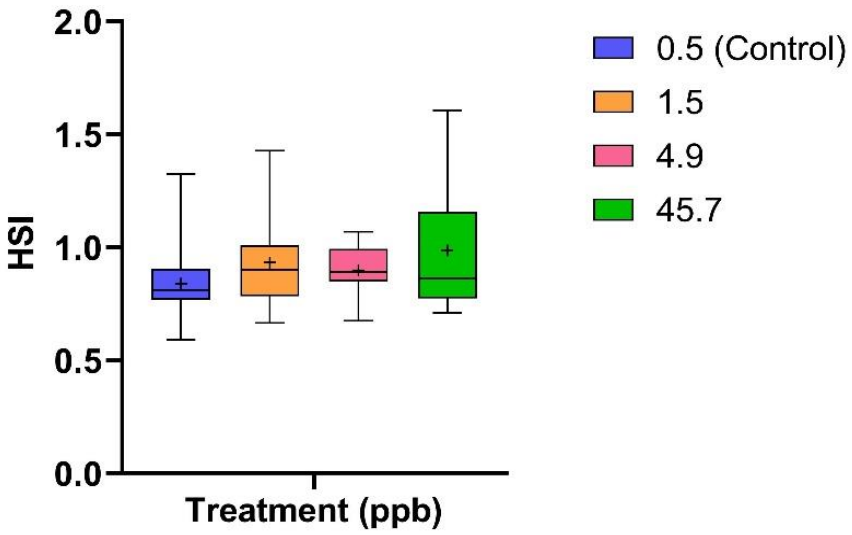

Figure D1: Hepatosomatic Index (HSI) of rainbow trout exposed to nickel. Boxplot represents the 25th, 50th (median) and 75th quantiles with outliers. Mean of group is represented by a '+' sign. N=15. No significant effect was observed with a Kruskal-Wallis test with a Dunn's multiple comparison test ($p > 0.05$). Plots were created using GraphPad 9.3.1

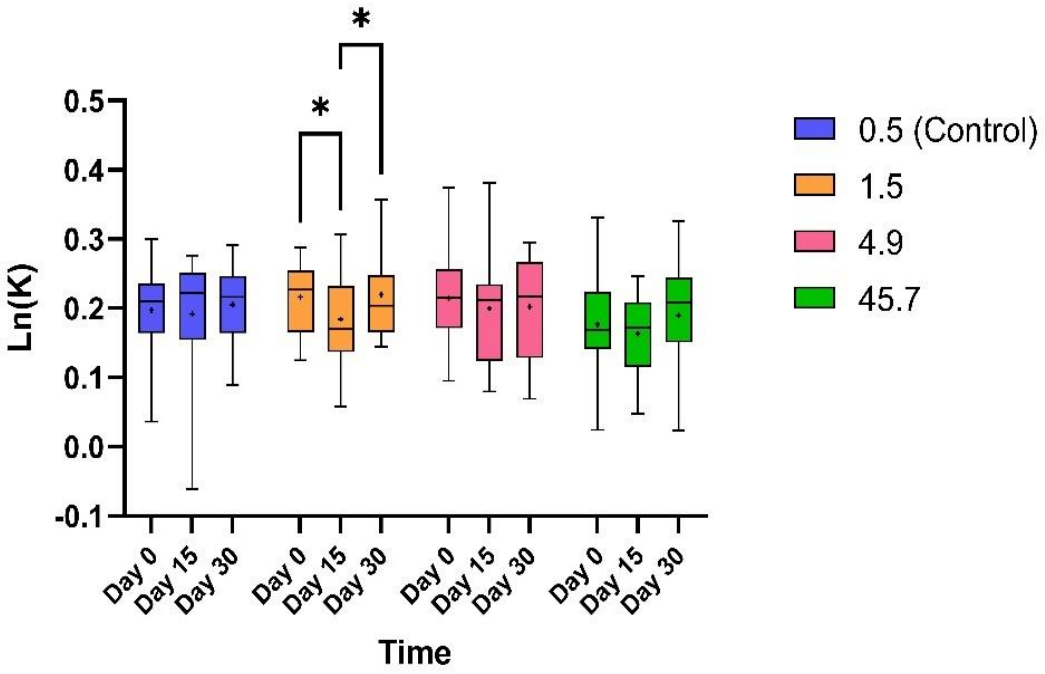

Figure D2. Natural logarithm transformed values of condition factor of rainbow trout. Boxplot represents the 25th, 50th (median) and 75th quantiles with outliers. Mean of group is represented by a '+' sign. N=15. A two-way ANOVA with Tukey test for multiple comparisons was performed; alpha < 0.05. Significant pairwise comparisons are indicated with a '*'. Plots were created using GraphPad 9.3.1

Appendix E. PCA plots

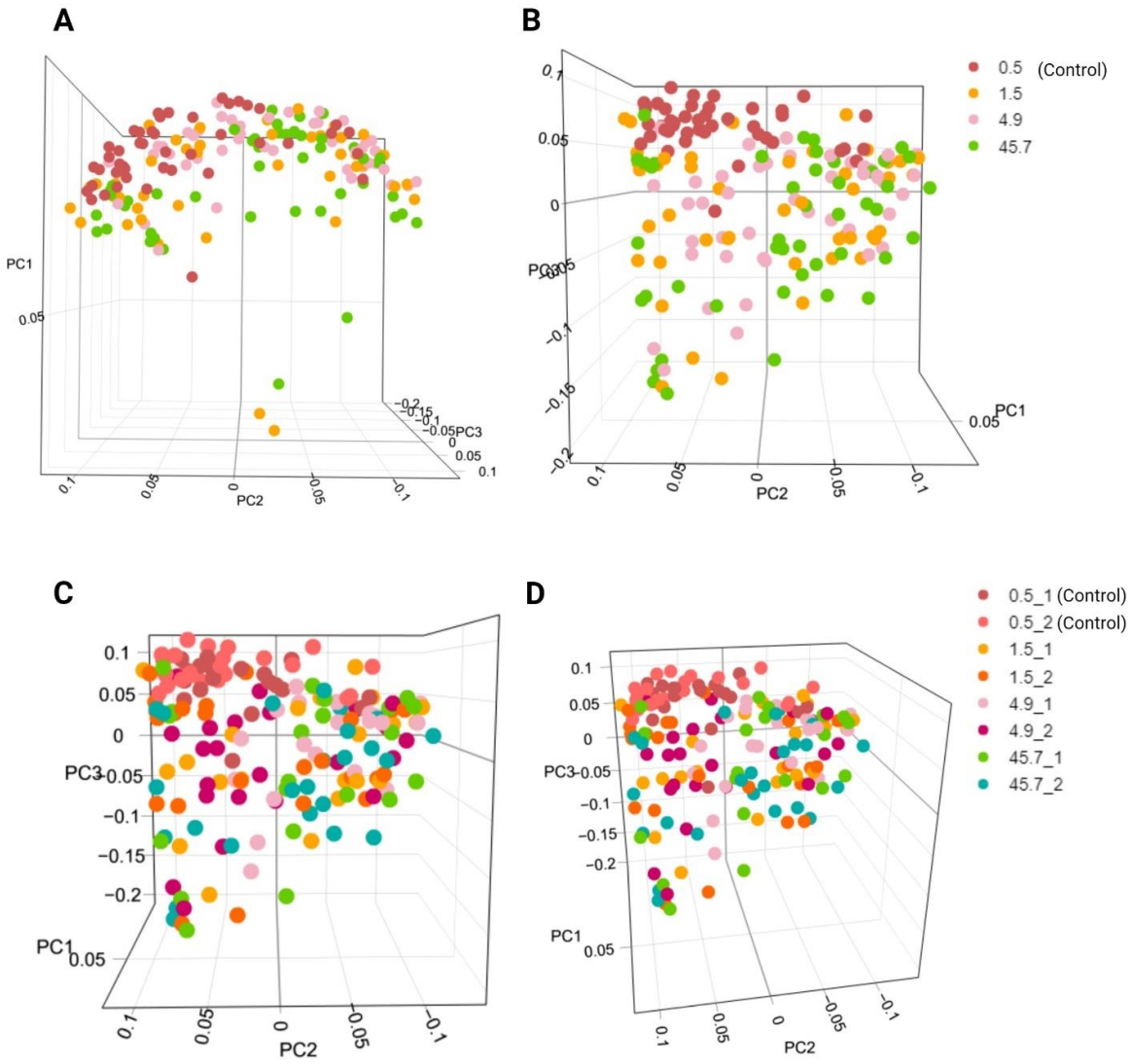

<u>Figure E1.</u> 3D PCA plots of mucus samples from different treatment groups based on protein intensities in the mucus proteome of rainbow trout. (A) and (B) Show the PCA plots of each treatment group, each data point is one fish (N=15, per sampling day). (C) and (D) show the PCA plots of replicate tank 1 (N=7, per sampling day) and replicate tank 2 (N=8, per sampling day) for each treatment group, each data point is one fish. Datapoints were not labelled by the sampling day since there were no clear clusters formed and to make visualization of groups formed by treatment group easier.

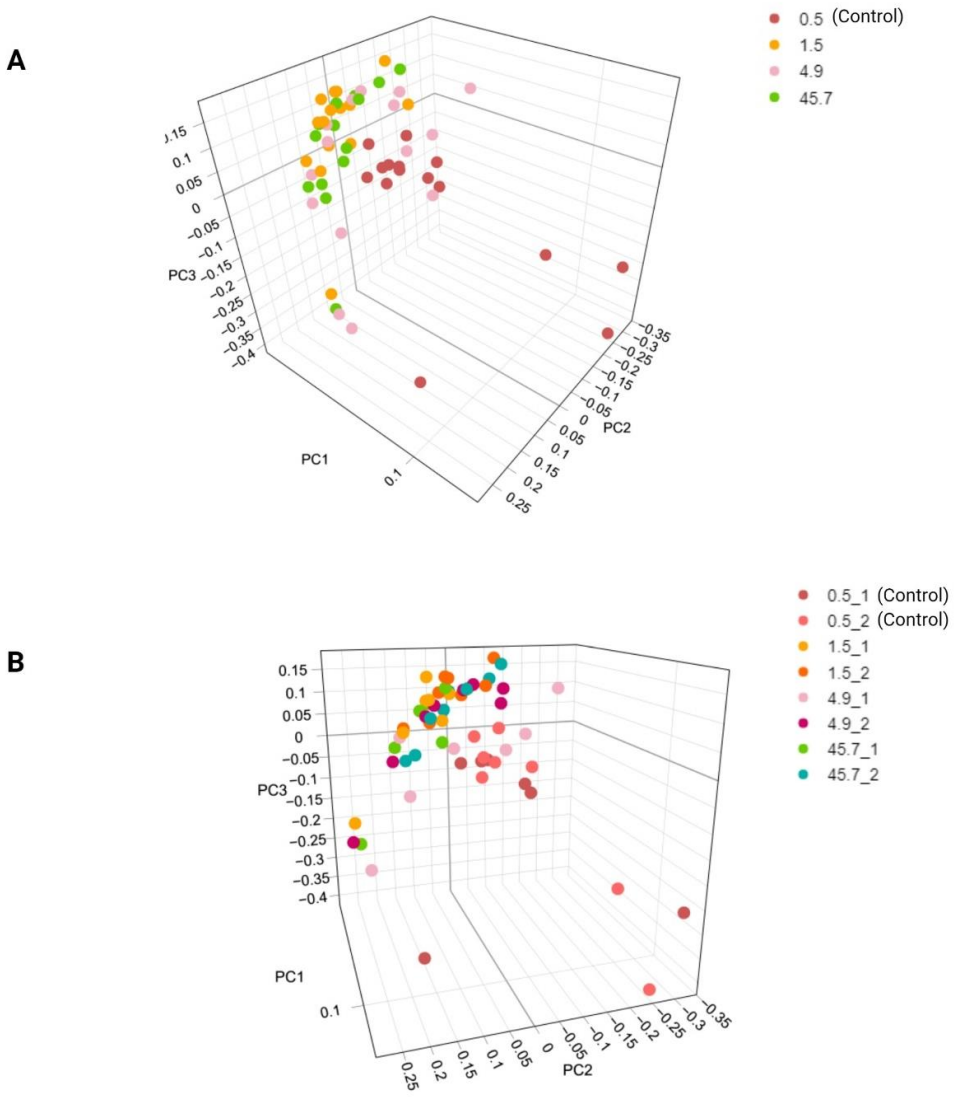

<u>Figure E2.</u> 3D PCA plots of blood plasma samples from different treatment groups based on protein intensities in the blood plasma proteome of rainbow trout on day 30. (A) and (B) Show the PCA plots of each treatment group, each data point is one fish (N=15). (C) and (D) show the PCA plots of replicate tank 1 (N=7) and replicate tank 2 (N=8) for each treatment group, each data point is one fish.

Appendix F. Over-represented pathways and GO terms in CPDB networks

Table F1: Over-represented GO biological processes in mucus proteins of rainbow trout significantly affected by nickel treatment.

The list of 51 proteins significantly affected by nickel treatment were searched against the Consensus Pathway database (CPDB) to find over-represented gene ontology (GO) biological processes involved in response to nickel exposure ($p < 0.01$).

P-Value	GO Term ID	GO Term	Proteins from Input List
0.00020213	GO:0038155	interleukin-23-mediated signaling pathway	JAK2; IL12B
0.00050704	GO:0050910	detection of mechanical stimulus involved in sensory perception of sound	LHFPL5; TMC2
0.00084727	GO:0061298	retina vasculature development in camera-type eye	PDGFRB; CLIC4
0.00110779	GO:0032989	cellular component morphogenesis	PDGFRB; NGF; MYO9A; DIP2B; CLIC4; CFDP1; NPTX1; AMIGO1; LHFPL5
0.00134649	GO:0070848	response to growth factor	PDGFRB; NGF; CTDSPL2; LRIT3; IL12B; KIF16B; TPR
0.00229147	GO:0070887	cellular response to chemical stimulus	IRF2; NGF; GPAM; PDGFRB; LRIT3; CTDSPL2; IL12B; KIF16B; CREBRF; JAK2; TPR; AMIGO1; STOX1; MYBL2; CLIC4; AS3MT
0.00237594	GO:0050793	regulation of developmental process	PDGFRB; NGF; GPAM; LINGO2; DIP2B; CFDP1; ZNF219; IL12B; ANKRD26; JAK2; NF2; MYO9A; AMIGO1; CNOT4
0.00256516	GO:0009653	anatomical structure morphogenesis	PDGFRB; NGF; MYO9A; KIF16B; DIP2B; ZNF219; IL12B; MYO6; NF2; NPTX1; AMIGO1; LHFPL5; CLIC4; CFDP1
0.00256973	GO:0000902	cell morphogenesis	NGF; MYO9A; DIP2B; CLIC4; CFDP1; NPTX1; AMIGO1; LHFPL5
0.00268838	GO:0050974	detection of mechanical stimulus involved in sensory perception	LHFPL5; TMC2
0.00338569	GO:0048660	regulation of smooth muscle cell proliferation	PDGFRB; JAK2; IL12B
0.00352815	GO:0022407	regulation of cell-cell adhesion	GPAM; JAK2; IL12B; MAGI1; NF2
0.00354028	GO:0048659	smooth muscle cell proliferation	PDGFRB; JAK2; IL12B
0.00412535	GO:0042127	regulation of cell proliferation	DNAJA2; PDGFRB; NGF; GPAM; STOX1; IL12B; JAK2; NF2; KSR1; CFDP1
0.00437413	GO:0051094	positive regulation of developmental process	PDGFRB; NGF; GPAM; LINGO2; ZNF219; IL12B; JAK2; NF2; AMIGO1
0.00481269	GO:0035315	hair cell differentiation	LHFPL5; MYO6
0.00530031	GO:0071363	cellular response to growth factor stimulus	PDGFRB; NGF; CTDSPL2; LRIT3; IL12B; KIF16B
0.00560973	GO:0051347	positive regulation of transferase activity	PDGFRB; NGF; IL12B; STOX1; KSR1; JAK2

0.00572626	GO:0061245	establishment or maintenance of bipolar cell polarity	CLIC4; MYO9A
0.00572626	GO:0035088	establishment or maintenance of apical/basal cell polarity	CLIC4; MYO9A
0.00572626	GO:0035722	interleukin-12-mediated signaling pathway	JAK2; IL12B
0.00597966	GO:0022604	regulation of cell morphogenesis	AMIGO1; NGF; DIP2B; CFDP1; MYO9A
0.00621049	GO:0050982	detection of mechanical stimulus	LHFPL5; TMC2
0.00627827	GO:0007259	JAK-STAT cascade	JAK2; IL12B; NF2
0.00645939	GO:0070671	response to interleukin-12	JAK2; IL12B
0.00672739	GO:0051049	regulation of transport	PDGFRB; ANKRD13D; TMC2; CTDSPL2; MYO6; IL12B; JAK2; TPR; AMIGO1; CLIC4
0.00684817	GO:0097696	STAT cascade	JAK2; IL12B; NF2
0.00695595	GO:0007264	small GTPase mediated signal transduction	PDGFRB; NGF; JAK2; MYO9A; KSR1
0.00701539	GO:0071310	cellular response to organic substance	IRF2; NGF; GPAM; PDGFRB; LRIT3; CTDSPL2; IL12B; KIF16B; AMIGO1; JAK2; TPR; CREBRF; MYBL2
0.00716915	GO:0007169	transmembrane receptor protein tyrosine kinase signaling pathway	PDGFRB; NGF; KIF16B; LRIT3; IL12B; JAK2
0.00750571	GO:0000904	cell morphogenesis involved in differentiation	NGF; DIP2B; CLIC4; NPTX1; AMIGO1; LHFPL5
0.00757154	GO:0050954	sensory perception of mechanical stimulus	LHFPL5; MYO6; TMC2
0.00832623	GO:0051965	positive regulation of synapse assembly	AMIGO1; LINGO2
0.00836745	GO:0031175	neuron projection development	NGF; MYO9A; DIP2B; JAK2; NPTX1; AMIGO1; LHFPL5
0.0087387	GO:0048839	inner ear development	PDGFRB; MYO6; LHFPL5
0.00886367	GO:0007265	Ras protein signal transduction	PDGFRB; NGF; JAK2; KSR1
0.00887453	GO:0033002	muscle cell proliferation	PDGFRB; JAK2; IL12B
0.00888703	GO:0048699	generation of neurons	NGF; MYO9A; DIP2B; MYO6; JAK2; NF2; NPTX1; AMIGO1; LHFPL5
0.00895995	GO:0007423	sensory organ development	PDGFRB; CLIC4; LHFPL5; NF2; MYO6
0.00941211	GO:0051169	nuclear transport	CTDSPL2; JAK2; TPR; IPO11
0.00979031	GO:0043388	positive regulation of DNA binding	NGF; JAK2
0.00979031	GO:0042490	mechanoreceptor differentiation	LHFPL5; MYO6
0.00986703	GO:0048869	cellular developmental process	PDGFRB; NGF; NPTX1; DIP2B; CFDP1; ZNF219; IL12B; MYO6; ANKRD26; JAK2; NF2; MYO9A; AMIGO1; LHFPL5; POMZP3; CLIC4; SPATA6; CNOT4
0.0099031	GO:0051338	regulation of transferase activity	PDGFRB; NGF; STOX1; IL12B; JAK2; NF2; KSR1

Table F2: Over-represented pathways in mucus proteins of rainbow trout significantly affected by nickel treatment. The list of 51 proteins significantly affected by nickel treatment were searched against the Consensus Pathway database (CPDB) to find over-represented pathways from different pathway databases involved in response to nickel exposure ($p < 0.01$).

P-value	Pathway	Pathway Database	Proteins From Input List
7.19E-05	IL-23 signaling	INOH	JAK2; IL12B
0.00010054	IL-12 signaling	INOH	JAK2; IL12B
0.00017188	Interleukin-12 signaling	Reactome	JAK2; IL12B
0.00017188	Interleukin-23 signaling	Reactome	JAK2; IL12B
0.00017188	no2-dependent il-12 pathway in nk cells	BioCarta	JAK2; IL12B
0.00030027	SHP2 signaling	PID	PDGFRB; NGF; JAK2
0.00049715	il12 and stat4 dependent signaling pathway in th1 development	BioCarta	JAK2; IL12B
0.0007214	Interleukin-12 family signaling	Reactome	JAK2; IL12B
0.00090763	Pathways in clear cell renal cell carcinoma	Wikipathways	PDGFRB; TPI1; KSR1
0.00151548	IL27-mediated signaling events	PID	JAK2; IL12B
0.00151548	S1P3 pathway	PID	PDGFRB; JAK2
0.0025871	RAF activation	Reactome	KSR1; JAK2
0.00278006	PDGFR-beta signaling pathway	PID	PDGFRB; JAK2; KSR1
0.00305858	IL23-mediated signaling events	PID	JAK2; IL12B
0.00305858	Type II interferon signaling (IFNG)	Wikipathways	IRF2; JAK2
0.00356727	ErbB2/ErbB3 signaling events	PID	JAK2; NF2
0.00392683	Signaling downstream of RAS mutants	Reactome	KSR1; JAK2
0.00392683	Signaling by RAS mutants	Reactome	KSR1; JAK2

0.00392683	Paradoxical activation of RAF signaling by kinase inactive BRAF	Reactome	KSR1; JAK2
0.00392683	Signaling by moderate kinase activity BRAF mutants	Reactome	KSR1; JAK2
0.00392683	Signaling by RAF1 mutants	Reactome	KSR1; JAK2
0.00396171	Brain-derived neurotrophic factor (BDNF) signaling pathway	Wikipathways	KSR1; NGF; JAK2
0.00403935	Factors involved in megakaryocyte development and platelet production	Reactome	KIF16B; JAK2; IRF2
0.00550353	JAK-STAT signaling pathway - Homo sapiens (human)	KEGG	PDGFRB; JAK2; IL12B
0.00552546	Sensory processing of sound by outer hair cells of the cochlea	Reactome	LHFPL5; TMC2
0.00596451	Signaling events mediated by PTP1B	PID	PDGFRB; JAK2
0.00618985	Sensory processing of sound by inner hair cells of the cochlea	Reactome	LHFPL5; TMC2
0.00725058	Tuberculosis - Homo sapiens (human)	KEGG	KSR1; JAK2; IL12B
0.007374	Sensory processing of sound	Reactome	LHFPL5; TMC2
0.00748591	PI3K-Akt signaling pathway - Homo sapiens (human)	KEGG	PDGFRB; NGF; JAK2; MAGI1
0.00812984	Signaling by BRAF and RAF fusions	Reactome	KSR1; JAK2
0.00865235	IL12-mediated signaling events	PID	JAK2; IL12B

Table F3: Over-represented GO biological processes in plasma proteins of rainbow trout significantly affected by nickel treatment.

The list of 1240 proteins significantly affected by nickel treatment were searched against the Consensus Pathway database (CPDB) to find over-represented gene ontology (GO) biological processes involved in response to nickel exposure ($p < 0.01$). The list here only includes manually selected terms from all the over-represented pathways that best represent the networks of interest.

P-Value	GO Term ID	GO Term	Proteins from Input List
3.61E-16	GO:0120036	plasma membrane bounded cell projection organization	DNAH17; MOV10; HSPA5; DYNLL2; NRCAM; CHRNA3; CHN1; CAPRIN1; LRRC49; DAB1; SEMA4D; SYNE2; EEF2K; AKIRIN1; NTNG2; DCC; NTRK2; SLC12A5; ZSWIM6; MANF; CDH1; SLITRK4; PLK2; RAB5A; LRRC7; CEP192; LRP1; OMG; LINGO1; KIF1A; BMP7; TWF2; SGK1; RFX4; LIMA1; PTK2B; ACSL4; RFX3; CEP70; PLEKHA1; FAT4; APC; WNT7A; VLDLR; UNC119B; ITGA1; ANO6; L1CAM; ITGA6; AKAP9; NPTX1; VANGL2; VIM; FNBP1L; FAM161A; TUBA1A; HAUS5; OTX2; VIL1; TBC1D24; RPGRIP1; TRPM2; LZTS1; PLPPR4; TBC1D2B; DPYSL2; SEPTIN6; FARP1; TRAPPC4; HERC1; CUX2; DAG1; PAX2; FHDC1; SARM1; PLA2G10; LRIG2; CAMSAP2; CAMSAP3; DNAH8; CDHR5; UNC13A; BBS12; FLNA; RSPH1; EHD3; GHRL; SDCBP; MAPK15; TNIK; PLCE1; DYNC2I2; DYNC2I1; DOCK10; HYDIN; FRMD7; ARF1; MYH9; CSF1R; TBC1D5; MARK4; SPTAN1; SEZ6; FBXO45; LAMA3; CELSR2; FER; ARFGEF1; TAPT1; PRDM12; FRY; VASH2; SEMA3A; AGRN; SEMA3B; SEMA3E; RASGRF1; SOS1; NTN1; PIP5K1A; USP9X; IRS2; TBC1D9B; SEPTIN2; MYO9A; COBL; HSP90AA1; MYO10; OCRL; NCKAP1L; DNM3; PTK7; LIMK2; KALRN; HMGB1; EGFR; ODAD4; CNTNAP1; MEGF8; LGI1; SLITRK2; SPTBN5; SPTBN4; SPTBN1; PTPN23; RAB35; MACF1; GRIN3A; TNN; CILK1; YWHAG; PLXNB2; CDH23; TMEM106B; TTLL3; PRKCA; ACAP3; DICER1; CCDC40; RAB3A; TRIP11; CNTN4; RAB25; IFT172; KIT; GRIN2B; PTPRF; ANK3; SCN1B; ABCC4; CFAP206; TBC1D10C; TBC1D10A; CKAP5
1.15E-10	GO:0031175	neuron projection development	MOV10; HSPA5; NRCAM; PLK2; CHN1; L1CAM; DAB1; SEMA4D; EEF2K; NTNG2; DCC; NTRK2; SLC12A5; CHRNA3; MANF; CDH1; SLITRK4; SLITRK2; LRRC7; LRP1; CAPRIN1; OMG; LINGO1; KIF1A; BMP7; TWF2; SGK1; PTK2B; ACSL4; VIM; FAT4; WNT7A; VLDLR; ITGA1; MACF1; ITGA6; TRAPPC4; NPTX1; PLXNB2; OTX2; TBC1D24; LZTS1; PLPPR4; DPYSL2; FARP1; HERC1; CUX2; DAG1; PAX2; FRMD7; SARM1; PLA2G10; LRIG2; CAMSAP2; CAMSAP3; FLNA; GHRL; TNIK; DOCK10; TNN; ARF1; CSF1R; ZSWIM6; SPTAN1; SEZ6; FBXO45; LAMA3; CELSR2; ARFGEF1; UNC13A; PRDM12; FRY; VASH2; SEMA3A; SEMA3B; SEMA3E; RASGRF1; SOS1; NTN1; USP9X; IRS2; SEPTIN2; MYO9A; COBL; HSP90AA1; NCKAP1L; DNM3; PTK7; KALRN; HMGB1; EGFR; CNTNAP1; MEGF8; LGI1; SPTBN5; SPTBN4; SPTBN1; RAB35; GRIN3A; DICER1; CDH23; TMEM106B; PRKCA; ACAP3; RAB3A; TRIP11; CNTN4; PTPRF; ANK3; SCN1B
3.57E-06	GO:0030036	actin cytoskeleton organization	MYO1H; NCKAP1L; SVIL; PTK7; GHRL; LIMK2; SPTAN1; NISCH; NEB; TNXB; SDCBP; XIRP2; SHROOM2; PTK2B; STARD13; AKAP13; MYO1C; PDCD10; TMOD1; FZD10; KRT8; SPTBN4; SPTBN5; SPTBN1; TNNT2; MYH6; GAS2L3; ARF1; MYH9; CSF1R; MICAL2; RICTOR; VIL1; CAPN10; IQGAP2; CDC42BPB; TRPM7; DAPK3; TRPM2; EPB41L1; EHBP1L1; CLASP2; DAAM1; EHBP1; RHOBTB2; CELSR1; COBL; FRMD7; TJP1; FER; CFL2; SERPINF2; TWF2; SMTNL2; FHDC1; FMN1; LRP1; SEMA3E; MYO18A; LIMA1; PIP5K1A; TNIK; ROCK2; KIT; INF2; FAT1; MYO19; MYOZ2; FLNA; FLNB; AMOT; ARFGEF1

2.92E-05	GO:0043087	regulation of GTPase activity	OCRL; RASGRP2; NCKAP1L; PLCB1; KALRN; ITGA6; DOCK5; AGRN; CHN2; PTK2B; STARD13; FZD10; RASAL2; SEMA4D; IQGAP2; PLXNB2; TBC1D9; CHML; AMOT; DOCK10; ARHGAP19; TBC1D5; NTRK2; ARHGAP22; ADAP2; RGS3; RALGAPA2; GIT1; TBC1D2B; TBC1D24; ACAP2; ACAP3; RICTOR; SRGAP3; SGSM1; DEPDC1B; SH3BP4; RASGRF1; SOS1; TBC1D10C; PIP5K1A; CHN1; RIN3; PREB; TBC1D9B; MYO9B; MYO9A; ARHGAP39; IPO5; RGP1; TBC1D10A; ARFGEF1
0.00015368	GO:0048015	phosphatidylinositol-mediated signaling	EGFR; CAT; PLCE1; CBL; SEMA4D; FLT1; KBTBD2; ZP3; CSF1R; NTRK2; PIK3CG; NLRC3; PLCB1; C1QBP; PDGFD; PLCD4; PLCD3; PLCD1; MUC5AC; OGT; PIP5K1A; IRS2; KIT; PLEKHA1; PITPNM2
0.00015755	GO:0007411	axon guidance	VLDLR; NRCAM; SPTAN1; CHN1; LGI1; CNTN4; L1CAM; DAB1; SPTBN4; SEMA4D; SPTBN5; SPTBN1; PLXNB2; CSF1R; DCC; OTX2; ZSWIM6; KALRN; SEMA3A; LAMA3; DPYSL2; PRKCA; SEMA3B; DAG1; SEMA3E; BMP7; LRP1; PLA2G10; SOS1; NTN1; MEGF8; IRS2; SCN1B
2.92E-05	GO:0043087	regulation of GTPase activity	OCRL; RASGRP2; NCKAP1L; PLCB1; KALRN; ITGA6; DOCK5; AGRN; CHN2; PTK2B; STARD13; FZD10; RASAL2; SEMA4D; IQGAP2; PLXNB2; TBC1D9; CHML; AMOT; DOCK10; ARHGAP19; TBC1D5; NTRK2; ARHGAP22; ADAP2; RGS3; RALGAPA2; GIT1; TBC1D2B; TBC1D24; ACAP2; ACAP3; RICTOR; SRGAP3; SGSM1; DEPDC1B; SH3BP4; RASGRF1; SOS1; TBC1D10C; PIP5K1A; CHN1; RIN3; PREB; TBC1D9B; MYO9B; MYO9A; ARHGAP39; IPO5; RGP1; TBC1D10A; ARFGEF1
0.00015368	GO:0048015	phosphatidylinositol-mediated signaling	EGFR; CAT; PLCE1; CBL; SEMA4D; FLT1; KBTBD2; ZP3; CSF1R; NTRK2; PIK3CG; NLRC3; PLCB1; C1QBP; PDGFD; PLCD4; PLCD3; PLCD1; MUC5AC; OGT; PIP5K1A; IRS2; KIT; PLEKHA1; PITPNM2
0.00015755	GO:0007411	axon guidance	VLDLR; NRCAM; SPTAN1; CHN1; LGI1; CNTN4; L1CAM; DAB1; SPTBN4; SEMA4D; SPTBN5; SPTBN1; PLXNB2; CSF1R; DCC; OTX2; ZSWIM6; KALRN; SEMA3A; LAMA3; DPYSL2; PRKCA; SEMA3B; DAG1; SEMA3E; BMP7; LRP1; PLA2G10; SOS1; NTN1; MEGF8; IRS2; SCN1B
0.00070711	GO:0006869	lipid transport	VLDLR; ACE; GHRL; FABP6; ATP11C; ACSL4; FABP1; PITPNA; CHKA; ATP8B2; TMEM30B; CEL; ESYT2; ABCD3; CYP7A1; LIPC; ACACA; ENPP7; PITPNM2; ATP10D; AQP9; OSBPL2; PLA2G4A; ATG2B; SLC27A1; PLA2G4F; ABCA12; LRP1; PLA2G10; LIMA1; IRS2; SYT7; ITGAV; ABCA4; ABCA5; ABCA1; ABCC4; ABCC3
0.0010437	GO:0001654	eye development	MYOM1; TMOD1; LIMK2; CPAMD8; HMGB1; TGIF2; BAX; SLC4A5; SHROOM2; MED1; CRYBG3; RRM1; YY1; IGFN1; FLT1; ZHX2; SOX11; NTRK2; RPGRIP1; KDM2B; CRB1; MAN2A1; CRYBB1; PAX2; CTNS; BMP7; SOS1; LRP5; HCN1; IFT172; VIM; FREM2; COL5A1; XRN2; WNT7A; SLC1A1; WNT7B
0.00118111	GO:0033043	regulation of organelle organization	CLTRN; TMOD1; PARN; PLK2; HPS4; PTK2B; PDCD10; EHD3; ZW10; SMG6; ESPL1; CAPN2; DYRK1A; RAB5A; HK2; MYO1C; PRMT6; LRP1; BRD4; SETD5; USP36; BMP7; SYT9; TWF2; LIMA1; AKAP9; PARP10; CEP70; ZNF274; APC; KDM5A; TASOR; TBC1D2B; SPTAN1; FMN1; UBE2L3; CLTC; XRCC1; FZD10; RICTOR; MPHOSPH8; CCSAP; TTK; VIL1; TBC1D24; TRPM2; PLCB1; SIRT6; FRMD7; ANAPC7; PRDM12; CAMSAP2; CAMSAP3; ATAD2; FLNA; HDAC5; KNTC1; NEB; SDCBP; MAPK15; AKAP13; INF2; ARF1; CSF1R; TBC1D5; MARK4; STOX1; RIF1; CELSR1; FER; ARFGEF1; SERPINF2; SYNE2; WAPL; TJP1; SEMA3E; LRP5; ATL3; PREB; TBC1D9B; MYO19; NCKAP1L; SVIL; LIMK2; BAX; SPTBN5; SPTBN4; SPTBN1; AASS; IQGAP2; DAPK3; YWHAG; CLASP2; KIF18A; TAPT1; RHOBTB2; CFL2; RAB3A; CCNB1; OGT; ROCK2; PDE2A; ATF5; TBC1D10C; TBC1D10A; CKAP5

2.92E-05	GO:0043087	regulation of GTPase activity	OCRL; RASGRP2; NCKAP1L; PLCB1; KALRN; ITGA6; DOCK5; AGRN; CHN2; PTK2B; STARD13; FZD10; RASAL2; SEMA4D; IQGAP2; PLXNB2; TBC1D9; CHML; AMOT; DOCK10; ARHGAP19; TBC1D5; NTRK2; ARHGAP22; ADAP2; RGS3; RALGAPA2; GIT1; TBC1D2B; TBC1D24; ACAP2; ACAP3; RICTOR; SRGAP3; SGSM1; DEPDC1B; SH3BP4; RASGRF1; SOS1; TBC1D10C; PIP5K1A; CHN1; RIN3; PREB; TBC1D9B; MYO9B; MYO9A; ARHGAP39; IPO5; RGP1; TBC1D10A; ARFGEF1
0.00015368	GO:0048015	phosphatidylinositol-mediated signaling	EGFR; CAT; PLCE1; CBL; SEMA4D; FLT1; KBTBD2; ZP3; CSF1R; NTRK2; PIK3CG; NLRC3; PLCB1; C1QBP; PDGFD; PLCD4; PLCD3; PLCD1; MUC5AC; OGT; PIP5K1A; IRS2; KIT; PLEKHA1; PITPNM2
0.00015755	GO:0007411	axon guidance	VLDLR; NRCAM; SPTAN1; CHN1; LGI1; CNTN4; L1CAM; DAB1; SPTBN4; SEMA4D; SPTBN5; SPTBN1; PLXNB2; CSF1R; DCC; OTX2; ZSWIM6; KALRN; SEMA3A; LAMA3; DPYSL2; PRKCA; SEMA3B; DAG1; SEMA3E; BMP7; LRP1; PLA2G10; SOS1; NTN1; MEGF8; IRS2; SCN1B
0.00070711	GO:0006869	lipid transport	VLDLR; ACE; GHRL; FABP6; ATP11C; ACSL4; FABP1; PITPNA; CHKA; ATP8B2; TMEM30B; CEL; ESYT2; ABCD3; CYP7A1; LIPC; ACACA; ENPP7; PITPNM2; ATP10D; AQP9; OSBPL2; PLA2G4A; ATG2B; SLC27A1; PLA2G4F; ABCA12; LRP1; PLA2G10; LIMA1; IRS2; SYT7; ITGAV; ABCA4; ABCA5; ABCA1; ABCC4; ABCC3
0.0010437	GO:0001654	eye development	MYOM1; TMOD1; LIMK2; CPAMD8; HMGB1; TGIF2; BAX; SLC4A5; SHROOM2; MED1; CRYBG3; RRM1; YY1; IGFN1; FLT1; ZHX2; SOX11; NTRK2; RPGRIP1; KDM2B; CRB1; MAN2A1; CRYBB1; PAX2; CTNS; BMP7; SOS1; LRP5; HCN1; IFT172; VIM; FREM2; COL5A1; XRN2; WNT7A; SLC1A1; WNT7B
0.00118111	GO:0033043	regulation of organelle organization	CLTRN; TMOD1; PARN; PLK2; HPS4; PTK2B; PDCD10; EHD3; ZW10; SMG6; ESPL1; CAPN2; DYRK1A; RAB5A; HK2; MYO1C; PRMT6; LRP1; BRD4; SETD5; USP36; BMP7; SYT9; TWF2; LIMA1; AKAP9; PARP10; CEP70; ZNF274; APC; KDM5A; TASOR; TBC1D2B; SPTAN1; FMN1; UBE2L3; CLTC; XRCC1; FZD10; RICTOR; MPHOSPH8; CCSAP; TTK; VIL1; TBC1D24; TRPM2; PLCB1; SIRT6; FRMD7; ANAPC7; PRDM12; CAMSAP2; CAMSAP3; ATAD2; FLNA; HDAC5; KNTC1; NEB; SDCBP; MAPK15; AKAP13; INF2; ARF1; CSF1R; TBC1D5; MARK4; STOX1; RIF1; CELSR1; FER; ARFGEF1; SERPINF2; SYNE2; WAPL; TJP1; SEMA3E; LRP5; ATL3; PREB; TBC1D9B; MYO19; NCKAP1L; SVIL; LIMK2; BAX; SPTBN5; SPTBN4; SPTBN1; AASS; IQGAP2; DAPK3; YWHAG; CLASP2; KIF18A; TAPT1; RHOBTB2; CFL2; RAB3A; CCNB1; OGT; ROCK2; PDE2A; ATF5; TBC1D10C; TBC1D10A; CKAP5
0.00130178	GO:0032970	regulation of actin filament-based process	NCKAP1L; SVIL; SPTAN1; NEB; AKAP9; PTK2B; AKAP13; TMOD1; FZD10; RICTOR; SPTBN4; SPTBN5; SPTBN1; FRMD7; ARF1; MYH9; CSF1R; VIL1; IQGAP2; DAPK3; TRPM2; CLASP2; MYO1C; RHOBTB2; CELSR1; TJP1; FER; CFL2; SERPINF2; TWF2; FMN1; LRP1; SEMA3E; LIMA1; HCN4; ROCK2; FLNA; PDE4D; ARFGEF1

0.00131357	GO:0015833	peptide transport	LIN7A; CLTRN; SCFD2; HSPA5; HSPA8; HPS4; PDCD10; CHML; SMG6; AHCYL1; CD209; SIX2; SLC12A2; CDH1; NUP210; AP1M1; RAB5A; RAB5C; NUP98; COG1; VPS13A; NUP93; MON2; ARRDC1; SEC24C; GNPAT; THOC2; USP36; SLC8B1; SYT9; AKAP6; NBAS; RFX6; ACSL4; SYT7; VIP; GRIP2; ANKRD50; VLDLR; DNAJC27; TRAK1; MACF1; MYO18A; MED1; ADAM8; CLTC; CAPN10; TBC1D9B; XPO4; ZIC1; SNX33; TBC1D2B; FRAS1; TBC1D9; EHBP1; DENND2A; MIA2; PAX8; TCAF2; ZDHHC3; CAMSAP3; RHBDF1; ATP6V0A2; IPO9; PDX1; IPO5; SSB; DTX3L; MYOM1; EHD3; SGSM1; GHRL; MYO1C; SDCBP; UPF2; FYTTD1; RFX3; VPS45; ARF3; ARF1; MYH9; TBC1D5; ARF5; UNC119B; TMEM30B; RPS26; CD63; ARRDC3; ARFGEF1; ARFGEF2; ZW10; LRP1; KIF1A; LRP5; VPS39; AGXT; IRS2; PREB; UBE2L3; MTCL1; ABCA1; HSP90AA1; STEAP3; KIF20A; CEMIP; RPS17; IPO11; IPO13; KALRN; SYNRG; EGFR; CAT; USP9X; PEX14; SPTBN1; PTPN23; RAB35; PMPCB; RAB5B; NUP188; VPS33A; CPSF1; KCNS3; DISP1; ATP6V1B2; DPP4; YWHAG; APPBP2; PRKCA; KIF18A; RAB3A; FLNA; RAB20; RAB25; DOP1B; ANK3; MON1B; CAMK2N1; TBC1D10C; SLC1A1; TBC1D10A
0.00410077	GO:0090183	regulation of kidney development	BMP7; FAT4; PDGFD; EGR1; SIX2; LIN28A; PAX2; PRKX; PAX8
0.00537499	GO:0090257	regulation of muscle system process	YY1; GHRL; DOCK5; PLCE1; EHD3; HCN4; TNNT2; KCNMA1; PIK3CG; GUCY1A1; TNNI3; PPP1R12B; SCN4A; DAPK3; PRKCA; DAG1; CHRNA3; AKAP6; G6PD; AKAP9; ROCK2; KIT; FLNA; PDE4D
0.00808683	GO:0070672	response to interleukin-15	PLCB1; STAT5A; ACSL4; JAK1
0.00879935	GO:0070102	interleukin-6-mediated signaling pathway	ST18; FER; SOCS3; CBL; JAK1
0.00913695	GO:0051130	positive regulation of cellular component organization	CLTRN; HSPA5; PARN; SERPINF2; HPS4; PTK2B; L1CAM; SEMA4D; EEF2K; MPP7; NTRK2; ESPL1; CAPN2; SLITRK2; HK2; LRRC7; BRD4; USP36; BMP7; SYT9; TWF2; AKAP9; KIT; APC; WNT7A; TASOR; VLDLR; ANO6; CAPRIN1; FMN1; ITGA6; DOCK5; MYO18A; MED1; UBE2L3; DNM3; RICTOR; FNBP1L; PLXNB2; MPHOSPH8; VIL1; C4B; PLCB1; SIRT6; CUX2; DAG1; FRMD7; ANAPC7; PRDM12; CBL; FLNA; GHRL; MYO1C; SDCBP; MAPK15; PLCE1; ARF1; TBC1D5; C1QBP; MARK4; HAS3; MACF1; RIF1; FRMPD4; FER; UNC13A; LGALS3; LRP1; AKIRIN1; LRP5; NTN1; ATL3; ABCA1; COBL; HSP90AA1; NCKAP1L; PTK7; KALRN; BAX; AGRN; MEGF8; CD63; IQGAP2; PTPN23; CAND1; YWHAG; CLASP2; GTF2H4; TAPT1; CFL2; CCNB1; OGT; RPA1; ROCK2; CUL4B; SCN1B; CKAP5
0.0095238	GO:0003338	metanephros morphogenesis	FRAS1; FMN1; SIX2; PAX2; PAX8; WNT7B

Table F4: Over-represented pathways in plasma proteins of rainbow trout significantly affected by nickel treatment. The list of 1240 proteins significantly affected by nickel treatment were searched against the Consensus Pathway database (CPDB) to find over-represented pathways from different pathway databases involved in response to nickel exposure ($p < 0.01$). The list here only includes manually selected terms from all the over-represented pathways that best represent the networks of interest.

P-value	Pathway	Pathway Database	Proteins from Input List
1.45E-06	Axon guidance	Reactome	VLDLR; LIMK2; ITGA1; HSPA8; EGFR; ITGA5; CLTC; SDCBP; CNTNAP1; ITGAV; DNM3; L1CAM; DAB1; SPTBN4; PITPNA; SPTBN5; SPTBN1; SEMA4D; MYH9; DCC; NRCAM; SRGAP3; KALRN; SCN4A; GRIN1; GIT1; DPYSL2; CLASP2; PRKCA; COL9A1; DAG1; ARHGAP39; SEMA3A; AGRN; RGMB; SEMA3E; SOS1; SPTAN1; NTN1; ROCK2; IRS2; GRIN2B; ANK3; SCN1B; MYO9B; HSP90AA1; COL6A3; MYO10
3.19E-06	RHO GTPase cycle	Reactome	OCRL; TMPO; NCKAP1L; KALRN; NISCH; SRGAP3; DOCK5; MOSPD2; USP9X; STARD13; AKAP12; AKAP13; CLTC; VANGL2; RASAL2; DOCK10; IQGAP2; FNBP1L; LBR; MPP7; C1QBP; HSP90AA1; ARHGAP22; SPTBN1; CDC42BPB; SPTAN1; FAM169A; ABCD3; NOXO1; GIT1; WDR6; CHN1; FARP1; DAAM1; DST; PKN2; RHOBTB2; SLK; DEPDC1B; TMEM87A; PLEKHG3; SOS1; CHN2; SLC4A7; MCF2L; ROCK2; VIM; SPEN; MAP3K11; MYO9B; MYO9A; ARHGAP39; STEAP3; SH3PXD2A; ARHGAP19
8.40E-06	Nervous system development	Reactome	VLDLR; LIMK2; ITGA1; HSPA8; EGFR; ITGA5; CLTC; SDCBP; CNTNAP1; ITGAV; DNM3; L1CAM; DAB1; SPTBN4; PITPNA; SPTBN5; SPTBN1; SEMA4D; MYH9; DCC; NRCAM; SRGAP3; KALRN; SCN4A; ROCK2; GIT1; DPYSL2; CLASP2; PRKCA; COL9A1; DAG1; HSP90AA1; GRIN1; SEMA3A; AGRN; RGMB; SEMA3E; SOS1; SPTAN1; NTN1; IRS2; GRIN2B; ANK3; SCN1B; MYO9B; ARHGAP39; COL6A3; MYO10
5.32E-05	Vesicle-mediated transport	Reactome	OCRL; CLTC; ACTR10; SPTAN1; HSPA8; MYO1C; MADD; COPS5; HPS4; RIN3; DNM3; RAB3A; SPTBN5; SPTBN4; PLA2G4A; SPTBN1; FNBP1L; VPS45; CHML; DENND2A; DENND2D; SCARA5; ARF3; ARF1; DYNLL2; SPARC; ARF5; TPD52L1; TRAPPC10; NBAS; YWHAG; RALGAPA2; AP1M1; RAB5A; RAB5C; RAB5B; COPS6; COG1; KIF18A; RAB35; MAN2A1; AAK1; LRP1; DENND5B; SEC24C; MIA2; HBA1; TRIP11; ZW10; COL7A1; SYT9; TJP1; KIF1A; TRAPPC8; AVPR2; TRAPPC4; CBL; PREB; ANK3; MON1B; KIF28P; HSP90AA1; EGFR; RGP1; TBC1D10A; KIF20A
0.00017213	ECM-receptor interaction - Homo sapiens (human)	KEGG	LAMA3; FRAS1; ITGB6; ITGA6; ITGA1; HSPG2; TNXB; ITGA5; ITGAV; COL9A1; AGRN; FREM2; FREM1; DAG1; COL6A3; TNN
0.00017946	Development of ureteric collection system	Wikipathways	MYCN; FRAS1; FAT4; CELSR1; FREM2; FREM1; GLI1; SIX2; PAX2; VANGL2; GREB1L
0.00101475	Phosphatidylinositol phosphate metabolism	EHMN	OCRL; PLCB1; NUP98; PIGA; ALG3; PIP5K1A; NUP93; PIK3CG; NUP188; ATP8B2; PLCD4; PLCE1; PLCD3; PLCD1; NUP210

0.00123874	IL2	NetPath	PTK2B; PLCB1; SOS1; SGK1; VIL1; CBL; PIK3CG; ETS2; STAT5A; SOCS3; IRS2; JAK1; HSP90AA1
0.0027987	Striated Muscle Contraction Pathway	Wikipathways	MYOM1; TNNT2; MYH6; DES; NEB; VIM; TNNI3; TMOD1
0.00358661	IL5	NetPath	SOS1; PTK2B; BAX; PIK3CG; STAT5A; CBL; JAK1; PLA2G4A; SDCBP
0.00413968	Sensory processing of sound	Reactome	EPB41L1; CDH23; TMC2; SPTAN1; MYH9; MYO1C; KCNMA1; TWF2; SPTBN1; XIRP2

Appendix G. Volcano plots

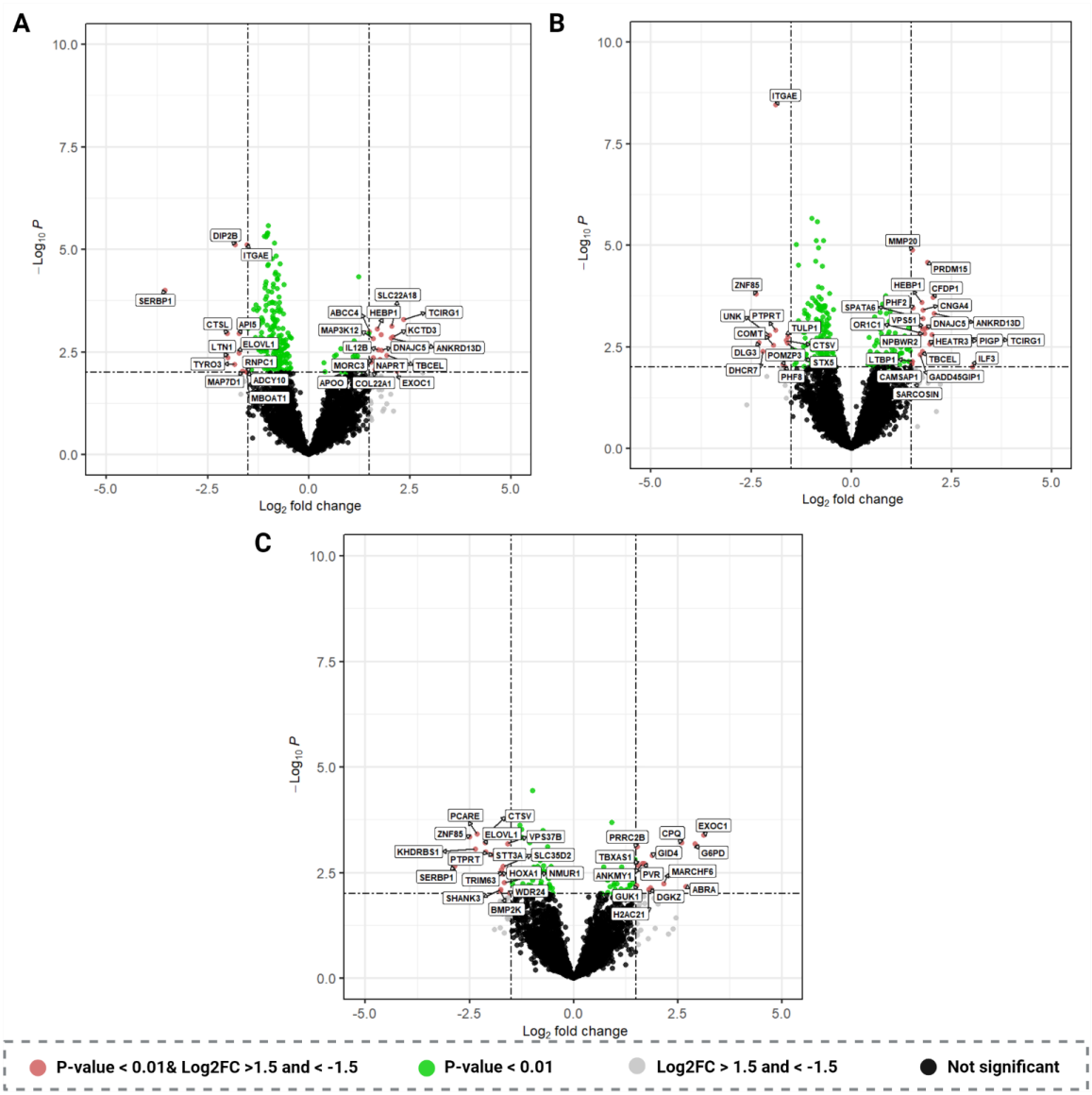

Figure G1 (A-C) – description below

<u>Figure G1:</u> Volcano plots representing log2 fold-change of abundance of mucus proteins of rainbow trout exposed to nickel treatments on day 15 compared to their controls on day 15. Volcano plot of log2 fold change of the abundance of proteins on day 15 in the nickel treatment: (**A**) 1.5 ppb compared to their abundance on day 15 in the control (0.5 pbb) group. (**B**) 4.9 ppb compared to their abundance on day 15 in the control (0.5 pbb) group. (**C**) 45.7 ppb compared to their abundance on day 15 in the control (0.5 pbb) group. Plots are labelled randomly with proteins that are significant ($p < 0.01$) and a fold-change greater or less than 1.5. Proteins with a log2 fold change greater or less than 1.5 with a p-value less than 0.01 are highlighted in pink. Proteins with a fold change with a p-value < 0.01 are highlighted in green, while proteins with a fold-change less or greater than 1.5 are highlighted in light grey. Proteins that are not significant at a p-value < 0.01 are highlighted in black

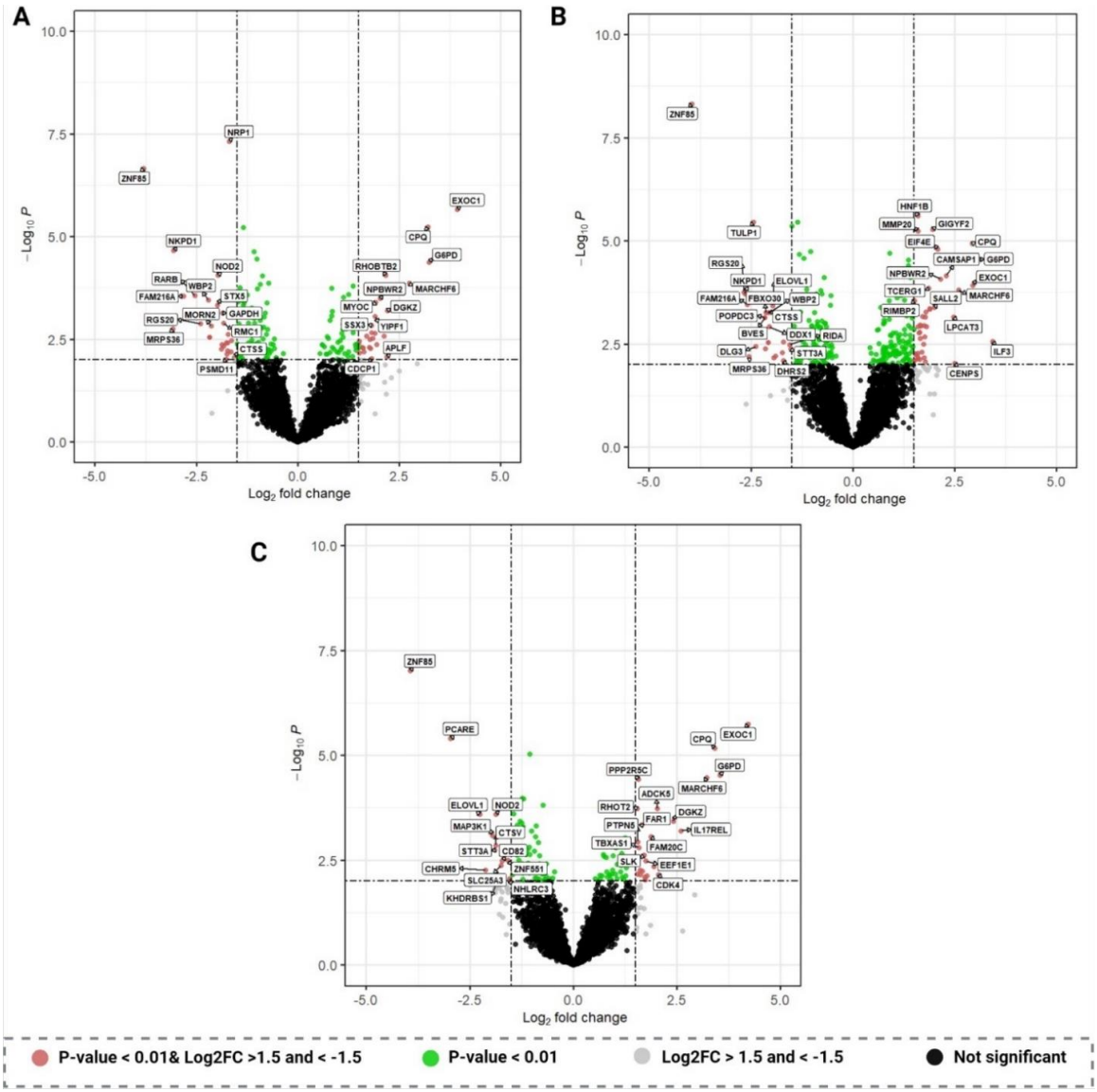

Figure G2 (A-C) – description below

<u>Figure G2:</u> Volcano plots representing log2 fold-change of abundance of mucus proteins of rainbow trout exposed to nickel treatments on day 30 compared to their controls on day 30. Volcano plot of log2 fold change of the abundance of proteins on day 30 in the nickel treatment: (A) 1.5 ppb compared to their abundance on day 30 in the control (0.5 pbb) group. (B) 4.9 ppb compared to their abundance on day 30 in the control (0.5 pbb) group. (C) 45.7 ppb compared to their abundance on day 30in the control (0.5 pbb) group. Plots are labelled randomly with proteins that are significant ($p < 0.01$) and a fold-change greater or less than 1.5. Proteins with a log2 fold change greater or less than 1.5 with a p-value less than 0.01 are highlighted in pink. Proteins with a fold change with a p-value < 0.01 are highlighted in green, while proteins with a fold-change less or greater than 1.5 are highlighted in light grey. Proteins that are not significant at a p-value < 0.01 are highlighted in black

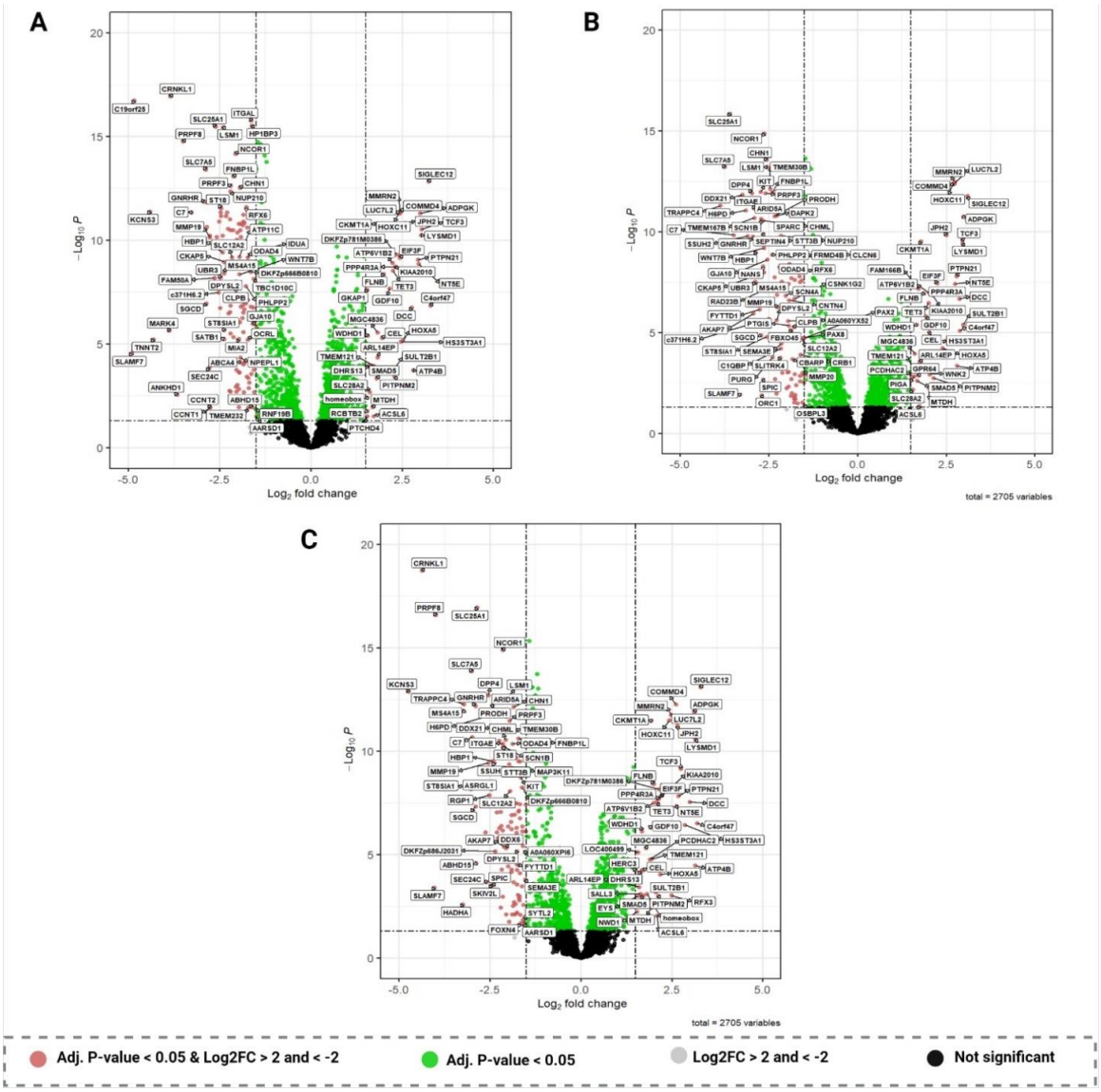

Figure G3 (A-C) – description below

<u>Figure G3:</u> Volcano plots representing log2 fold-change of abundance of blood plasma proteins of rainbow trout exposed to nickel treatments compared to the control. Volcano plot of log2 fold change of the abundance of proteins in the nickel treatment: (A) 1.5 ppb compared to their abundance in the control (0.5 pbb) group. (B) 4.9 ppb compared to their abundance in the control (0.5 pbb) group. (C) 45.7 ppb compared to their abundance in the control (0.5 pbb) group. Plots are labelled randomly with proteins that are significant ($p < 0.01$) and a fold-change greater or less than 2. Proteins with a log2 fold change greater or less than 2 with an adjusted p-value less than 0.05 are highlighted in pink. Proteins with an adjusted p-value < 0.05 are highlighted in green, while proteins with a fold-change less or greater than 2 are highlighted in light grey. Proteins that are not significant at a adjusted p-value < 0.05 are highlighted in black.